Historic and Future Extreme Weather Events over Southern Baffin Island

by

Danielle Desjardins

A Thesis submitted to the Faculty of Graduate Studies of

The University of Manitoba

in partial fulfillment of the requirements of the degree of

MASTER OF SCIENCE

Department of Environment and Geography

University of Manitoba

Winnipeg

ABSTRACT

Historic and future extreme precipitation and wind events over southern Baffin Island, more specifically Iqaluit, Kimmirut, Pangnirtung and Cape Dorset are examined.

Two sets of modeled re-analysis data, the Canadian Regional Climate Model (CRCM) forced with European Centre for Medium-Range Weather Forecasts Regional Analysis 40 (ERA40) and the other the North American Regional Re-analysis (NARR) dataset were used to characterize the atmosphere during historic events.

Two sets of CRCM data forced with Canadian Global Climate Model (CGCM) data, one from 1961-1990 and the other from 2041-2070, are compared to assess the changes in extreme events in the future.

Extreme events were defined by daily precipitation and sustained wind thresholds. Based on the CRCM future projection, events were inferred to increase in intensity for all communities and increase in frequency for 3 of the 4 communities. A shift in the Arctic storm season was also inferred in the future projection.

ACKNOWLEDGEMENTS

I would like to thank George Liu for all of his hard work in writing the scripts used to detect extreme events as well as Jason Knight for his help with the GrADs software. Also, a big thanks to my advisor, Dr. Ronald Stewart for all his support and guidance as well as Dr. John Hanesiak and Dan Fulton for all of their help and advice.

I would like to acknowledge the Data Access Integration team (DAI, see http://quebec.ccsn.ca/DAI/) for providing the data and technical support. The DAI data download gateway is made possible through collaboration among the Global Environmental and Climate Change Centre (GEC3), the Adaptation and Impacts Research Division (AIRD) of Environment Canada, and the Drought Research Initiative (DRI). The Ouranos Consortium (in Québec) also provides IT support to the DAI team.

Model data were from different sources. The Canadian Regional Climate Model time series data has been generated and supplied by Ouranos' Climate Simulations Team. NARR and NCEP/NCAR images and re-analysis data provided by the NOAA/ESRL Physical Sciences Division, Boulder, Colorado, USA, from their Web site at http://www.esrl.noaa.gov/psd/

DEDICATION

To my fiancé Shaun, who has been my rock from beginning to end and also to my parents who are unconditionally supportive of all my endeavours.

TABLE OF CONTENTS

LIST OF TABLES

LIST OF FIGURES

CHAPTER 1: INTRODUCTION AND OBJECTIVES

With temperatures rising due to climate change, the Arctic may become more prone to adverse weather. Storm tracks may, for example, shift northward and more mid-latitude storms may affect the region, which means that the Canadian Arctic may experience more frequent and severe storms in the future. The recent article on observational storm tracks shows that trends in cloud cover over the 1983-2008 periods are shifting towards the poles (Bender et al., 2011). Not only do these rising temperatures have an effect on storm tracks, but they may also influence precipitation amount and its type as well as the seasonality of events. As one example of this concern, the impacts of saltwater surges driven by storms are unprecedented in the thousand year history in the Canadian Arctic region (Hill, 2011). The model of the Canadian Centre for Climate Modeling and Analysis projects near-total melting of summer Arctic sea ice by 2100 due to a loss of snow and ice and an overall warming trend in the Arctic (ACIA, 2005).

It is essential that we understand the impacts that climate change is having on the Arctic and whether we are going to see more extreme and damaging events in this area in the future. However, relatively little research has actually addressed this issue.

This thesis contributes to addressing the impacts of climate change on the Arctic and will focus on severe weather events over a particular region of the Arctic. To begin addressing this topic, this study's overall objectives are to identify and characterize the atmosphere during extreme precipitation and wind events that have taken place in eastern

Nunavut over the southern Baffin Island area (Figure 1.1) and to use this information as a basis for examining future events using a regional climate model projection.

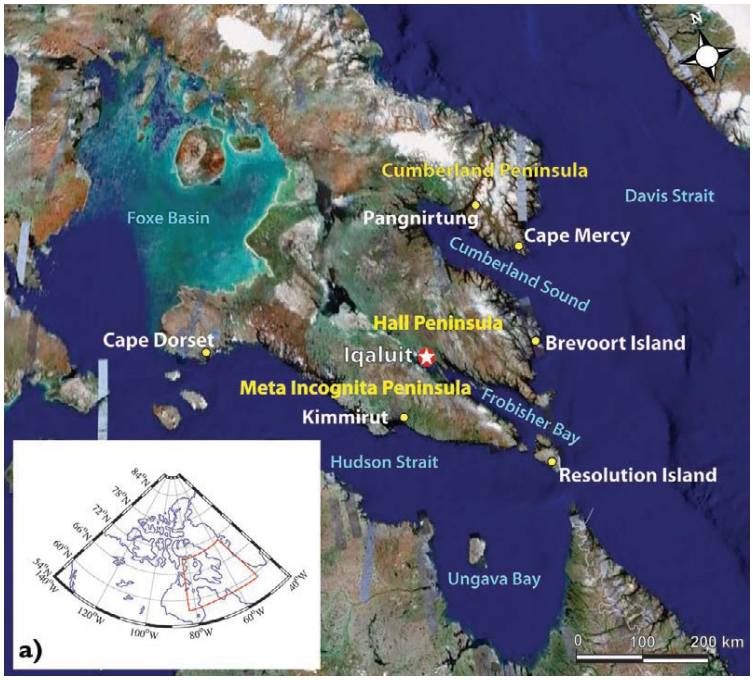

Figure 1.1: Map of southern Baffin Island and the four communities, adapted from Hanesiak et al. (2010). © American Meteorological Society. Reprinted with permission.

The specific objectives of this thesis are to identify past extreme wind and precipitation events, to assess the degree to which their overall features are replicated with a regional climate model, and to assess how such events may occur in the future.

Several datasets were used in order to address these objectives. These include three separate Canadian Regional Climate Model (CRCM) datasets as well as one North American Regional Re-analysis (NARR) dataset.

Extreme events were defined on the basis of precipitation and wind thresholds. Upon defining an extreme event, algorithms were developed that detected extreme wind

and precipitation events in model re-analysis and future projection datasets. These algorithms identified accumulated daily precipitation amounts three standard deviations above the mean accumulated daily precipitation to identify only the most extreme precipitation events. All days including 'nil' or 'trace' precipitation accumulations were included and as such the algorithms identified events of 5-7 mm/day (5-7 cm/day snow equivalent) as extreme precipitation threshold amounts. For wind events, sustained wind speeds of 60, 70 and 80 km/h or greater were identified based on the Environment Canada wind threshold criteria of sustained 70 km/h wind speeds to give a distribution of the extreme wind events. Both of these algorithms were applied to the historic datasets and compared to the future climate projection.

Analyses of the historic events were carried out using different critical levels to characterize the atmospheric patterns during extreme events. The surface, 850 mb and 500 mb are atmospheric levels commonly used in meteorology for analysis and diagnosis of the weather and were therefore used in this study to characterize the atmosphere.

Some of these events are analyzed in detail to isolate large scale as well as local factors that enhance these extreme events over southern Baffin Island. Once these events and flow patterns have been characterized, this study will correlate the CRCM re-analysis data with NARR re-analysis data and real historic observations to see how well the CRCM re-analysis replicated these events. Patterns characterized in the historic re-analysis may also be apparent in future extreme precipitation and wind events inferred the future projection data.

Future projection analyses were carried out using the algorithms to detect only the most extreme events from the CRCM forced with Canadian Global Climate Model

(CGCM) datasets. A comparison of the CRCM hindcast to the future projection would reveal any change in the seasonality, frequency and intensity of extreme precipitation and wind events.

CHAPTER 2: LITERATURE REVIEW

Extratropical cyclones are the main weather-makers in the Arctic. A considerable amount is known about these systems and they have been identified using numerous methods of detection, on seasonal as well as decadal time scales.

Chang and Fu (2002) studied interdecadal variability in Arctic storm tracks in the winter using the National Centers for Environmental Prediction-National Center for Atmospheric Research (NCEP-NCAR) re-analysis data. They showed a relationship between mean flow anomalies and the variability of the storm tracks. They also found an association between the Arctic Oscillation (AO) index and storm track variability.

Zhang et al. (2004) studied annual cyclonic variability in the Arctic from 1948-2002. Their study concluded that there is a strengthening trend in cyclonic activity, in both frequency and intensity throughout this period. They also observed a northward shift in cyclonic activity, which was most prominently observed in the summer. During the summer months the cyclones occurred more frequently and lasted longer but were less intense. In winter the cyclones were generally less frequent, decayed more rapidly but were more intense. An association between the decrease in mean sea level pressure and increased cyclonic activity was observed between 1988 and 1991. Zhang et al. associated this relationship partly with the AO index as well as other large-scale atmospheric phenomena.

Raible et al. (2008) studied three ways to track and detect extratropical cyclones in the northern hemisphere as well as comparing the ERA-40 re-analysis data with the NCEP-NCAR re-analysis data. The three approaches to detect extratropical cyclones

were the University of Hamburg (HAM) method, which uses a 1000 mb minimum with a minimum pressure gradient to track the storms. The second approach was the Swiss Federal Institute of Technology (ETH) method which uses a 1000 mb minimum as well as an algorithm to eliminate any other minimum within a certain radius of the main storm to track the cyclones. The third approach was the Australian (AUS) method which used a bicubic spline method to detect 1000 mb minima, which allowed for the detection of the storms between grid points. They pointed out that cyclone tracking does not only depend on the dataset used but also the algorithm used to detect them. The ERA-40 and NCEP-NCAR re-analysis datasets not only yielded a different number of cyclones, but their intensities differed as well between each of the approaches. The NCEP-NCAR data tended to show more significant trends than the ERA-40 data; however both the datasets showed similar seasonality in the results. The slight differences between these detection methods showed the most variation in detecting winter and summer cyclones as opposed to annual cyclonic variability.

Intihar and Stewart (2005) studied the relationship between extratropical cyclones and precipitation in the Canadian Archipelago during the cold season. They noted that, in general, snowfall accumulation increased from the northwest to the southeast, with maximum values occurring at Hall Beach, Clyde River and Iqaluit. Another relationship they noted was the southern sites, which are closer to the jet stream, experienced more cyclones on average as opposed to sites that are farther north and hence farther from the jet stream. Extratropical cyclones were not always the greatest factor when producing high precipitation events. An example of this is Alert, where orographic processes and lift were deemed to be the most important factors.

Roberts and Stewart (2008) studied freezing rain and ice pellets from 1980-2004. Synoptic patterns, vertical profiles as well as surface conditions were analyzed and it was determined that warm air advection as well as cyclonic vorticity advection were two of the main factors that were responsible for the freezing rain and ice pellet occurrences. They also suggest that subsequent studies should examine the impacts that a northward shift of storms will have on freezing rain and ice pellets in the future.

Gascon et al. (2010) studied extreme cold-season precipitation events at Iqaluit, Nunavut from 1955-1996. They examined 194 events, all which exceeded the 97th percentile of daily precipitation accumulation normal. This study determined that 40% of these events originated from the South, 29% from the West and 23% from the Atlantic Ocean, with the main storm tracks featured in Figure 2.1. Gascon et al. (2010) noted that the Southern originating storms formed over the United States or the Great Lakes and propagated northward until they re-intensified slightly over the Hudson Strait and then decayed over Baffin Island The Western-originating cyclones initiated as a result of either lee-cyclogenesis east of the Rocky Mountains or over the plains, due to orographical features. After reaching the Foxe Basin, the storms tended to split – either veering northward and decaying over Foxe Basin or maintaining their propagation towards the east, moving over the Hudson Strait and finally veering northward towards the southern part of Baffin Island. The Atlantic-originating cyclones generally formed over the northeastern coast of the United States and either followed the coast of Labrador or continued up the Atlantic Ocean and decayed over northeastern Baffin Island.

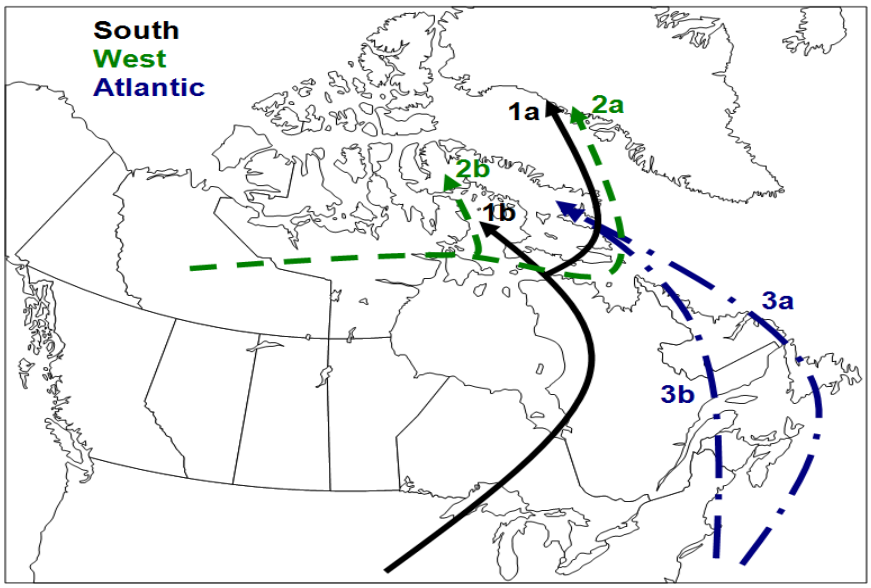

Figure 2.1: Main storm propagation of cold-season heavy precipitation events adapted from Gascon et al. (2010). © Arctic Institute of North America. Reprinted with permission.

Roberts et al. (2008) studied storms that passed over Southern Baffin Island during autumn of 2005 with a focus on storm structure and evolution. Six storms were studied in depth; similarities were found between the surface and vertical atmospheric conditions. Four of the six storms were associated with frontal passages; and warm temperatures were associated with all of the storms and were attributed to southeasterly winds. Above-average temperatures were observed for most of the study period, with record high temperatures observed on three days. There is concern that these storms may increase in frequency in the future because of greater moisture and temperature advection.

Henson et al. (2010) studied the three of the largest precipitation events over Iqaluit during the STAR field campaign; which ran from October 15, 2007 to December 5, 2007. This study used surface observations, soundings and radar to characterize the atmosphere during these events. Their results suggested that sublimation and advection of precipitation downstream from Iqaluit played important roles in the amount of precipitation recorded at Iqaluit itself. Another important conclusion was that the Global Precipitation Measurement satellite might not detect much of the precipitation in the region because of the low reflectivity values detected by the radar.

Nawri and Stewart (2008) studied the channeling of high-latitude boundary-layer flow over Cape Dorset and Iqaluit. Their research indicated that high-latitude winds over complex terrain are strongly affected by blocking and channeling affects due to the stability of boundary–layer stratification. They also suggested that when modeling surface winds, modeling large-scale pressure distribution might be more representative than modeling highly variable surface winds directly.

Nadeau (2007) analyzed atmospheric conditions that produced strong surface wind events at Iqaluit from 1979-2007. He defined a strong wind event as a surface wind speed of 10 m/s or greater lasting a minimum of three hours. The majority (approximately 2/3) of these events were from the northwest. Out of all the northwesterly strong wind events, his study showed that the top 5 events occurred during the cold season (October-April).

Deacu et al. (2010) simulated the November 7-8, 2006 wind event over Iqaluit using the Global Environmental Multiscale-Limited Area Model (GEM-LAM 2.5 km). Their study supports that an interaction between wind channeling over Frobisher Bay

driven by the large-scale pressure gradient force as well as downslope winds over the eastern slope of Hall Peninsula intensified the surface winds at Iqaluit during this event. A comparison between the observations at Iqaluit and the simulation of this event also detected a directional wind shift at the site, which was attributed to this interaction between the channeled and downslope winds. Another important aspect of this study was that the GEM-LAM grid point that represented Iqaluit during the simulation was not the most representative of the observations at Iqaluit. Alternately, a grid point located approximately 8 km to the west of Iqaluit represented the observations the best.

Collectively, it is apparent that some research has been conducted on high latitude extreme events; but it is still a relatively small amount in relation to what is needed. This project will specifically examine one gap and that is to examine how severe events may change in the future for one part of the Canadian Arctic.

CHAPTER 3: DATA AND METHODS

3.1 Introduction

This chapter identifies and describes the four communities involved in this study, the datasets that were used to analyze the extreme events as well as the methods used to identify the extreme events.

3.2 Site Description

As climate change continues, communities and the infrastructure upon which they rely is increasingly vulnerable (Nielsen, 2007). Baffin Island, located in the eastern Canadian Arctic, is particularly vulnerable to climate change because it is also susceptible to sea-level rise as well as storm surges (Nielsen, 2007). Situated between mainland Canada and Greenland, Baffin Island is the largest island of the Canadian Arctic Archipelago and is surrounded by numerous bodies of water. Davis Strait and Baffin Bay are situated to its north and east and Hudson Strait and Foxe Basin are situated to its south and west.

Iqaluit, the capital of Nunavut, Canada, is located near the head of Frobisher Bay at 63.8ºN and 68.5ºW. It is surrounded by the Meta Incognita Peninsula to its southwest and the Hall Peninsula to its northeast. Topographically, this community is situated in the middle of a valley where the Sylvia Grinnell River empties into Frobisher Bay. This often leads to a northwest-southeast 'channeling' of wind because of the orientation of the valley (Nawri and Stewart, 2006). Iqaluit averages approximately 6 blizzards a year (Prairie and Arctic Storm Prediction Centre (PASPC), personal communication, 2010).

The predominant winds are from the northwest during the winter months with a secondary wind direction from the southeast. Northwest winds can be unexpectedly strong in winter even under a weak ridge of high pressure. In the summer months, winds from the southeast are just as common as winds from the northwest.

The community of Pangnirtung is located on the southeastern shore of the Pangnirtung Fjord on the north shore of Baffin Island's Cumberland Sound. It is approximately 297 km northeast of Iqaluit, and has the coordinates 66.2ºN and 65.7ºW. Mount Duval lies east of the site, whereas the Kolik River flows into the community to its east as well. Southwest winds are most dominant at Pangnirtung during the summer months due to sea breezes up the valley fjord. Ahead of a synoptic system, easterly winds are dominant with significantly higher temperatures observed as a result to a Chinook Effect (PASPC, personal communication, 2010). With a population of approximately 1325 (2006 Census), the community is among one of the more populated areas of Baffin Island. Pangnirtung is very sensitive to excessive rainfall amounts due to the changes in riverbed, underground drainage and the impact of climate change on permafrost conditions (Bisson, 2008).

The community of Kimmirut is located on the south side of the Meta Incognita Peninsula on the shore of Hudson Strait. Its coordinates are 62.9ºN and 69.9ºW. It is a relatively sheltered community with predominantly light north winds in the winter. In the summer, southerly winds are dominant. Because Kimmirut is close to Hudson Strait, a west-southwest wind and open water can result in the community being affected by streamers in the shoulder seasons (PASPC, personal communication, 2010). Kimmirut, formerly known as Lake Harbour until 1996, has a population ranging from 425 to 550

people depending on the time of year. It was formerly a Hudson Bay trading post and was established in 1909, making it one of Nunavut's oldest communities.

Cape Dorset is located on Dorset Island near Foxe Peninsula and just south of Foxe Basin. An east-west channel between Mallik and Dorset Islands produces a channeling of the winds around this community. A strong low pressure system will cause strong, gusty winds at Cape Dorset. Like Kimmirut, Cape Dorset is also susceptible to streamers originating over Hudson Straight during the shoulder seasons (PASPC, personal communication, 2010). Its coordinates are 64.2N and 76.5W. With a population of over 1200, it is another large community on Baffin Island. Cape Dorset is known as the "Capital of Inuit Art" and has been a centre for drawing, printmaking and carving.

3.3 Datasets

The datasets were used for two overall purposes in this study. The first purpose was to assess the capability of the models to recreate historic extreme events and characterize the atmosphere during these extreme events. The second purpose was to compare model output that was run from two different time periods: A hindcast time frame and a future projection time frame to determine whether the model detected a change in frequency, intensity or climatology of extreme weather events in the future. The next two sections describe each dataset used in this study and their purpose. The different datasets used in this study are summarized in Table 3.1.

*Table 3.1: S*ummary of datasets and timescales used in this study.

Datasets for Historic Events	**Time Period**
Environment Canada observations and corrected	1961-1990
CRCM forced with ERA-40	1961-1990
NARR	1961-1990; 2008*
Datasets for Future Projection	
CRCM forced with CGCM Hindcast	1961-1990
CRCM forced with CGCM Future Projection	2041-2070

*This refers to the June 8-9, 2008 precipitation event at Pangnirtung

3.3.1 Datasets used for historic events

To compare the modeled data to the actual recorded occurrences of the extreme events, three datasets were used to compare the modeled output to actual observations. Firstly, the Environment Canada data archive (Environment Canada, 2011) was used for historic surface observations from the four communities. Corrected precipitation data were also obtained from the Iqaluit station (Mékis and Brown, submitted) to provide precipitation amounts. The corrected precipitation data used precipitation adjustments for snow and rain respectively to account for external factors that influence the accuracy of precipitation measurements. The rain adjustments took into account wind, undercatch, evaporation and gauge specific wetting loss and are further explained in Devine and Mékis (2008). The snow adjustment took into account density corrections based upon coincident ruler and Nipher snow gauge measurements and are further explained in Mékis and Hopkinson (2004). Due to incomplete historic datasets at Cape Dorset,

Kimmirut and Pangnirtung, complete corrected precipitation datasets were not available for these three communities.

The other two datasets were model based and were used to evaluate the Canadian Regional Climate Model (CRCM) simulation of historic extreme precipitation and wind events: The North American Regional Re-analysis (NARR) dataset (Mesinger et al., 2006) and the CRCM forced with European Regional Analysis (ERA-40) dataset (DAI Catalogue, 2009).

The NARR dataset was obtained from the National Oceanic and Atmospheric Administration (NOAA) website and runs from January 1948 to present day. The NARR dataset used a very high resolution NCEP Eta Model together with the Regional Data Assimilation system (RDAS), which simulates precipitation among other variables. The model has a 32 km and 45-layer resolution with 3-hourly output. The user customizes the date, the domain, the variable as well as the length of time they wish the variable to be averaged over. For this study, daily composites were chosen to be consistent with the other datasets.

The CRCM forced with ERA-40 dataset was run from 1961-2002 however only the years 1961-1990 were used for this study. The CRCM forced with ERA-40 re-analysis dataset is based on actual global weather observations as opposed to being forced with another model and in theory should have a more accurate depiction of the atmosphere during historic events. The model has a 45 km and 29-layer resolution with a 6-hourly output. Scripts were created to customize the domain as well as the daily averages.

Both the NARR and the CRCM forced with ERA-40 datasets are examples of Re-analysis datasets. A re-analysis reprocesses historic observational data that spans an extended period of time using a consistent analysis scheme aiming at producing a dataset that can be used for meteorological and climatological studies. The output from the re-analysis provides a 'best-fit' analysis of the model data and the available historical observational data, which also takes into account model and historic observational data errors.

3.3.2 Datasets used for future projection events

Two datasets were used for a comparison between the historic CRCM and future projection CRCM output. These two datasets used the CRCM forced with the Global Climate Model (CGCM) for two different time periods and were directly compared to assess differences in climatology, frequency and intensity of extreme events (DAI Catalogue, 2009). The hindcast CRCM dataset was run from 1961-1990 and the future projection dataset was run from 2041-2070.

Both of these datasets used the CGCM3 Global Climate Model version to force the CRCM data and is an example of modeled data being forced with another modeled dataset. The historic CRCM forced with CGCM dataset is an example of a hindcast. A hindcast is an integration of a numerical weather model where no historical observations have been assimilated. Climate forcings are entered into a climate model to test whether known events have been replicated or shown in the model output. More information regarding the parameterization schemes used in this version of the CGCM is available on the DAI website and references (DAI CGCM3 Predictors, 2008). Both the CRCM forced

with CGCM datasets had a 45 km and 29-layer resolution. The future projection scenario followed the Intergovernmental Panel on Climate Change (IPCC) SRES A2 version of Greenhouse Gas evolution (DAI CGCM3 Predictors, 2008).

Since the hindcast CRCM and the projection CRCM data were run using the same forcing schemes, a direct comparison between these two datasets could reveal future trends in extreme precipitation and wind events, and any model bias should be apparent in both the hindcast as well as the future projection analysis results.

3.3.3 Dataset variables and domain

All three of the datasets that used CRCM data were acquired through the Data Access Integration (DAI) website (DAI Portal, 2010). This website allows users to customize the domain they wish to acquire. Five variables were collected for each of the CRCM datasets; mean sea level pressure, 500 mb geopotential heights, mean amplitude of sustained wind at 10 m, vector wind at 850 mb as well as total precipitation rate. The data were in 6-hour blocks, and values were averaged over 24-hour periods. More information about the model physics and the datasets acquired is available on the DAI website (DAI Portal, 2010).

A larger domain for the mean sea level pressure, 850 mb wind and the 500 mb geopotential height variables (Figure 3.1) was obtained to get a large scale view of the atmosphere during the extreme events. With this larger domain, the synoptic patterns during the events were more apparent.

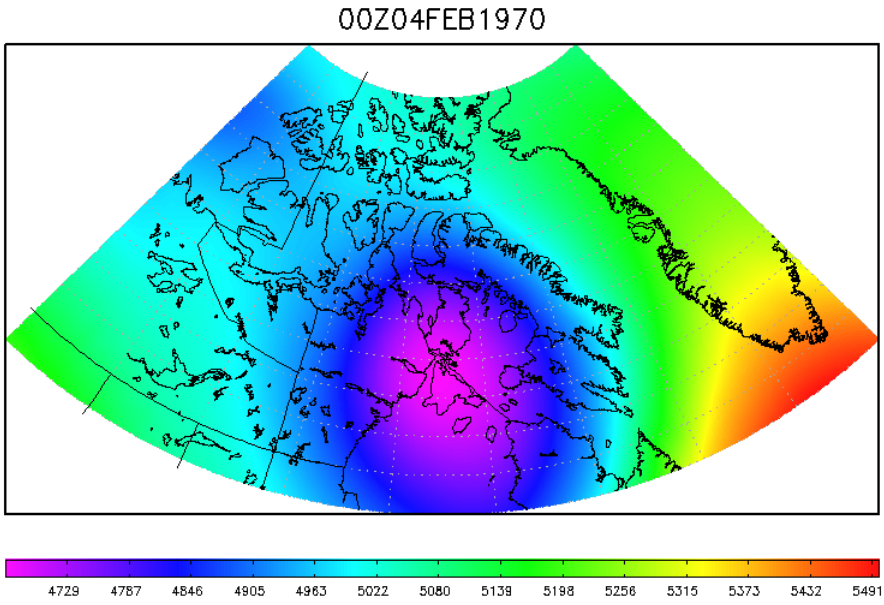

Figure 3.1: Sample grid box showing the domain chosen to depict the synoptic pattern during extreme events. This example shows 500 mb geopotential heights (m).

The area ranging from 61ºW to 68º W, and 60º N to 80ºN was chosen to depict daily precipitation amounts as well as the 10 m winds (Figure 3.2). The area encompassed 615 grid cells. Within this domain the four grid cells that surround each of the communities were chosen to represent that respective community. The average of these four grid cells was used as the representative value for daily precipitation amounts and daily sustained wind speeds for that site. The maximum precipitation amounts for each site were represented by the one grid cell surrounding the community that yielded the maximum daily accumulated precipitation.

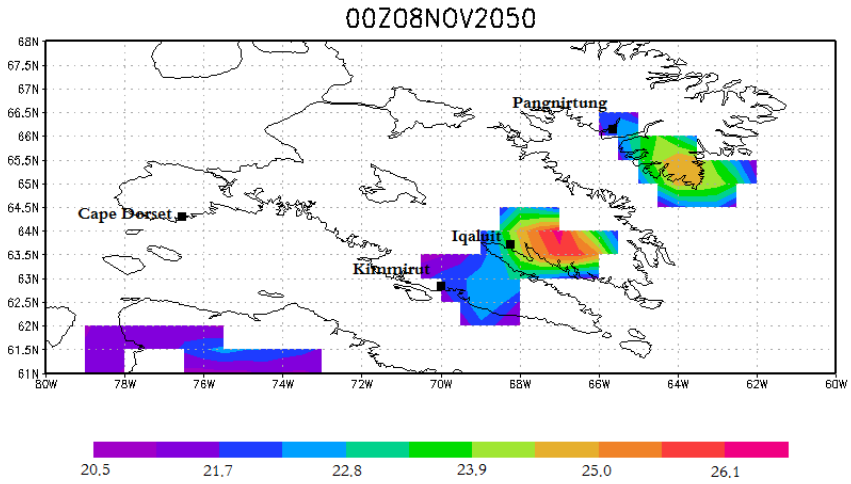

Figure 3.2: Sample grid box showing the domain chosen to represent Southern Baffin Island. This example shows the sustained surface wind speeds (m/s). The communities used in this study are identified.

3.4 Methods

The first step for detecting extreme precipitation and wind events was to analyze actual observations and pick out events that qualified as extreme events according to the definition. Once a date for the extreme event was selected, algorithms to plot out the mean sea level pressure, 850 mb winds and 500 mb geopotential heights were generated.

Secondly, the development of an algorithm that would detect only the most extreme precipitation and wind cases from the CRCM datasets was essential to assess the model performance during these events.

Precipitation amounts were calculated using the four grid cells surrounding each community. Initially, daily precipitation accumulations that exceeded two standard deviations above the mean, or precipitation accumulations above the 97th percentile were the criteria set in the scripts to be considered an 'extreme' amount of precipitation. Upon analysis of the data, too many anomalous days were detected with over 350 grid cells over the 30-year period being anomalous. Therefore, a decision to make the criteria for an extreme precipitation event more stringent was made. The script was altered to detect precipitation amounts that exceeded three standard deviations above the mean (above the 99th percentile). This new set of criteria yielded more reasonable results. The threshold values as detected by the precipitation algorithms were defined as events exceeding 5-7 mm/day (5-7 cm/day snow equivalent) depending on the community. The maximum precipitation event for each site was calculated using the grid cell that yielded the maximum precipitation amount out of the four grid cells that surrounded each community.

According to Environment Canada (2011), the thresholds for a rainfall-warning event at Iqaluit, Kimmirut, Cape Dorset and Pangnirtung are 50 mm in a 24-hour period, 75 mm in a 48-hour period, or an extenuating circumstance that causes flash flooding. The criteria for a snowfall-warning event are 10 cm or more in a 12-hour period. The precipitation algorithms used for this study yielded smaller values of daily precipitation than the Environment Canada threshold values. This means that the algorithms used in this study detected more extreme events as opposed to the Environment Canada thresholds. The algorithm values detected for each of the four communities were considerably low compared to the Environment Canada thresholds. These lower

threshold values were yielded by the algorithms because they took into account all non-precipitation event days, meaning days with trace or no recorded precipitation were included. Therefore, the means as well as the standard deviations were lowered because of the inclusion of the non-precipitation days in the algorithm output.

The wind thresholds defining an extreme event for this study were based on Environment Canada's current thresholds for a wind warning events. The current Environment Canada thresholds for wind warnings at Iqaluit, Kimmirut, Cape Dorset and Pangnirtung are sustained winds of 70 km/h (19.4 m/s) or more and wind gusts of 90 km/h (25.0 m/s) or greater. An algorithm was developed to detect sustained wind speeds of 60, 70 and 80 km/h (16.7, 19.4 and 22.2 m/s) or more within the CRCM data as the criterion for extreme wind events to show the distributions of high wind events over the study periods.

The Environment Canada warning criteria for a blizzard is when winds of 40 km/h (11.1 m/s) or greater are expected to cause widespread reductions in visibility to 400 m or less due to blowing snow, or blowing snow in combination with falling snow for at least 6 h.

When choosing case studies to analyze in detail, several factors were considered. These were the precipitation warning criteria, wind warning criteria, blizzard warning criteria as well as special circumstances where the site was particularly susceptible to the event.

CHAPTER 4: HISTORIC CASE STUDIES

4.1 Overview

Many extreme precipitation and wind events have occurred over southern Baffin Island during the study period. Four examples of these types of events are analyzed in this section (Table 4.1). These case studies were associated with conditions that met the definition of an extreme precipitation event, the Environment Canada warning criteria thresholds used in this study and by the societal impacts these events had on the northern communities. The top wind and the top precipitation event at Iqaluit from the study period were chosen to analyze in detail. Also, an extreme wind and precipitation event at Iqaluit that was identified in Gascon et al. (2010) and Nadeau (2007) was chosen. Finally, an extreme precipitation event from Pangnirtung that had a devastating impact on the community was chosen as the fourth case study.

Table 4.1: Historic case studies.

Event Date	Location	Type
April 5, 1962	Iqaluit	Wind
July 14, 1968	Iqaluit	Precipitation
December 4, 1982	Iqaluit	Precipitation and Wind
June 8-9, 2008	Pangnirtung	Precipitation

4.2 April 5, 1962 Blizzard at Iqaluit

On April 5, 1962 Iqaluit experienced one of its strongest wind events of the study period. Actual Environment Canada observations showed a sustained wind speed of 116

km/h (32.2 m/s) and gusts up to 153 km/h (42.5 m/s) at the event's peak. With 12 hours of near zero visibilities in blowing snow and warning level sustained wind speeds, this event was considered a blizzard according to Environment Canada's blizzard criterion.

Table 4.2: Environment Canada hourly observations at Iqaluit April 5, 1962. C refers to clear, MC refers to mainly clear and BS refers to blowing snow.

Condition Time (UTC)	Visibility (km)	Wind Direction (°)	Wind Speed (km/h)	Air Temperature	Weather Condition
1962/04/05/04:00:00	16.1	50	42	-25	MC
1962/04/05/05:00:00	16.1	50	42	-23.9	C
1962/04/05/06:00:00	8	50	53	-23.9	BS
1962/04/05/07:00:00	6.4	50	51	-24.4	BS
1962/04/05/08:00:00	6.4	320	63	-25.6	BS
1962/04/05/09:00:00	0.2	320	72	-28.3	BS
1962/04/05/10:00:00	0.2	320	84	-29.4	BS
1962/04/05/11:00:00	0	320	90	-29.4	BS
1962/04/05/12:00:00	0	320	77	-28.9	BS
1962/04/05/13:00:00	0	320	84	-27.8	BS
1962/04/05/14:00:00	0	320	95	-27.8	BS
1962/04/05/15:00:00	0	320	116	-26.1	BS
1962/04/05/16:00:00	0	320	109	-25	BS
1962/04/05/17:00:00	0	320	108	-23.9	BS
1962/04/05/18:00:00	0	320	105	-23.3	BS
1962/04/05/19:00:00	0	320	89	-22.8	BS
1962/04/05/20:00:00	0	320	79	-22.2	BS
1962/04/05/21:00:00	0	320	72	-22.2	BS
1962/04/05/22:00:00	0.8	320	63	-21.7	BS
1962/04/05/23:00:00	12.9	320	51	-21.7	MC
1962/04/06/00:00:00	12.9	320	37	-22.8	MC
1962/04/06/01:00:00	19.3	320	29	-22.2	MC
1962/04/06/02:00:00	24.1	320	21	-21.7	C
1962/04/06/03:00:00	24.1	320	27	-22.8	MC

4.2.1 NARR re-analysis of April 5, 1962

The NARR surface re-analysis showed a 995 mb low situated over Davis Strait, between southern Baffin Island and the southern tip of Greenland (Figure 4.1). Conceptually, the re-analysis data showed that Iqaluit was on the 'back side' of the low pressure system, meaning the community would be under the influence of cold, northwesterly winds. This matches well with the observed Environment Canada data, which showed the winds changing from a northeasterly direction at 50° to northwesterly direction at 320° as the low passed over Iqaluit. A ridge of high pressure was located over the Kivalliq region of Nunavut and extending southeastward into northern Manitoba and northern Ontario.

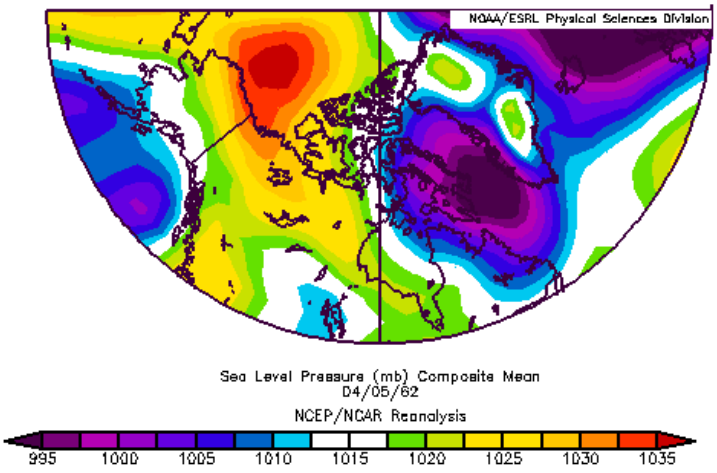

Figure 4.1: Composite mean sea level pressure (mb) from 00 UTC April 5, 1962 to 00 UTC April 6, 1962.

The 500 mb geopotential height chart showed a 4900 m upper low located right over southern Baffin Island, with the low center almost directly over Iqaluit (Figure 4.2). A weak ridge is apparent east of Davis Strait and extending into southern Greenland.

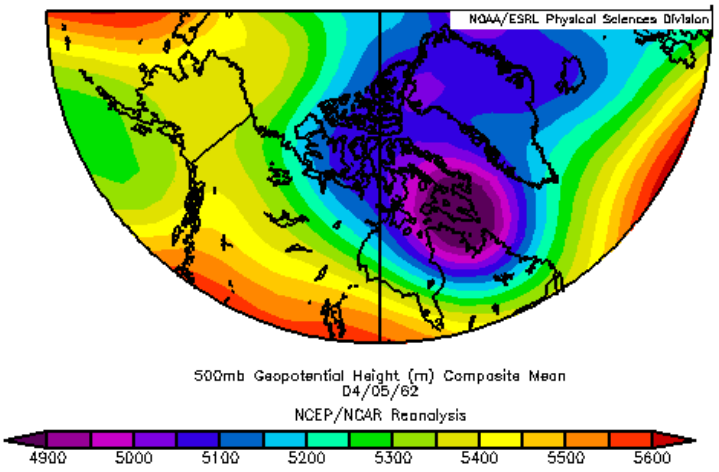

Figure 4.2: Composite mean 500 mb geopotential height (m) from 00 UTC April 5, 1962 to 00 UTC April 6, 1962.

The 1000-500 mb thickness chart showed the coldest air right over southern Baffin Island (Figure 4.3), in approximately the same location as the 500 mb low (Figure 4.2). This is indicative that the low has become a 'cold low', or a mature system with no strong advection apparent in the southern Baffin Island area. Figure 4.3 also shows a weak ridge of warm air over the same location as the 500 mb ridge extending into southern Greenland.

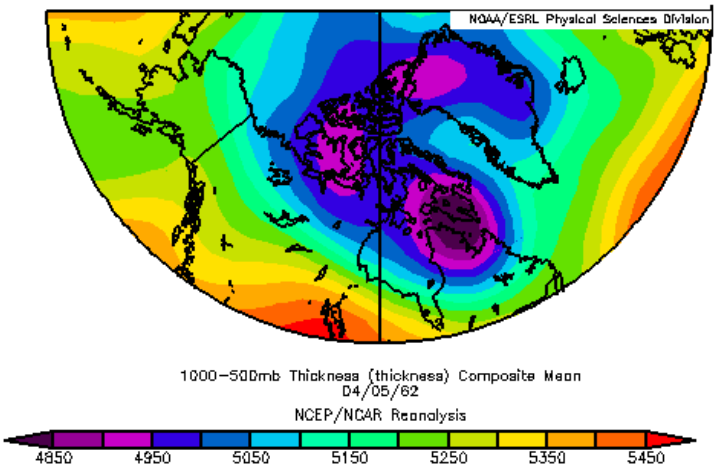

Figure 4.3: Composite mean 1000-500 mb thickness (m) from 00 UTC April 5, 1962 to 00 UTC April 6, 1962.

The 1000 mb wind fields showed a northwesterly jet maximum over the Kivalliq region of Nunavut, with wind speeds up to 12 m/s in its core (Figure 4.4). A secondary jet maximum of 12 m/s is apparent just south of Baffin Island with a westerly flow. Conceptually, the westerly jet south of Baffin Island could have been the jet affecting the Iqaluit area that day. However, the model has this jet slightly south of Iqaluit over Ungava Bay with values of approximately 7 m/s over Iqaluit itself. This could either indicate that the model has not resolved a small-scale feature producing locally higher winds at Iqaluit or that the model has the jet displaced too far south.

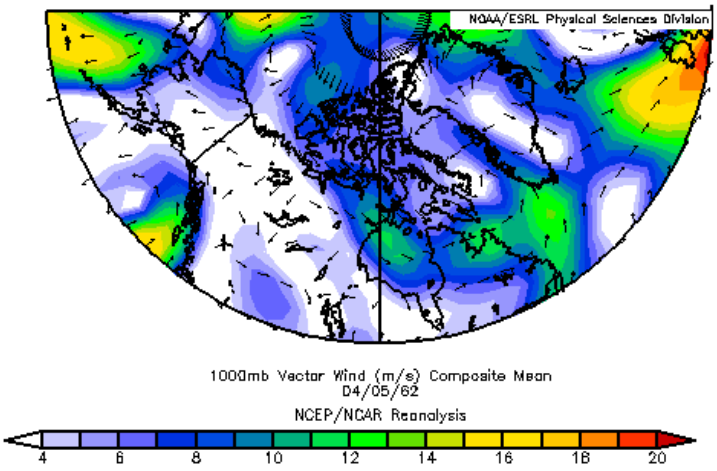

Figure 4.4: Composite mean 1000 mb vector wind speed (m/s) from 00 UTC April 5, 1962 to 00 UTC April 6, 1962.

The 850 mb wind chart showed a more prominent jet maximum over northern Quebec just south of Ungava Bay, with values of 18m/s in its core (Figure 4.5). According to the NARR re-analysis, there is no 850 mb jet core over Iqaluit. Much like the 1000 mb wind re-analysis, the model has either displaced the 850 mb jet south of Iqaluit or it has too coarse of a resolution to pick up on enhanced 850 mb winds at Iqaluit. Light 850 mb winds were analyzed over the Iqaluit area.

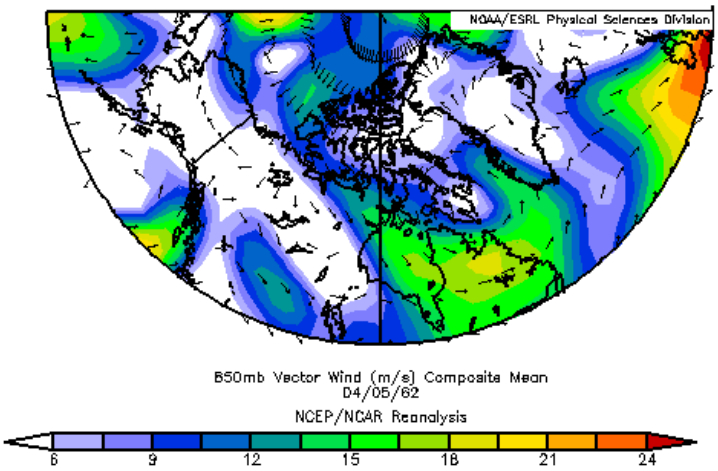

Figure 4.5: Composite mean 850 mb vector wind speed (m/s) from 00 UTC April 5, 1962 to 00 UTC April 6, 1962.

4.2.2 CRCM re-analysis of April 5, 1962

The following section analyzes the CRCM forced with the ERA-40 output of the April 5, 1962 event at Iqaluit.

Figure 4.6 shows the mean sea level pressure for this event. According to the re-analysis, a 995 mb surface low was analyzed over Baffin Bay. Relative to the NARR, the CRCM re-analysis has placed the surface low northwest of the NARR re-analysis had it analyzed but the surface lows were analyzed at similar strengths.

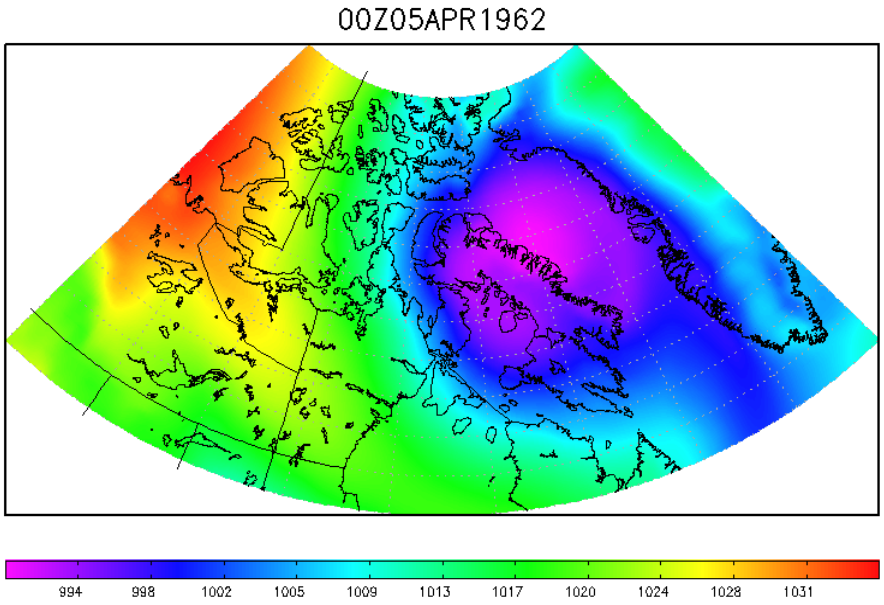

Figure 4.6: Composite mean sea level pressure (mb) from 00 UTC April 5, 1962 to 00 UTC April 6, 1962.

Figure 4.7 shows the 500 mb geopotential height chart for this event. A 4780 m upper low was located over central Baffin Island with Iqaluit being south of the low centre. In this region, Iqaluit would be in a good position for upper-level forcing, being slightly downstream of the upper low. The CRCM re-analysis has the 500 mb low placed farther north than the NARR re-analysis and has the low approximately 120 m deeper than the NARR re-analysis.

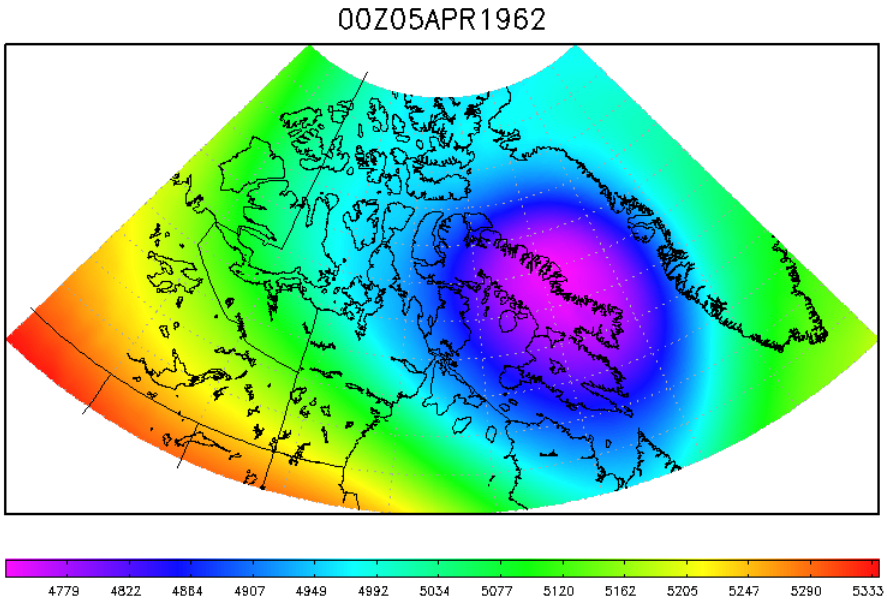

Figure 4.7: Composite mean 500 mb geopotential height (m) from 00 UTC April 5, 1962 to 00 UTC April 6, 1962.

The 850 mb wind charts show a jet maximum over the Kivalliq region of Nunavut, with a jet core of approximately 18-20 m/s (Figure 4.8). Wind speeds of approximately 10 m/s were inferred over Iqaluit itself. Like the NARR re-analysis, this could be indicative that the model has not resolved a small-scale feature over Iqaluit or that the jet was displaced too far west. The strength of the 850 mb jet west of Iqaluit is similar to the NARR re-analysis, although the CRCM has the jet a bit farther north than the NARR re-analysis.

A CRCM surface wind chart from April 5, 1962 was omitted from this thesis as there were no sustained surface wind speeds over 60 km/h detected by the CRCM re-analysis over southern Baffin Island for this event.

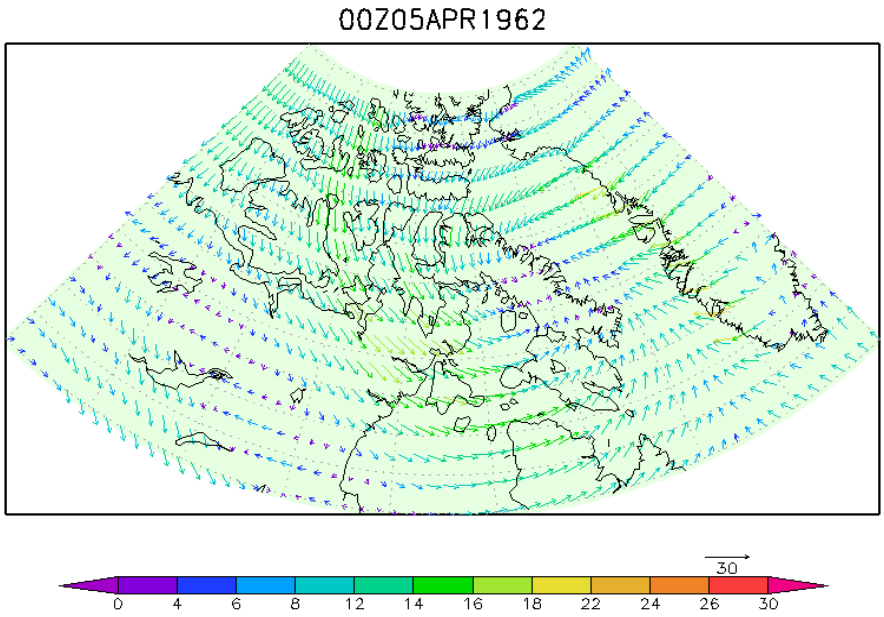

Figure 4.8: Composite mean 850 vector wind speed (m/s) from 00 UTC April 5, 1962 to 00 UTC April 6, 1962.

The CRCM precipitation 4-panel chart showed a region of precipitation over southern Baffin Island for this event, with insignificant (less than 1 mm) amounts for the day (Figure 4.9b). Over Iqaluit, the re-analysis detected 0.5 mm of precipitation for this event. As this was primarily a wind event, no significant precipitation amounts were expected in the model output. No anomalous precipitation amounts were detected over southern Baffin Island by the model for this event (Figure 4.9d).

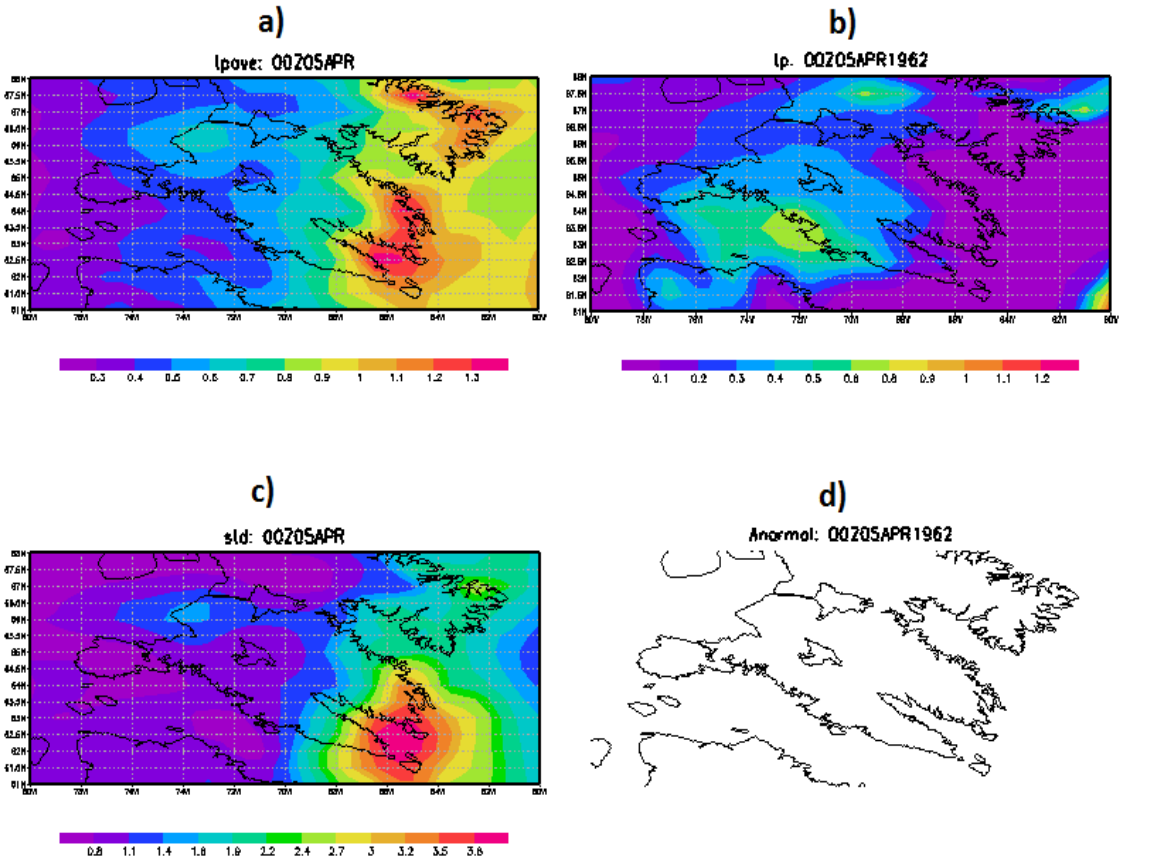

Figure 4.9: Daily values for CRCM precipitation (mm/day) data forced with ERA-40 data output. (a) shows the composite average daily precipitation amount from 00 UTC April 5 to 00 UTC April 6 for the 30-year period. (b) shows the precipitation amount from 00 UTC April 5, 1962 to 00 UTC April 6, 1962 specifically. (c) shows the standard deviation of the daily precipitation from 00 UTC April 5 to 00 UTC April 6 for the 30-year period. (d) shows precipitation amounts 3 standard deviations above (a) from 00 UTC April 5, 1962 to 00 UTC April 6, 1962 specifically.

4.2.3 April 5, 1962 Summary

Overall, the NARR re-analysis and the CRCM re-analysis of the Iqaluit blizzard showed similarities and differences. Both models detected a surface low in the vicinity of Iqaluit with identical strength, although their placement differed. The NARR re-analysis placed the surface low over Davis Strait whereas the CRCM re-analysis placed the low over Baffin Bay. Both models detected an upper low over southern Baffin Island, although the strength of the low was different slightly for each model run. The NARR had the 500 mb low analyzed at 4900 m whereas the CRCM was deeper at 4780 m. Both of the re-analyses detected an 850 mb jet over the Kivalliq region of Nunavut with a secondary jet just south of Baffin Island. In this case, the re-analyses may not have displaced the 850 mb jet; the resolution of the models may not have been sufficient to detect a small scale wind event at Iqaluit. The surface winds for both of the re-analyses did a poor job at representing the Iqaluit winds, with 8 m/s winds detected over Iqaluit according to the NARR re-analysis and sustained surface of less than 60 km/h detected in the CRCM re-analysis.

4.3 July 14, 1968 Top Precipitation Event at Iqaluit

On July 14, 1968 Iqaluit experienced its most extreme precipitation event of the study period. Corrected precipitation data (Mékis and Brown, submitted) showed 55.1 mm of rain fell within 14 h. Climatologically, Iqaluit typically experiences 59.2 mm of rain in the month of July. This event produced over 90% of the monthly precipitation at Iqaluit in just 14 hours.

Table 4.3: Hourly Environment Canada Observations at Iqaluit July 14 and 15, 1968. CL refers to cloudy, MC refers to mostly cloudy, R refers to rain, MR refers to moderate rain and F refers to fog.

Condition Time (UTC)	Visibility (km)	Wind Direction (°)	Wind Speed (km/h)	Air Temperature (°C)	Weather Condition
1968/07/14/10:00:00	24.1	140	23	6.7	MC
1968/07/14/11:00:00	24.1	140	19	6.7	MC
1968/07/14/12:00:00	24.1	140	24	6.7	CL
1968/07/14/13:00:00	24.1	140	24	7.8	MC
1968/07/14/14:00:00	19.3	140	27	6.7	R
1968/07/14/15:00:00	12.9	140	26	6.7	R
1968/07/14/16:00:00	11.3	140	24	6.7	R
1968/07/14/17:00:00	11.3	140	27	5.6	R
1968/07/14/18:00:00	9.7	140	27	5.6	R, F
1968/07/14/19:00:00	9.7	140	26	5.6	R, F
1968/07/14/20:00:00	9.7	140	27	5.6	R, F
1968/07/14/21:00:00	4	140	21	5.6	R, F
1968/07/14/22:00:00	8	140	39	5	R, F
1968/07/14/23:00:00	8	160	40	5	MR, F
1968/07/15/00:00:00	8	140	37	4.4	MR, F
1968/07/15/01:00:00	8	140	35	4.4	R, F
1968/07/15/02:00:00	8	140	29	4.4	R, F
1968/07/15/03:00:00	11.3	140	32	4.4	R
1968/07/15/04:00:00	11.3	140	35	4.4	R
1968/07/15/05:00:00	12.9	140	21	6.1	CL
1968/07/15/06:00:00	16.1	140	18	7.8	CL
1968/07/15/07:00:00	24.1	160	18	6.7	MC
1968/07/15/08:00:00	24.1	160	11	8.9	MC
1968/07/15/09:00:00	24.1	160	21	7.8	MC
1968/07/15/10:00:00	24.1	140	6	7.2	MC

4.3.1 NARR re-analysis of July 14, 1968

Mean sea level pressure charts for the NARR re-analysis showed a large 995 mb surface low just west of Hudson Bay, over northern Manitoba and the Kivalliq region of Nunavut (Figure 4.10). A surface trough was extending northeastward from this low

across Hudson Bay and into Foxe Basin with Iqaluit being impacted by the eastern edge of this trough.

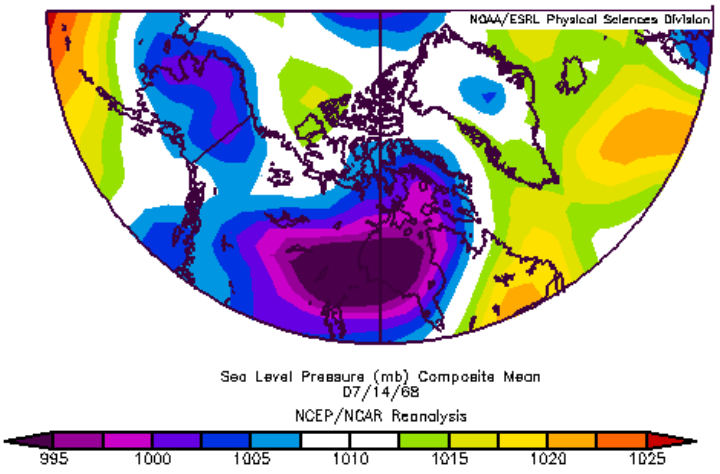

Figure 4.10: Composite mean sea level pressure (mb) from 00 UTC July 14, 1968 to 00 UTC July 15, 1968.

The 500 mb geopotential height chart showed a 5400 m upper low located right over Foxe Basin (Figure 4.11). With the positioning of this upper low, the storm would have had upper level support at 500 mb. The 500 mb low was analyzed to the northwest of Iqaluit, making Iqaluit in a prime area for enhanced lift.

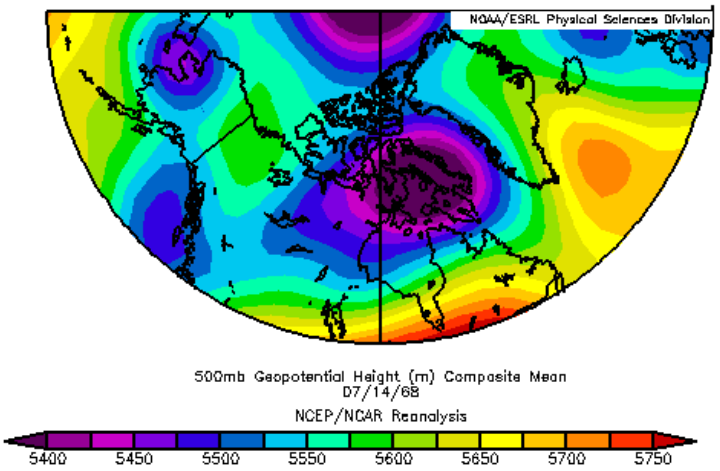

Figure 4.11: Composite mean 500 mb geopotential height (m) from 00 UTC July 14 1968 to 00 UTC July 15, 1968.

The 1000-500 mb thickness chart showed the coldest air right over Baffin Island with a trough of colder air that extended southward over the northeastern shore of Quebec (Figure 4.12). A ridge of warmer air was located over the eastern shore of Greenland as well as over Ontario. The main baroclinic zone was located over Hudson Bay and extending into extreme southern Baffin Island. This baroclinic zone would provide ample potential energy to this system.

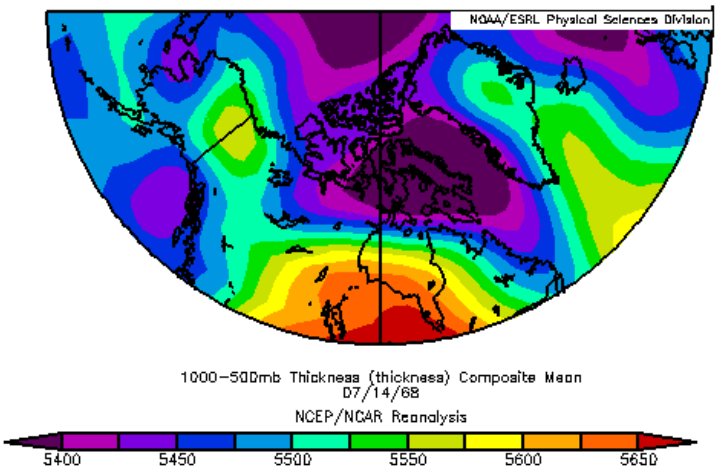

Figure 4.12: Composite mean 1000-500 mb thickness (m) from 00 UTC July 14, 1968 to 00 UTC July 15, 1968.

Surface winds showed cyclonic rotation over Foxe Basin with a southwesterly flow at Iqaluit with a weak jet maximum of 9 m/s (Figure 4.13). A stronger jet maximum of 14 m/s was detected over northern Manitoba and also the southeastern portion of Hudson Bay, and was being advected into the Iqaluit area.

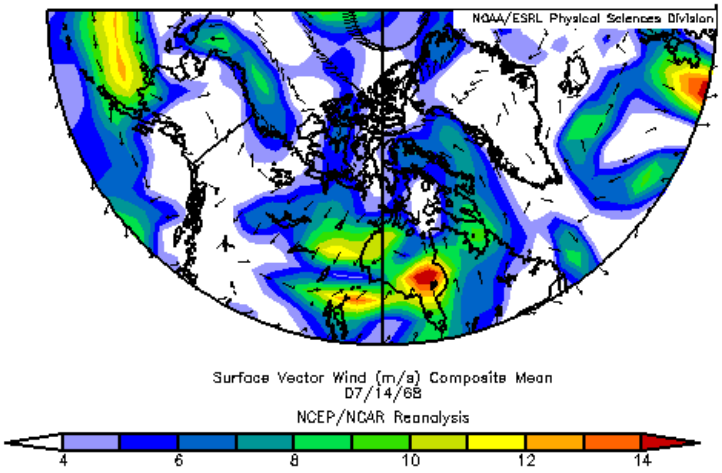

Figure 4.13: Composite mean surface vector wind (m/s) from 00 UTC July 14, 1968 to 00 UTC July 15, 1968.

The 850 mb wind chart showed the strongest jet maximum located over northern Ontario at 20 m/s (Figure 4.14). The left-exit region of this jet maximum was extending into southern Baffin Island. Wind speeds up to 12 m/s were detected over the Iqaluit area. The left exit region denotes an area of greater lift, which would again help support the system with more dynamic energy. Although the main jet core was analyzed over northern Ontario, enhanced 850 mb winds were analyzed over Iqaluit. The model may not have been able to pick up on a localized event such as channeled winds at Iqaluit because of the coarse model resolution.

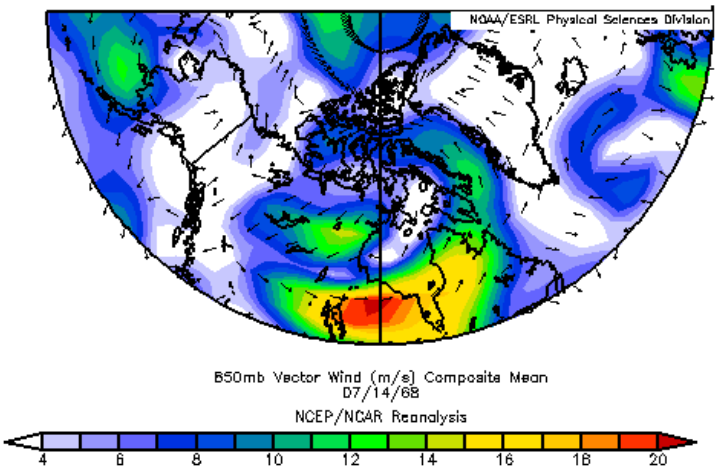

Figure 4.14: Composite mean 850 mb vector wind speed (m/s) from 00 UTC July 14, 1968 to 00 UTC July 15, 1968.

Approximately 20 mm of precipitable water was analyzed over Iqaluit (Figure 4.15). Higher values of approximately 35 mm located over Hudson Bay were being advected by the 850 mb jet into the Iqaluit area. The precipitable water anomaly chart showed a similar pattern with highly anomalous values of 15 mm detected over Hudson Bay (Figure 4.16). Although there were no anomalous precipitable water values analyzed over Iqaluit on this date, the atmospheric pattern suggests that these values were being advected into the Iqaluit by the southwesterly flow over Hudson Bay.

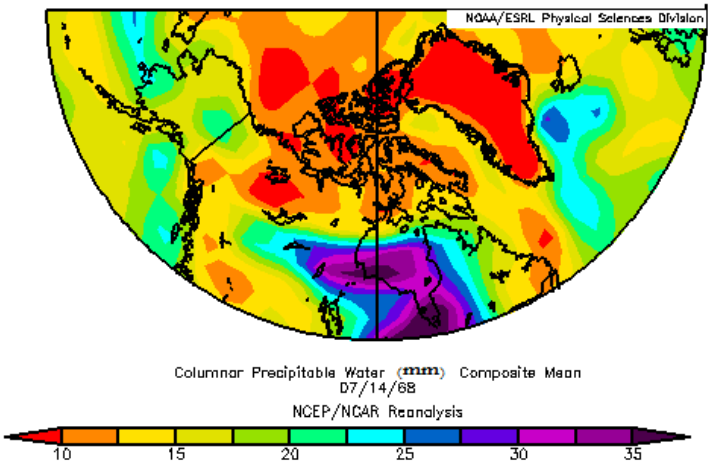

Figure 4.15: Composite mean columnar precipitable water (mm) from 00 UTC July 14, 1968 to 00 UTC July 15, 1968.

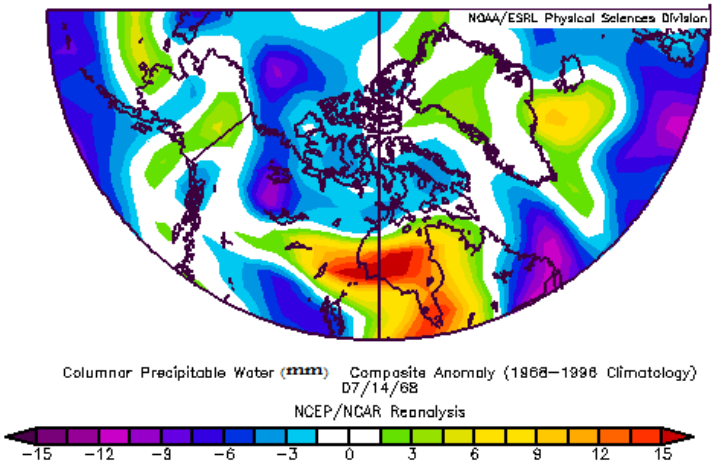

Figure 4.16: Composite mean columnar precipitable water anomaly (mm) from 00 UTC July 14, 1968 to 00 UTC July 15, 1968.

4.3.2 CRCM re-analysis of July 14, 1968

To determine if the CRCM re-analysis data forced with the ERA-40 captured historic events accurately, a comparison of the ERA-40 dataset with the NARR dataset was carried out. This event occurred between July 14, 1968 and July 15, 1968. Because the CRCM re-analysis of this event detected this event partially on July 14, 1968 and partially on July 15, 1968 the charts from both days are included in the analysis of this event.

Figure 4.17 shows the mean sea level pressure for this event on July 14, 1968. A 965 mb surface low was analyzed over Hudson Bay, well southwest of Baffin Island and the Iqaluit area. The NARR re-analysis had the low analyzed farther west over the Kivalliq area, and it wasn't nearly as deep at 993 mb.

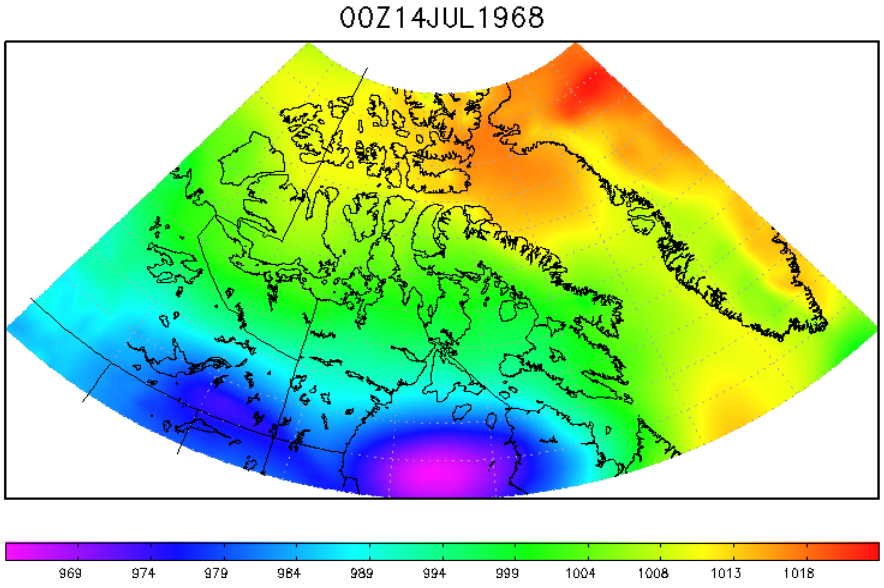

Figure 4.17: Composite mean sea level pressure (mb) 00z July 14, 1968 to 00z July 15, 1968.

Figure 4.18 shows the mean sea level pressure for this event on July 15, 1968. The low was analyzed at 963 mb and had moved from Hudson Bay, across northern Quebec and was analyzed over eastern Hudson Strait. Conceptually, Iqaluit would be under the influence of a southeasterly flow.

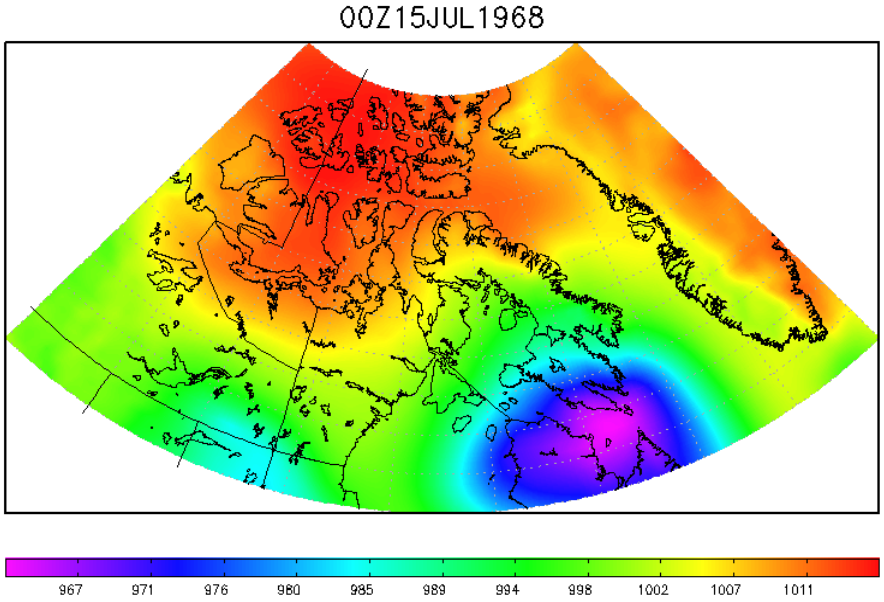

Figure 4.18: Composite mean sea level pressure (mb) 00z July 15, 1968 to 00z July 16, 1968.

Figure 4.19 shows the 500 mb geopotential heights for the event. A 5320 m upper low was located over central Baffin Island. Relative to the upper low, Iqaluit was just south of the low centre. The NARR re-analysis had the 500 mb low analyzed at 5400 m and had it analyzed over Foxe Basin.

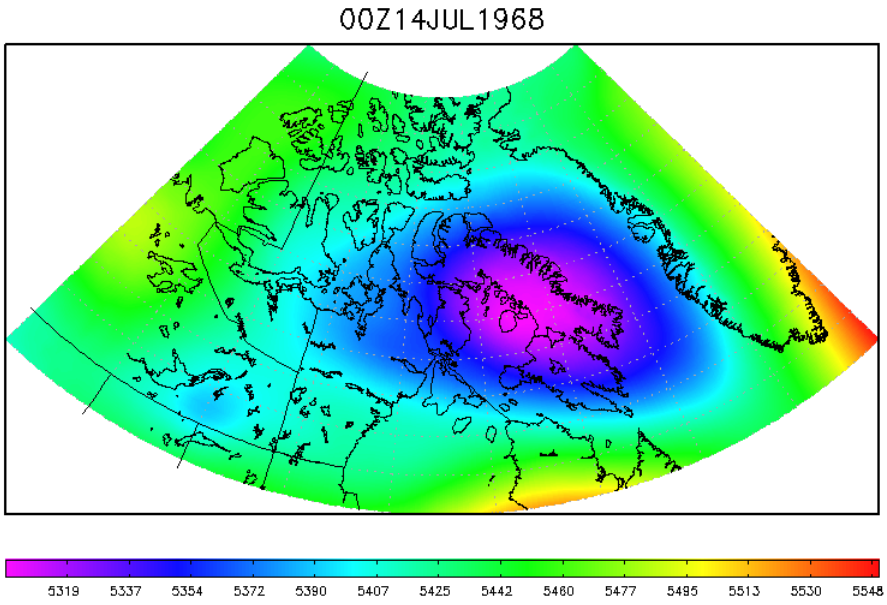

Figure 4.19: Composite mean 500 mb geopotential heights (m) 00z July 14, 1968 to 00z July 15, 1968.

Figure 4.20 showed the 850 mb winds for July 14, 1968. A 20 m/s jet maximum was located over southern Hudson Bay and northern Quebec on this date, however light and variable winds were detected in the Iqaluit area. Relative to the NARR re-analysis, the jet was more progressive with the CRCM re-analysis but was similar in strength.

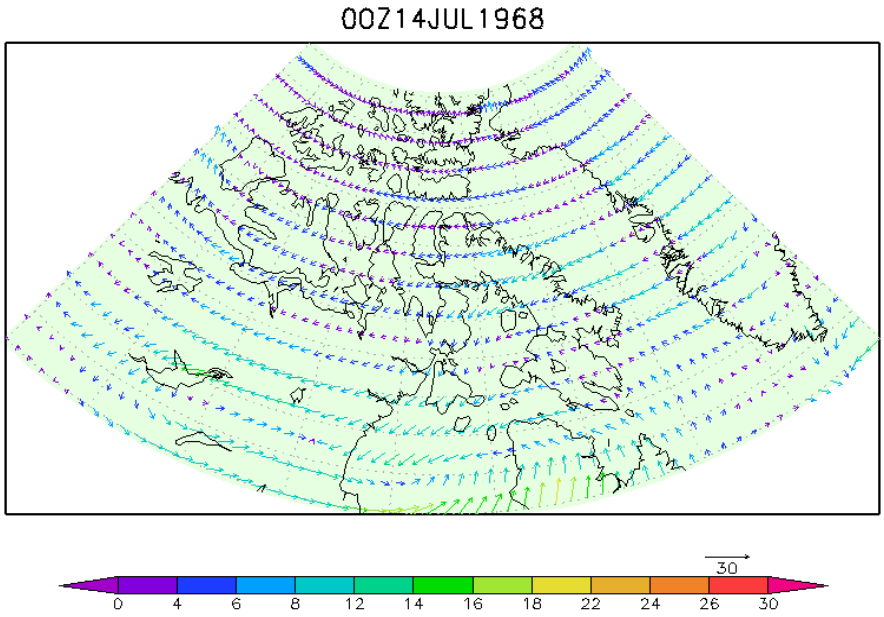

Figure 4.20: Composite mean 850 mb vector wind speed (m/s) from 00 UTC July 14, 1968 to 00 UTC July 15, 1968.

On July 15, 1968 the 850 mb wind chart (Figure 4.21) detected that the jet maximum had moved into the Iqaluit area with an easterly 24 m/s jet maximum located over Iqaluit.

Surface wind output from the CRCM showed no sustained winds over 60 km/h over southern Baffin Island on July 14, 1968 as well as July 15, 1968 therefore the surface wind chart was omitted from this study.

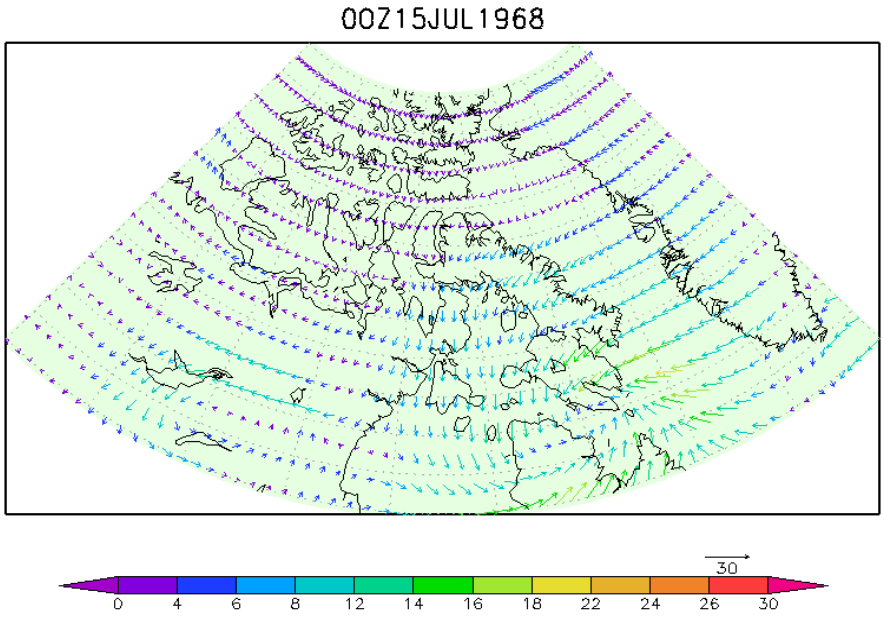

Figure 4.21: Composite mean 850 mb vector wind speed (m/s) from 00 UTC July 15, 1968 to 00 UTC July 16, 1968.

The 4-panel precipitation chart from the CRCM output showed an area of enhanced precipitation just southeast of Iqaluit. Amounts of 49 mm/day were detected over the Davis Strait (Figure 4.22b). The CRCM also detected anomalous precipitation values that were 3 standard deviations above the mean of approximately 17 mm over Davis Straight (Figure 4.22d).

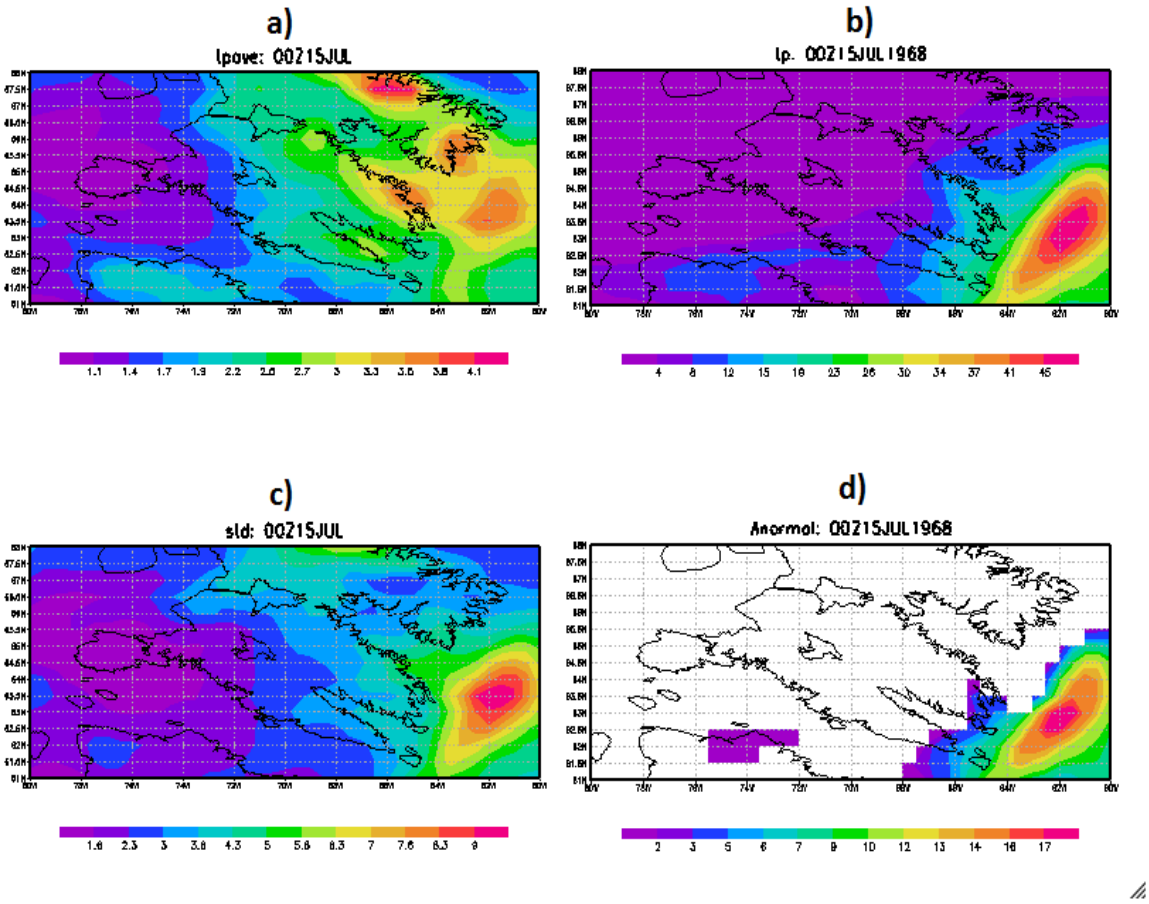

Figure 4.22: Daily values for CRCM precipitation (mm/day) data forced with ERA-40 data output. (a) shows the composite average daily precipitation amount from 00 UTC July 15 to 00 UTC July 16 for the 30-year period. (b) shows the precipitation amount from 00 UTC July 15, 1968 to 00 UTC July 16, 1968 specifically. (c) shows the standard deviation of the daily precipitation from 00 UTC July 15 to 00 UTC July 16 for the 30-year period. (d) shows precipitation amounts 3 standard deviations above (a) from 00 UTC July 15, 1968 to 00 UTC July 16, 1968 specifically.

4.3.3 July 14, 1968 Summary

The July 14, 1968 extreme event at Iqaluit was fairly well detected in the gross sense by both the NARR and the CRCM re-analysis. Both models detected a surface low in the Baffin Island area that was associated with this event. The placement and the strength of the low were very different between both models. The CRCM had the low analyzed at 965 mb whereas the NARR had the low analyzed at 995 mb. This could be an issue of averaging the daily values as part of the re-analysis; since this event occurred over the span of two days, the timing of the even could have an influence on low placement and strength between the NARR and the CRCM. Both models detected a deep upper low over central Baffin Island with similar strengths and similar placement. Also, each model detected a low level 850 mb jet in the vicinity of Iqaluit, although the timing of the jet was slightly displaced in each model run. The precipitable water charts in the NARR re-analysis showed higher raw values and higher anomalous values being advected into the Iqaluit area. The CRCM re-analysis showed an area of enhanced daily precipitation accumulations in the vicinity of Iqaluit although the amount of precipitation compared to the corrected precipitation data was slightly underdone.

4.4 December 4, 1982 Precipitation and Wind Event at Iqaluit

December 4, 1982 met the Environment Canada blizzard criteria for the community of Iqaluit. Actual observations at the Iqaluit airport reported over 5 h of sustained wind speeds greater than 90 km/h (25.0 m/s) with a maximum sustained wind speed of 111 km/h (30.8 m/s) from the northwest. Corrected snowfall accumulations (Mékis and Brown, submitted) were estimated at 11 cm for the day. Visibilities dropped to nearly 0 km for 10 hours, improving marginally the next day. Table 4.4 shows the Environment Canada hourly observations from the Iqaluit airport from 5:00 UTC December 4 to 9:00 UTC on December 5, 1982. The air temperature at Iqaluit dropped substantially as the wind speed increased and as visibilities dropped indicating the passage of a cold front. Snow fell until 7:00 UTC on December 5, indicated under the 'weather condition' column by the S- symbol. As wind speeds increased, the combination of snow and blowing snow (indicated by the BS symbol under 'weather condition') caused the visibilities to drop to 0 km.

Table 4.4: Environment Canada Hourly Observations at Iqaluit December 4, 1982. S- refers to light snow, and BS refers to blowing snow.

Condition Time (UTC)	Visibility (km)	Wind Direction (°)	Wind Speed (km/h)	Air Temperature (°C)	Weather Condition
1982/12/04/05:00	16.1	90	22	-9.9	S-
1982/12/04/06:00	12.9	120	22	-9.3	S-
1982/12/04/07:00	4	110	17	-9.3	S-
1982/12/04/08:00	1.6	90	28	-9.6	S-, BS
1982/12/04/09:00	2.4	100	26	-9.4	S-
1982/12/04/10:00	4.8	130	22	-9	S-
1982/12/04/11:00	1	70	48	-9.9	S-, BS
1982/12/04/12:00	2	120	19	-9.3	S-
1982/12/04/13:00	2	160	19	-9.6	S-
1982/12/04/14:00	2.4	110	15	-9.3	S-
1982/12/04/15:00	1.2	100	20	-9.2	S-, BS
1982/12/04/16:00	1	70	22	-9.5	S-, BS
1982/12/04/17:00	1.2	70	24	-9.4	S-, BS
1982/12/04/18:00	0.8	50	46	-9	S-, BS
1982/12/04/19:00	1	50	44	-9.1	S-, BS
1982/12/04/20:00	2.4	60	37	-8.5	S-, BS
1982/12/04/21:00	0	320	59	-14.2	S-, BS
1982/12/04/22:00	0	320	83	-18.9	S-, BS
1982/12/04/23:00	0	320	100	-21.1	S-, BS
1982/12/05/00:00	0	320	96	-21.8	S-, BS
1982/12/05/01:00	0	320	111	-22.5	S-, BS
1982/12/05/02:00	0	330	104	-23.1	S-, BS
1982/12/05/03:00	0	330	104	-23.1	S-, BS
1982/12/05/04:00	0	330	104	-23.4	S-, BS
1982/12/05/05:00	0	320	100	-23.8	S-, BS
1982/12/05/06:00	0	320	89	-23.8	S-, BS
1982/12/05/07:00	0	330	83	-24.1	BS
1982/12/05/08:00	0.4	320	70	-24.6	BS
1982/12/05/09:00	0.4	310	59	-25.1	BS

4.4.1 NARR re-analysis of December 4, 1982

According to the NARR re-analysis data, a 985 mb surface low-pressure system was situated over Ungava Bay, just south of the study area (Figure 4.23). Iqaluit was under the influence of the northern edge of the low, which conceptually would mean that

an east-southeasterly flow would have been present at Iqaluit. This would correspond to the pre-frontal conditions apparent at Iqaluit before the blizzard had occurred.

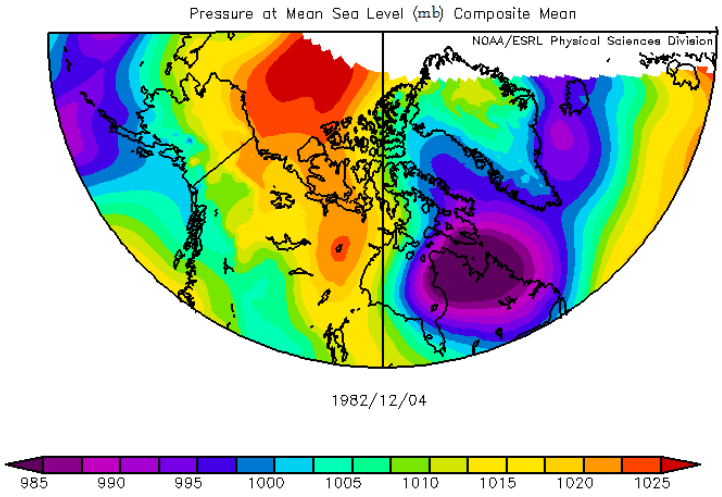

Figure 4.23: Composite mean sea level pressure (mb) from 00 UTC December 4, 1982 to 00 UTC December 5, 1982.

At 500 mb, a 5000 m upper low was situated in the high Arctic between Northern Baffin Island and northwestern Greenland with a trough extending southward from the main low into southern Baffin Island (Figure 4.24). This would provide some upper support for the surface low. A broad 500 mb ridge was located between southern Baffin Island and Southern Greenland, putting Iqaluit in a prime area for upward motion, being on the downstream side of the upper low and the upstream side of the ridge.

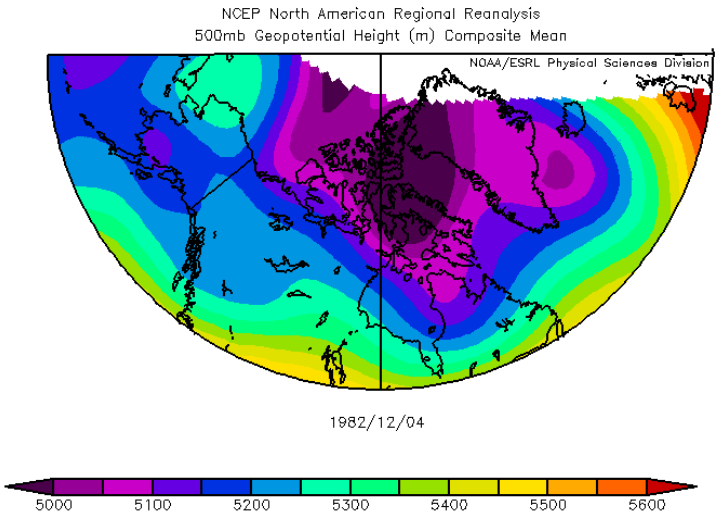

Figure 4.24: Composite mean 500 mb geopotential height (m) from 00 UTC December 4, 1982 to 00 UTC December 5, 1982.

The 1000-500 mb thickness chart (Figure 4.25) showed that the coldest air was situated over northern Baffin Island with a thermal ridge located over Davis Strait, in between southern Baffin Island and the southern tip of Greenland. Upon examining both the 500 mb geopotential heights and the 1000-500 mb thickness charts simultaneously, it is apparent that the model detected that cold air was being advected into southern Baffin Island.

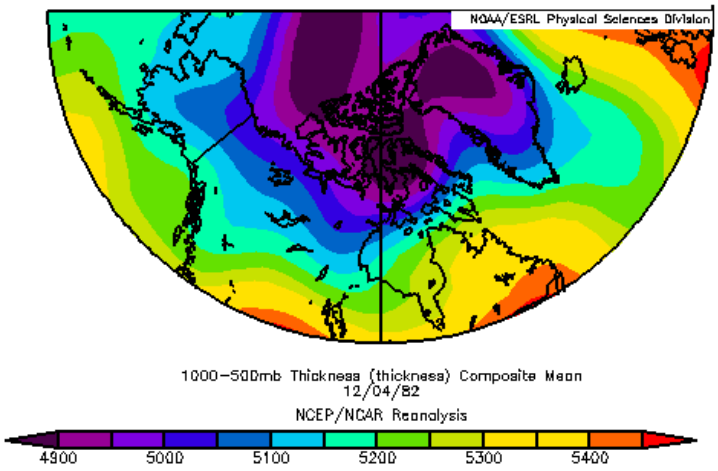

Figure 4.25: Composite mean 1000-500 mb thickness (m) from 00 UTC December 4, 1982 to 00 UTC December 5, 1982.

The 1000 mb wind chart (Figure 4.26) showed a southeasterly flow over Iqaluit parallel to Frobisher Bay with a jet maximum of 10 m/s over Iqaluit. The 850 mb winds were also southeasterly with a jet maximum of approximately 22 m/s right over the Iqaluit area (Figure 4.27). According to the surface observations, the winds shifted from southeast to northwest as the cold front passed over Iqaluit however the 1000 mb and 850 mb wind charts picked up on the southeasterly pre-frontal winds at Iqaluit for this event.

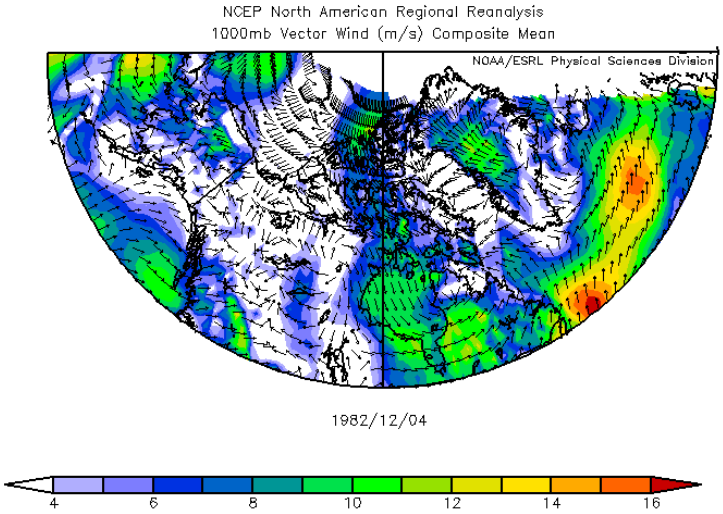

Figure 4.26: Composite mean 1000 mb vector wind speed (m/s) from 00 UTC December 4, 1982 to 00 UTC December 5, 1982.

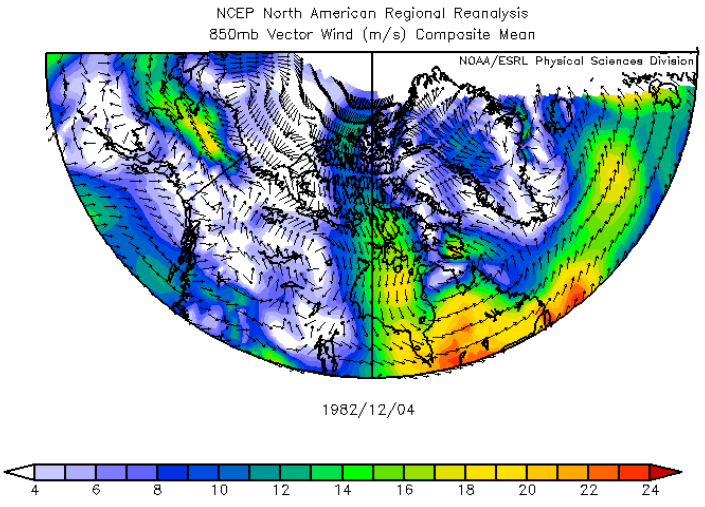

Figure 4.27: Composite mean 850 mb vector wind speed (m/s) from 00 UTC December 4, 1982 to 00 UTC December 5, 1982.

The precipitable water chart (Figure 4.28) showed a moist ridge of higher values extending up from northern Quebec into the southern tip of Baffin Island. Precipitable water values of approximately 7-9 mm over the Iqaluit area were detected. Values of 11-13 mm were detected farther south of the community. With the southeasterly flow, however, the higher precipitable water values were likely being advected into the region.

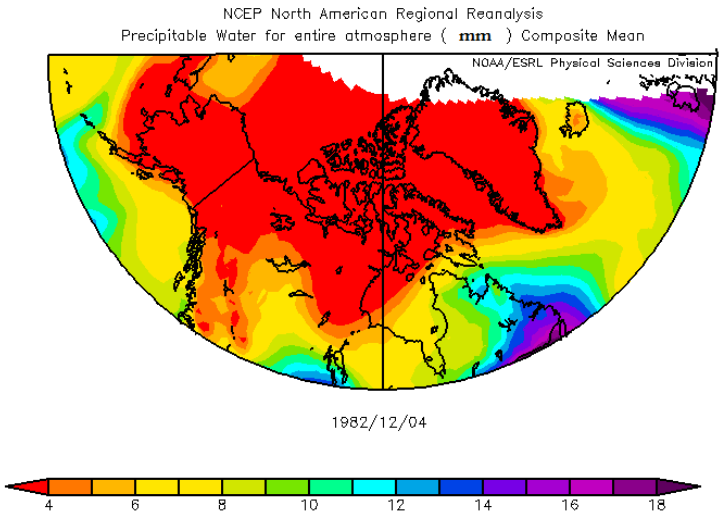

Figure 4.28: Composite mean columnar precipitable water (mm) from 00 UTC December 4, 1982 to 00 UTC December 4, 1982.

The precipitable water anomaly chart showed some of the highest values over Iqaluit, with values of 4-5 mm above normal detected over Iqaluit (Figure 4.29). The values detected over Iqaluit are the northern extent of a ridge of anomalous precipitable water values originating from eastern Quebec. These higher values were likely also being advected into the Iqaluit area with a southeasterly flow.

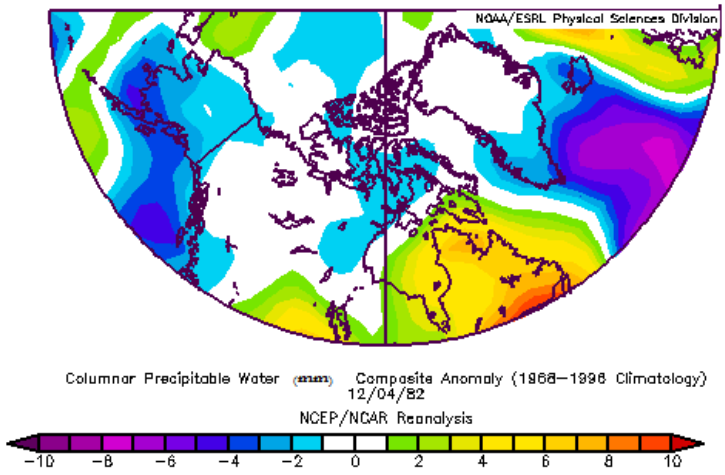

Figure 4.29: Composite mean columnar precipitable water anomaly (mm) from 00 UTC December 4, 1982 to 00 UTC December 5, 1982.

Daily accumulated precipitation values, according to the NARR re-analysis, were approximately 11 mm/day over Iqaluit (Figure 4.30). This translates to values of approximately 11 cm/day snow equivalent over Iqaluit with higher values of approximately 18 mm/day (18 cm/day snow equivalent) northeast of Quebec. These values correspond well with the corrected precipitation data that showed that 11 cm of snow fell at Iqaluit that day.

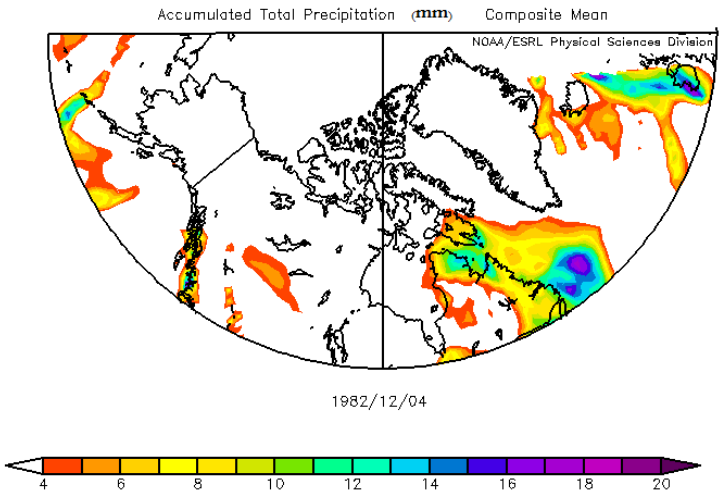

Figure 4.30: Composite mean accumulated total precipitation (mm) from 00 UTC December 4, 1982 to 00 UTC December 5, 1982.

4.4.2 CRCM re-analysis of December 4, 1982

To determine if the CRCM re-analysis data forced with the ERA-40 data captured events accurately, a comparison of the CRCM output with the NARR output was carried out.

Figure 4.31 shows the mean sea level pressure detected by the CRCM output. A surface low pressure system was analyzed over northeastern Quebec with a pressure center of 986 mb detected. A strong ridge of higher pressure was located over the Kivalliq area of Nunavut, providing a large pressure gradient over southern Baffin Island. Compared to the NARR, the low is displaced farther southeast though they are similar in strength.

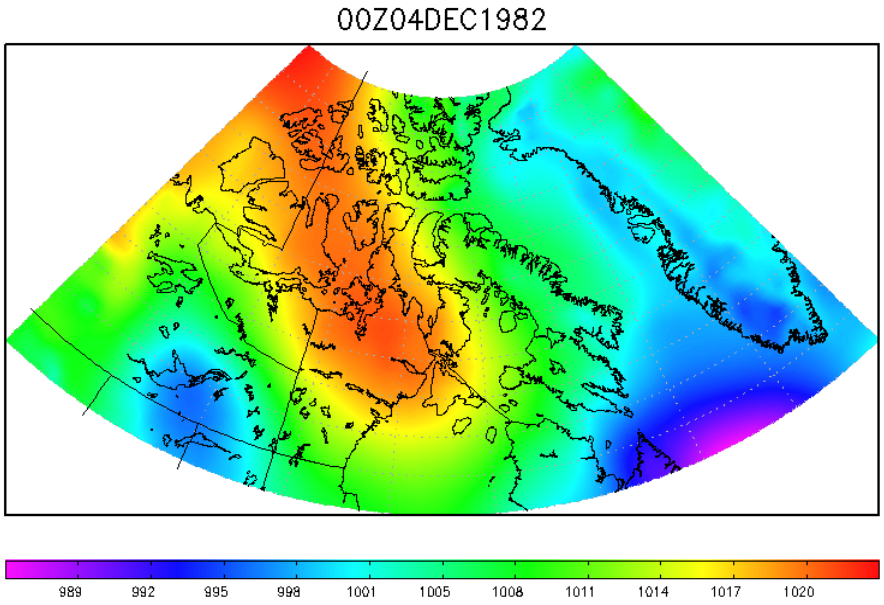

Figure 4.31: Composite mean sea level pressure (mb) from 00 UTC December 4, 1982 to 00 UTC December 5, 1982.

The 500 mb geopotential height chart (Figure 4.32) showed a 4810 m upper low over northeastern Baffin Island with a trough extending southward from the main low into the Iqaluit area. Iqaluit was located in a prime area for upper level lift relative to the low, being downstream of the upper low and upstream of a ridge apparent over southern Greenland. Compared to the NARR re-analysis, the CRCM has the low deeper than the NARR however the trough extending into southern Baffin Island was broader than the NARR re-analysis.

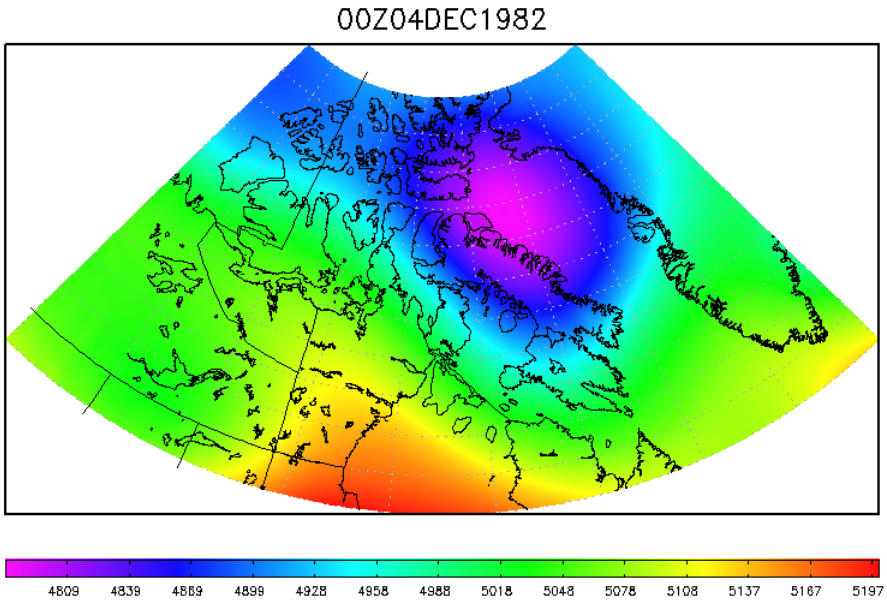

Figure 4.32: Composite mean 500 mb geopotential height (m) from 00 UTC December 4, 1982 to 00 UTC December 5, 1982.

The 850 mb wind chart from the CRCM output (Figures 4.33) showed a 20 m/s northwesterly low level jet over northern Baffin Island that was being advected into the Iqaluit area. Values of 10 m/s were apparent over Iqaluit itself. This matches the direction of the winds observed at Iqaluit after the passage of the cold front. The outflow from the surface ridge combined with the inflow into the surface low could be responsible for these enhanced winds. The NARR re-analysis had a southeasterly 850 mb jet analyzed over Iqaluit with this system, which could signify that the NARR was slower with the progression of this storm.

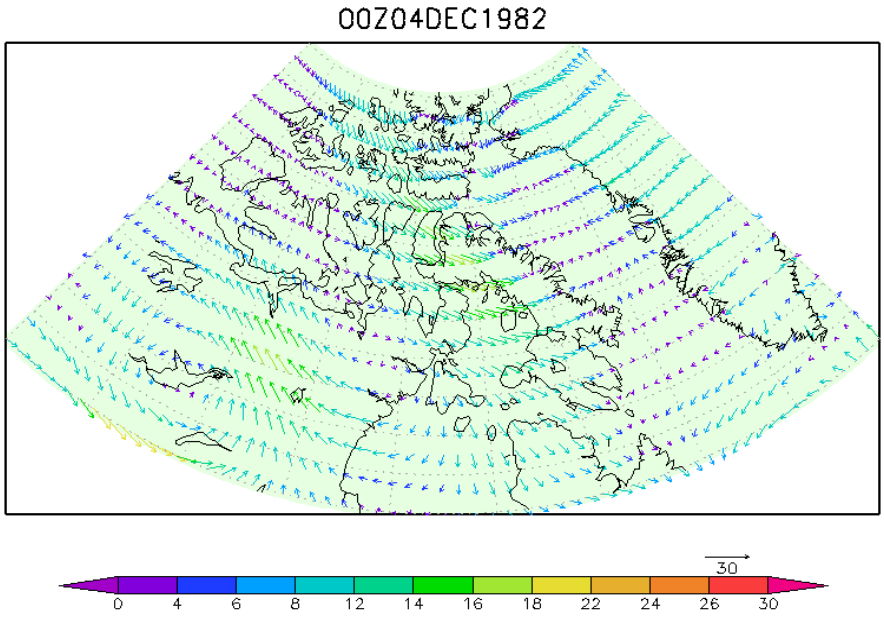

Figure 4.33: Composite mean 850 mb vector wind speed (m/s) from 00 UTC December 4, 1982 to 00 UTC December 5, 1982.

A graph showing the 10 m wind speeds on December 4, 1982 over southern Baffin Island was omitted from the analysis because no values over 60 km/h were detected on that day.

The 4-panel daily precipitation graph showed a maximum daily precipitation value of approximately 4 mm in the vicinity of southern Baffin Island just east of Pangnirtung but only about 2 mm over Iqaluit (Figure 4.34b). No anomalous values were detected over southern Baffin Island for this day using the CRCM forced with ERA-40 forcing scheme (Figure 4.34d). The lack of enhanced precipitation over southern Baffin Island indicates that the CRCM re-analysis under-represented precipitation for this event.

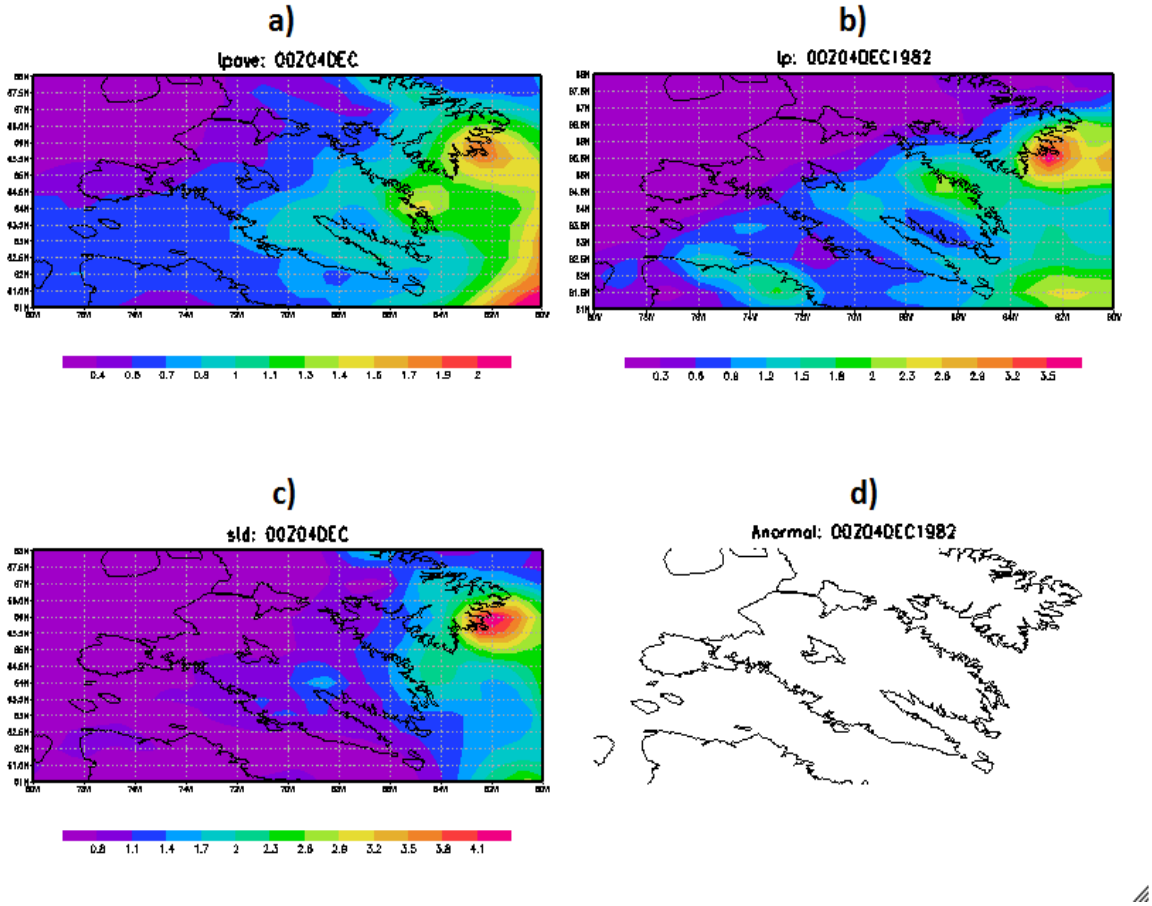

Figure 4.34: Daily values for CRCM precipitation (mm/day) data forced with ERA-40 data output. (a) shows the composite average precipitation amount from 00 UTC December 4 to 00 UTC December 5 for the 30-year period. (b) shows the precipitation amount from 00 UTC December 4, 1982 to 00 UTC December 5, 1982 specifically. (c) shows the standard deviation of the daily precipitation from 00 UTC December 4 to 00 UTC December 5 for the 30-year period. (d) shows precipitation amounts 3 standard deviations above (a) from 00 UTC December 4, 1982 to 00 UTC December 5, 1982 specifically.

4.4.3 December 4, 1982 Summary

The December 4, 1982 event at Iqaluit had mixed results from the model output. The large scale factors, such as the 500 mb low was placed in the same general area for both of the re-analyses however their strengths differed. The winds and the precipitation were not detected as well in both the NARR and the CRCM results. The placement of the surface low differed between the two re-analyses. The NARR placed the low farther west and indicated pre-blizzard conditions at Iqaluit whereas the CRCM placed the low farther east when the low had passed over Iqaluit and the blizzard had started. The NARR re-analysis showed an 850 mb low level jet right over Iqaluit on the same date of the event; however it was a southeasterly jet as opposed to the northwesterly winds that were observed at Iqaluit. The CRCM detected an 850 mb jet maximum northwest of Iqaluit however the direction matched well with the surface observations. The difference in wind direction between the NARR and the CRCM could be due to the timing of the passage of the cold front with the CRCM being more progressive with the storm. The CRCM model did not detect stronger surface winds nor did it detect high precipitation amounts over the Iqaluit area whereas the NARR did detect a 10 m/s 1000 mb wind as well as higher precipitation amounts over southern Baffin Island.

4.5 June 8-9, 2008 Extreme Flooding Event at Pangnirtung

On June 8 and 9, 2008 Pangnirtung experienced an extreme flooding event that devastated the community. Within 24 hours, 40 mm of rain fell at the site and though this amount is well below the Environment Canada warning criteria of 50 mm in 24 hours, this amount of rain is unusual for Pangnirtung and had many negative impacts on

the community. This event may have subjectively qualified under the ‘extenuating circumstances that cause flash flooding’ Environment Canada warning criteria. On June 8, extremely warm temperatures at Pangnirtung aided in the melting of the snowpack. The maximum temperature at Pangnirtung was 13°C on June 8, 2008 leading up to this event whereas the average maximum temperature for June is 8°C. The melting of the snowpack combined with the falling precipitation on June 9, 2008 enhanced runoff and contributed to the severity of this event.

Although this event occurred outside of the CRCM forced with ERA-40 dataset timeline, the societal impacts on the community were so great that this event was deemed important enough to analyze in depth to characterize the atmosphere. Lots of observational data were available for this event. Large crevasses, a collapsed bridge and other structural damage occurred in the community making travel difficult and disrupted normal living. Abnormal amounts of water flowed through the Duval River causing major soil erosion as well.

The METAR observations at Pangnirtung showed a maximum sustained wind speed of 59 km/h and a maximum gust of 78 km/h from the east. Normally, this is a downslope wind at Pangnirtung. Visibilities were reported as low as 8 km. While an actual observer manned the station, moderate rain was the most intense precipitation reported. When the station was not manned by an actual observer, note that the automatic weather station at Pangnirtung does not report precipitation or visibilities.

Table 4.5: METAR observations at Pangnirtung June 8 and 9, 2008. RA refers to moderate rain and –RA refers to light rain.

CYXP	081600Z	07039G63KMH 24KM VCSH OVC040 11/03 A2927 RMK SC8 SLP914
CYXP	081622Z	09026G48KMH 13KM -RA OVC040 RMK SC8 SKYXX=
CYXP	081700Z	08037G63KMH 13KM -RA OVC040 08/05 A2926 RMK SC8 SLP910 SKYXX=
CYXP	081708Z	08035G59KMH 8KM RA OVC040 RMK SC8 SKYXX=
CYXP	081733Z	09052G65KMH 13KM -RA OVC040 RMK SC8 SKYXX=
CYXP	081800Z	09054G67KMH 13KM -RA OVC040 07/05 A2924 RMK SC8 SLP903 57024
CYXP	081820Z	11059G78KMH 8KM RA OVC040 RMK SC8 SKYXX=
CYXP	081844Z	11044G63KMH 13KM -RA OVC040 RMK SC8 SKYXX=
CYXP	081900Z	11059G74KMH 13KM -RA OVC040 06/04 A2925 RMK SC8 SLP906 SKYXX=
CYXP	082000Z	09057G78KMH 16KM -RA OVC030 06/04 A2923 RMK SC8 11.0/6.0/2.2/LAST
CYXP	082100Z	AUTO 12041G57KMH 09/04 A2925=
CYXP	082200Z	AUTO 11050G61KMH 09/04 A2924=
CYXP	082300Z	AUTO 11037G61KMH 07/04 A2927=
CYXP	090000Z	AUTO 10035G65KMH 06/05 A2927=
CYXP	090100Z	AUTO 10024G56KMH 07/05 A2927=
CYXP	090200Z	AUTO 08052G76KMH 07/05 A2924=
CYXP	090300Z	AUTO 11043G63KMH 06/04 A2925=
CYXP	090400Z	AUTO 11052G69KMH 06/04 A2923=
CYXP	090500Z	AUTO 09052G93KMH 06/04 A2920=
CYXP	090600Z	AUTO 11043G67KMH 06/04 A2923=
CYXP	090700Z	AUTO 09028G61KMH 06/04 A2922=
CYXP	090800Z	AUTO 12037G63KMH 06/03 A2924=
CYXP	090900Z	AUTO 10024G46KMH 06/03 A2926=
CYXP	091000Z	AUTO 10030G56KMH 06/02 A2929=
CYXP	091100Z	09035G50KMH 24KM -RA OVC030 07/02 A2932 RMK SC8 9.6/5.4/35.4
CYXP	091200Z	09031G46KMH 24KM -RA OVC030 07/01 A2935 RMK SC8 SLP942 52036
CYXP	091232Z	09030G54KMH 24KM BKN030 RMK SC7 SKY99=
CYXP	091300Z	09046G57KMH 24KM BKN030 07/00 A2940 RMK SC7 SLP957 SKY99=
CYXP	091400Z	11022G39KMH 24KM BKN030 06/00 A2945 RMK SC7 SLP974 SKY99=
CYXP	091500Z	13031KMH 19KM VCSH BKN030 05/00 A2950 RMK SC7 SLP990 52048
CYXP	091527Z	14009G19KT 8SM -RA BKN020 OVC030 RMK SC5SC3 SKYXX=
CYXP	091600Z	06003KT 8SM -RA SCT012 OVC025 04/00 A2956 RMK ST3SC5 SLP011
CYXP	091700Z	16007KT 8SM -RA SCT012 OVC025 03/00 A2962 RMK ST4SC4 SLP030

4.5.1 NARR re-analysis of June 8-9, 2008

The NARR re-analysis data showed a 995 mb surface low pressure system situated over northern Quebec with a trough that extended northwestward from this low

through Cape Dorset, Hall Beach and Igloolik (Figure 4.35). Relative to the trough, Pangnirtung was in a prime area for vertical motion, being on the downstream side of the low pressure system.

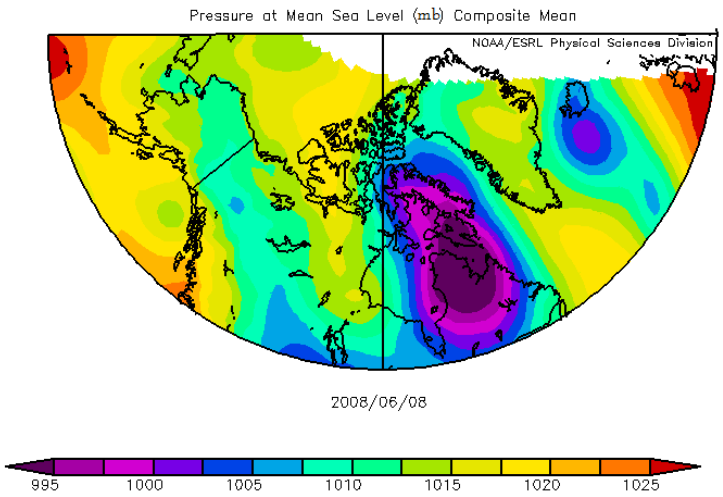

Figure 4.35: Composite mean sea level pressure (mb) from 00 UTC June 8, 2008 to 00 UTC June 9, 2008.

At 500 mb, a 5350 m upper low was situated right over Foxe Basin (Figure 4.36). A ridge of high pressure was situated just east of Baffin Island over Davis Strait, meaning that Pangnirtung was on the downstream side of the low. This region is primed at for upper level lift, which is indicating more energy and support for this system.

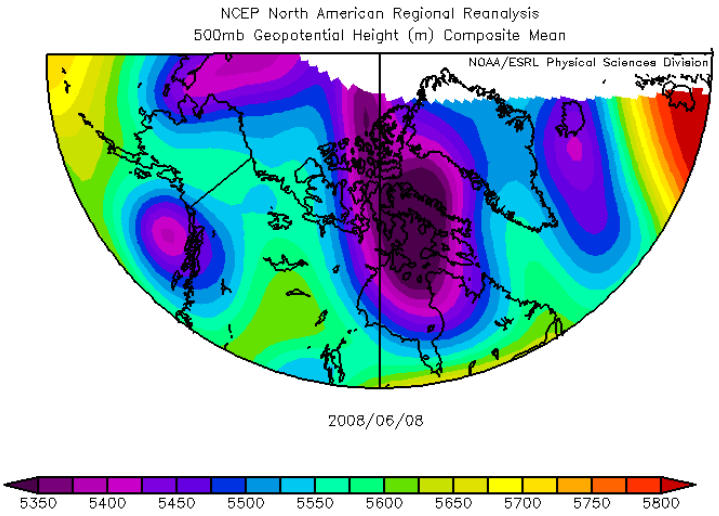

Figure 4.36: Composite mean 500 mb geopotential height (m) from 00 UTC June 8, 2008 to 00 UTC June 8, 2008.

A 1000 mb jet maximum was located just southeast of Pangnirtung with maximum values of approximately 14 m/s (Figure 4.37). The re-analysis shows that the winds over Pangnirtung were from the southeast, which matches the actual observed data quite well. During the peak of the actual event, observed winds were being reported between 90° and 120°, which is only a slight deviation from the southeasterly winds detected in the model re-analysis.

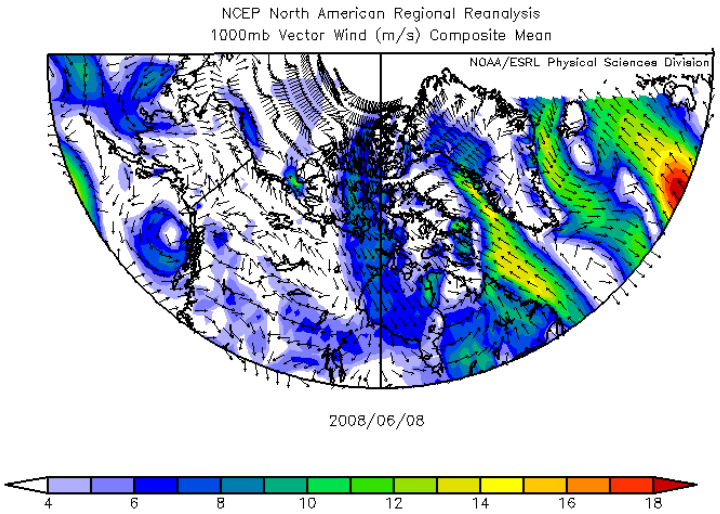

Figure 4.37: Composite mean 1000 mb vector wind speed (m/s) from 00 UTC June 8, 2008 to 00 UTC June 9, 2008.

At 850 mb, a 20 m/s jet maximum was located just southeast of Pangnirtung which was in the same vicinity as the 1000 mb jet maximum (Figure 4.38). Values of approximately 18 m/s were detected above Pangnirtung. The re-analysis indicated a south-southeasterly flow over Pangnirtung at 850 mb.

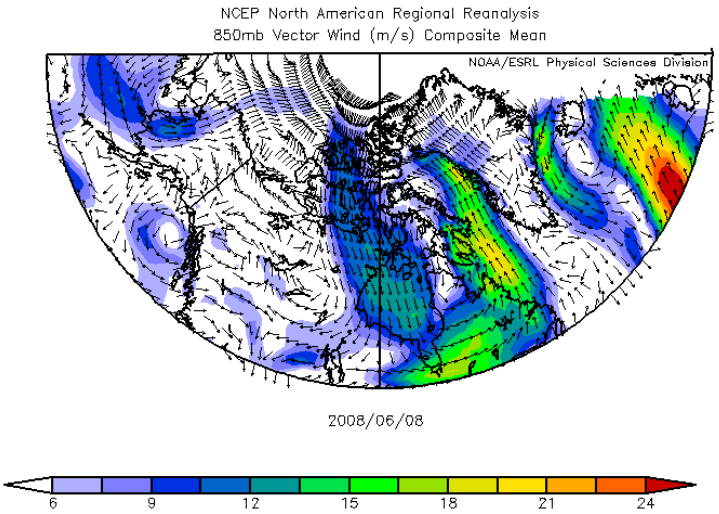

Figure 4.38: Composite mean 850 mb vector wind speed (m/s) from 00 UTC June 8, 2008 to 00 UTC June 9, 2008.

According to the NARR re-analysis data, the accumulated precipitation amount for June 8, 2008 was approximately 24 mm over Pangnirtung (Figure 4.39). These higher accumulated precipitation amounts were well placed according to the re-analysis, although still under-represented compared to the actual observed 40 mm that fell during the course of this event.

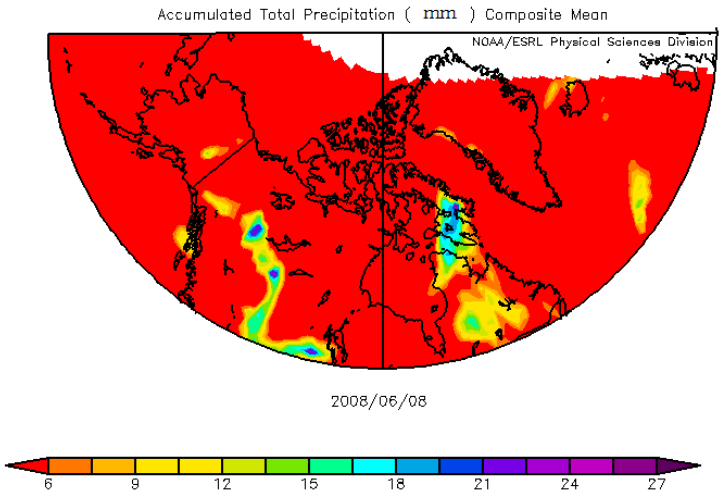

Figure 4.39: Composite mean accumulated precipitation (mm) from 00 UTC June 8, 2008 to 00 UTC June 9, 2008.

The precipitable water chart showed a ridge of higher values that extended up from Northern Quebec being advected into the Kimmirut region of southern Baffin Island (Figure 4.40). Although the highest values remained south of Baffin Island, according to the re-analysis data 25-30 mm of precipitable water was located over the Kimmirut and Iqaluit areas, and values of approximately 20 mm were detected over Pangnirtung.

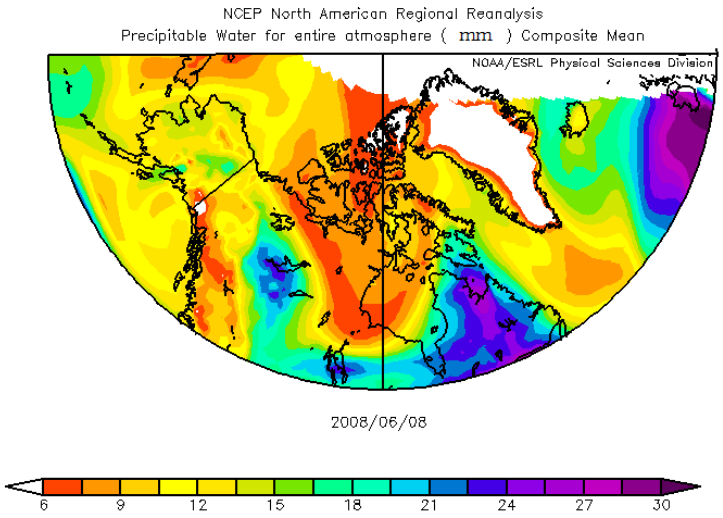

Figure 4.40: Composite mean columnar precipitable water (mm) from 00 UTC June 8, 2008 to 00 UTC June 9, 2008.

Precipitable water anomaly values showed a ridge of maximum anomalous values extending into southern Baffin Island from northern Quebec (Figure 4.41). At Pangnirtung, these values were approximately 12 mm above normal. By examining both the precipitable water values and the precipitable water anomaly values, it is evident that, despite having lower precipitable water amounts over southern Baffin Island compared to Northern Quebec, these values are nonetheless unusual. This may be an indication that Baffin Island does not need to experience precipitable water amounts as high as other parts of Canada to produce extreme precipitation events because precipitation may be produced more efficiently.

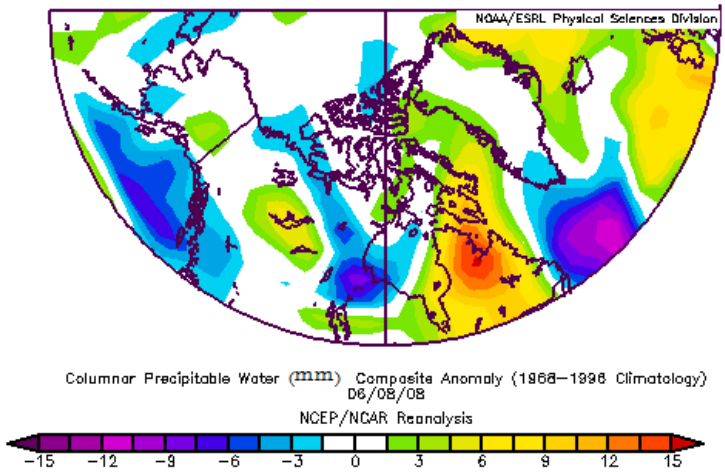

Figure 4.41: Composite mean columnar precipitable water anomaly (mm) from 00 UTC June 8, 2008 to 00 UTC June 9, 2008.

4.5.2 CRCM re-analysis of June 8-9, 2008

Since the CRCM forced with ERA40 run included only the years 1961-2002, a comparison between the NARR output and the ERA-40 was not possible because the Pangnirtung precipitation event occurred in 2008. It was important, however, to include this event in this thesis to characterize the atmosphere during this extreme event because of its tremendous impact on Pangnirtung as well as the abundance of observational data available.

4.5.3 June 8-9, 2008 Summary

Overall, the NARR re-analysis did a good job at re-creating the June 8-9, 2008 Pangnirtung wind event. Surface and 500 mb low pressure systems were detected over a location that would conceptually be primed for a severe weather event at Pangnirtung. The 850 mb wind chart detected enhanced winds over the Pangnirtung area, denoting enhanced lift in the area. The 1000 mb wind chart also showed enhanced surface winds which were reflective of actual observations. The accumulated precipitation chart showed higher values over Pangnirtung although the amounts were underrepresented compared to the event itself. The precipitable water and precipitable water anomaly charts also showed enhanced values over Pangnirtung.

4.6 Summary of historic case studies

The NARR and CRCM re-analyses of the historic case studies showed both strengths and weaknesses in replicating historic severe weather events. The upper levels were generally consistent in detecting a 500 mb low or trough in the Baffin Island area with similar strengths. In some cases, timing and placement of the surface low caused discrepancies between the NARR and the CRCM re-analyses and the strength of the surface low also differed more than the 500 mb low. In general, the 850 mb winds showed a low level jet in the general area, whereas the surface winds were more hit and miss. For some events at Iqaluit, both re-analyses did not detect enhanced surface or 850 mb winds. This could indicate that model resolution was too coarse to detect enhanced winds caused by local factors. The CRCM did not detect the surface winds well in the historic cases. Although total precipitation and precipitable water values consistently

showed higher amounts over the affected site, the values were consistently under represented by both the models.

CHAPTER 5: HINDCAST AND FUTURE SCENARIOS

5.1 Introduction

The following sections describe the differences in precipitation amounts and wind events between the historic CGCM driven dataset and the future projection CGCM driven dataset.

Algorithms for deriving daily mean and maximum precipitation amounts were calculated and separated by month for the two CRCM datasets that were forced with CGCM data. This was done in order to examine changes between the historic dataset and the future projection. The mean daily precipitation algorithm included all of the days within the study period and was separated into monthly values. This means that days where 'nil' or 'trace' amounts of precipitation fell at the communities were included in the calculation of the mean. By including all of the days, the mean daily precipitation values are low relative to the precipitation amounts that occurred in any given event. The maximum precipitation charts picked out the single largest daily precipitation accumulation for each month from the hindcast and future projection datasets.

Furthermore, an algorithm was run to detect the number of wind events for each of the CRCM driven by CGCM datasets. The algorithm detected sustained wind speeds of 60, 70 and 80 km/h or greater and the results are described in the subsequent sections.

Results are discussed as well as possible reasons for the differences in results between the hindcast and the future projection datasets.

5.2 Precipitation Assessment

The following sections will describe the climatology of the precipitation events between the 1961-1990 and the 2041-2070 CRCM forced with CGCM dataset. Each of the communities showed an overall increase in the mean annual precipitation in the future projection. On an annual scope, Iqaluit showed an increase from 291 mm/year to 349 mm/year, Pangnirtung showed an increase from 269 mm/year to 300 mm/year, Cape Dorset showed an increase from 243 mm/year to 301 mm/year and Kimmirut showed an increase from 340 mm/year to 420 mm/year.

5.2.1 Iqaluit precipitation assessment

The daily mean precipitation amounts were calculated for each month at Iqaluit. Figure 5.1 shows this variable. Every month showed a higher mean precipitation amount for the future projection scenario as opposed to the hindcast dataset. The biggest increases were in the summer months with June through September having a 0.4 mm/day higher average. The other months also showed an increase of between 0.1-0.3 mm/day in the mean.

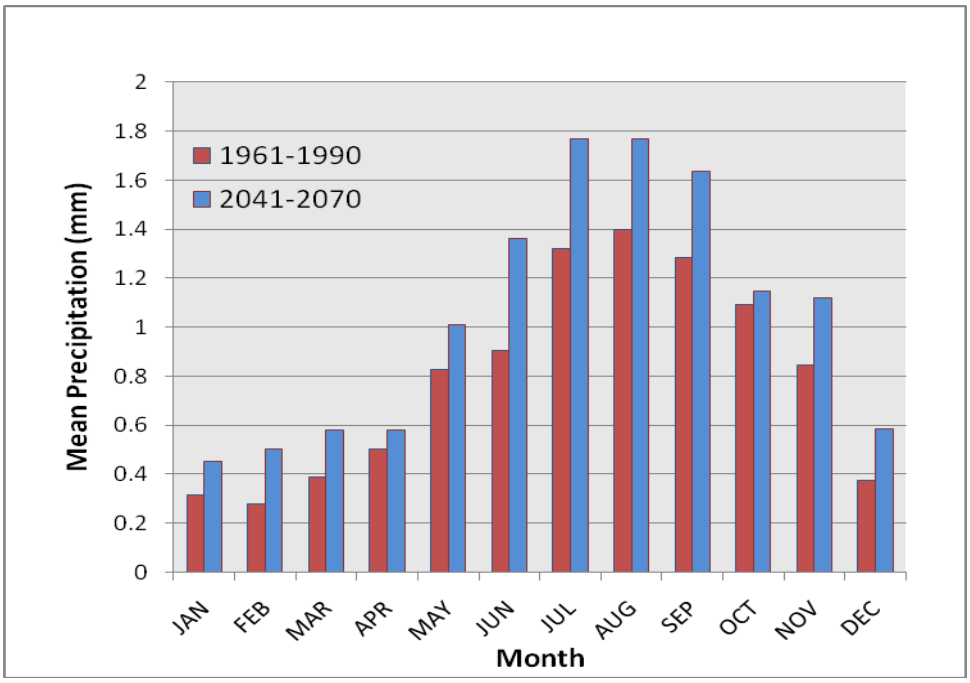

Figure 5.1: Mean daily precipitation for Iqaluit (mm/day) by month over the 1961-1990 and 2041-2070 periods. Results were from the CRCM forced by CGCM over these two periods.

Secondly, an algorithm was developed to detect the daily precipitation amounts at each site. Figure 5.2 shows the results at the Iqaluit site. The vast majority of the daily precipitation amounts fell into the 0-5 mm category with over 10,000 days for each of the model simulations. The hindcast detected more events in the 0-5 mm category with 10,604 days whereas the future projection detected 10,562 days. For all of the other categories, more events were detected in the future projection simulation. Most notably, the future projection simulation detected one event in the 30-35 mm category as well as the 35-40 mm category whereas the hindcast didn't detect any in either the 30-35 or the

35-40 mm category. The maximum event detected by the hindcast was in the 25-30 mm category.

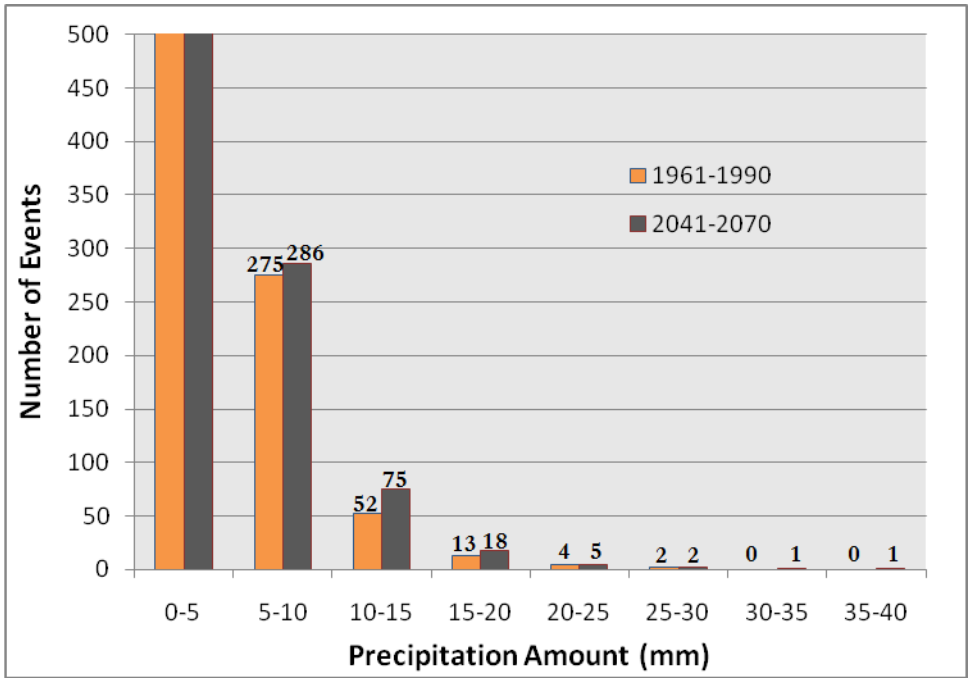

Figure 5.2: The number of events as a function of daily precipitation amount for Iqaluit over the 1961-1990 and 2041-2070 periods. Results were from the CRCM forced by CGCM over these two periods. The vertical axis was scaled down to a maximum of 500 days so that the more extreme precipitation categories were visible and the number of events is shown at the top of each bar.

Figure 5.3 shows the maximum precipitation event for each month within the analysis period at Iqaluit. Aside from the months of May and July, the 2041-2070 period showed a great increase in the maximum precipitation event, most markedly in the months of October and November. The hindcast run showed a maximum precipitation

event of 19 mm in October and 16 mm in November, whereas the future projection showed a 37 mm event in October and a 33 mm event in November.

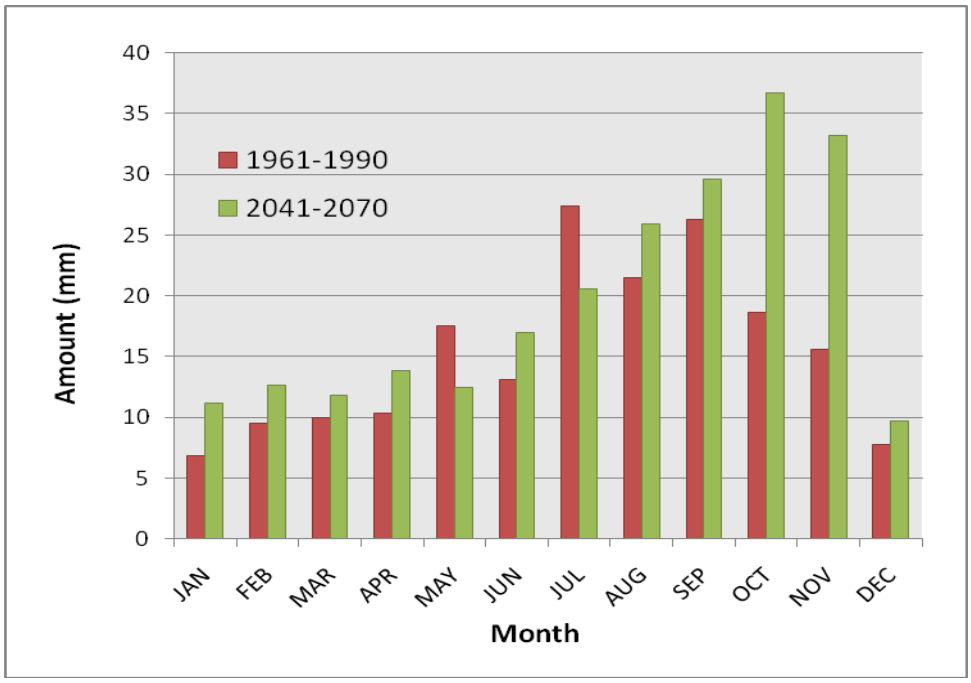

Figure 5.3: Maximum daily precipitation from events at Iqaluit (mm) over the 1961-1990 and 2041-2070 periods. Results were from the CRCM forced by CGCM over these two periods.

5.2.2 Pangnirtung precipitation assessment

Figure 5.4 shows the mean daily precipitation amounts at Pangnirtung. For the winter months, Pangnirtung showed insignificant changes in daily precipitation amounts. For the months of April through to December, the hindcast dataset showed a higher mean monthly precipitation than the future projection, with the exception of June showing a

slightly higher mean precipitation in the future projection than the hindcast. The decrease in mean daily precipitation was on the order of 0.1-0.2 mm/day.

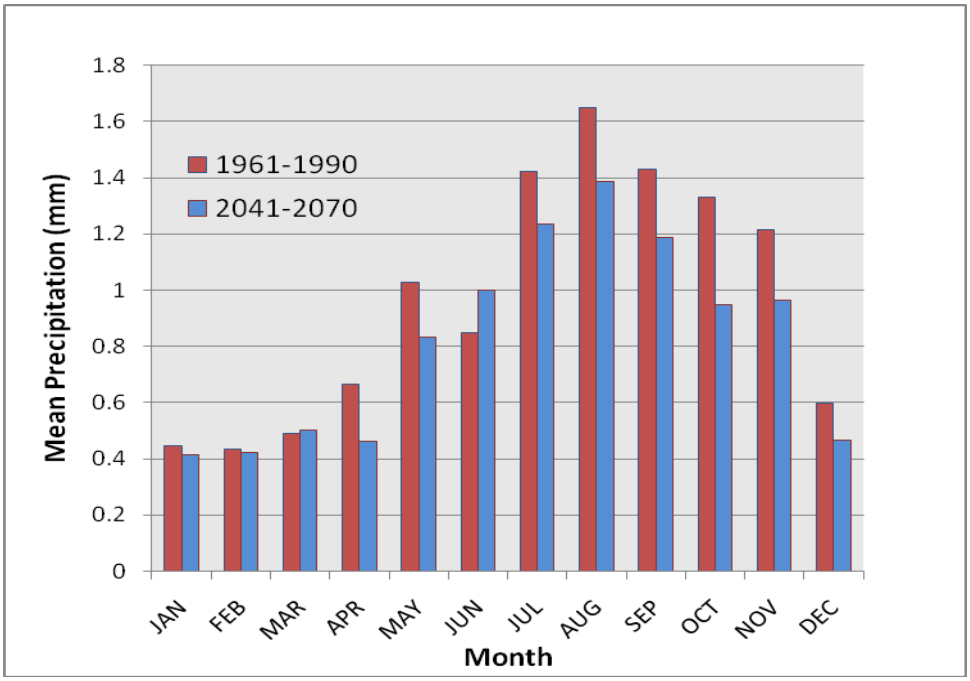

Figure 5.4: Mean daily precipitation for Pangnirtung (mm/day) by month over the 1961-1990 and 2041-2070 periods. Results were from the CRCM forced by CGCM over these two periods.

Figure 5.5 shows the daily precipitation events at Pangnirtung. The results for Pangnirtung were similar to those at Iqaluit; the hindcast showed more events in the 0-5 mm category than the future projection but fewer events in all the other categories. Most notably, there were 8 events detected in the 20-25 mm category in the future projection whereas the hindcast only detected 5. Also, the future projection detected 3 events in the 25-30 mm category whereas the hindcast only detected 2. These results may be indicating a trend towards heavier rainfall events at Pangnirtung.

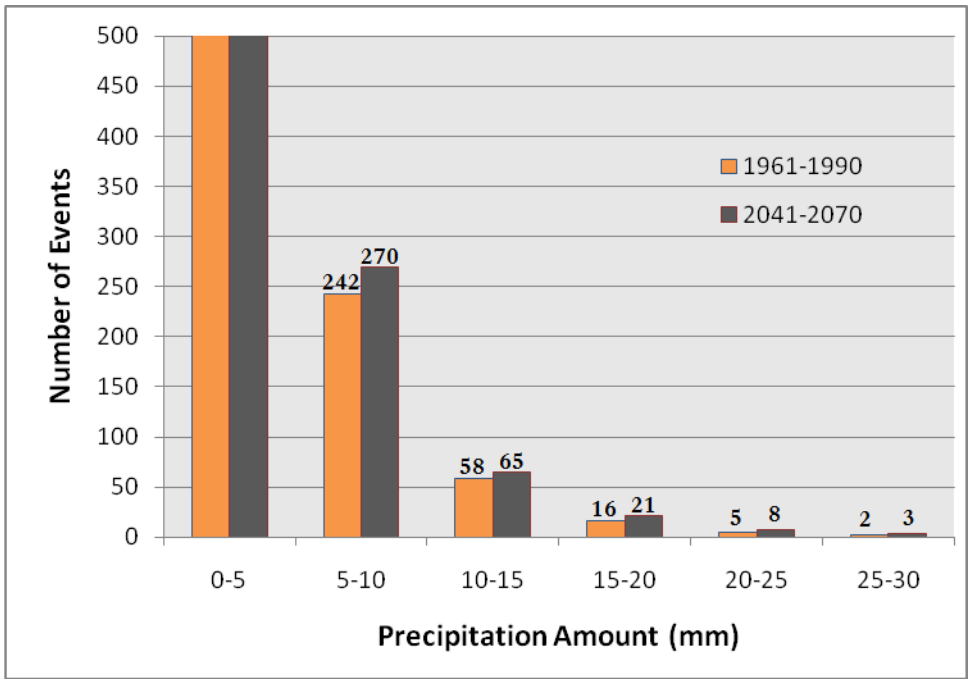

Figure 5.5: The number of events as a function of daily precipitation amount for Pangnirtung over the 1961-1990 and 2041-2070 periods. Results were from the CRCM forced by CGCM over these two periods. The vertical axis was scaled down to a maximum of 500 days so that the more extreme precipitation categories were visible and the number of events is shown at the top of each bar.

Figure 5.6 shows the maximum precipitation event in each month for the analysis period at Pangnirtung. The analysis showed that, for most months, there was an increase in the number of events within a category in the future projection period. However, there were several months with little difference or a decrease in the amount of precipitation from the future projection compared to the hindcast. August showed the biggest increase in precipitation amount with a 19 mm event detected in the hindcast and a 27 mm event detected in the future projection.

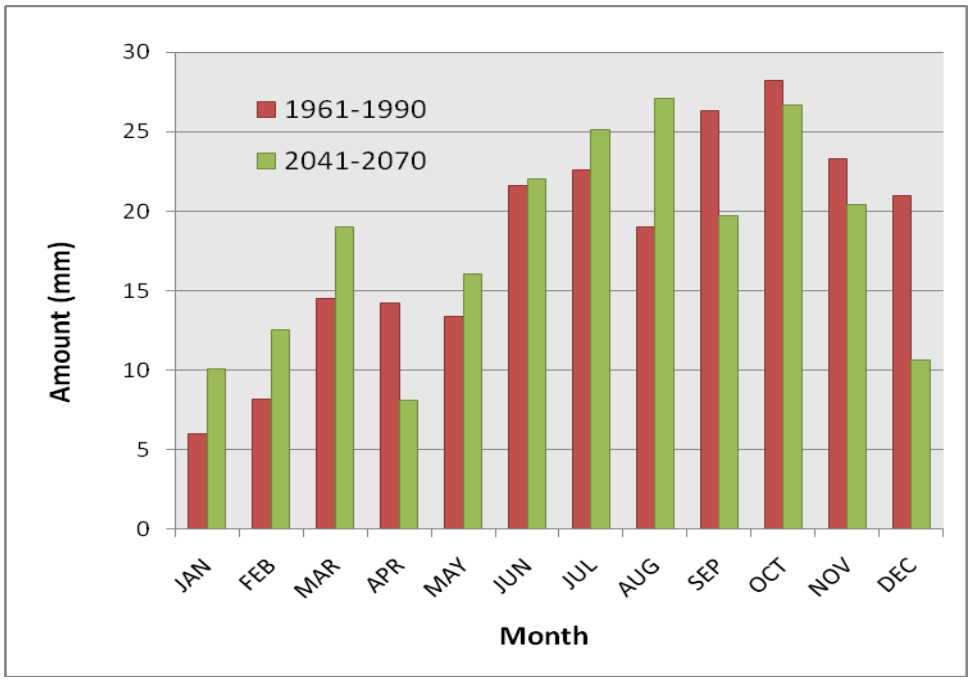

Figure 5.6: Maximum daily precipitation from events at Pangnirtung (mm) over the 1961-1990 and 2041-2070 periods. Results were from the CRCM forced by CGCM over these two periods.

5.2.3 Cape Dorset precipitation assessment

Figure 5.7 shows the mean daily precipitation amounts at Cape Dorset. All months showed a slight increase in the mean daily precipitation, with smaller increases during the winter months and slightly larger increases in July, September and November. July showed the largest increase in mean precipitation with a 0.4 mm greater mean in the period from 2041-2070 than in the hindcast period.

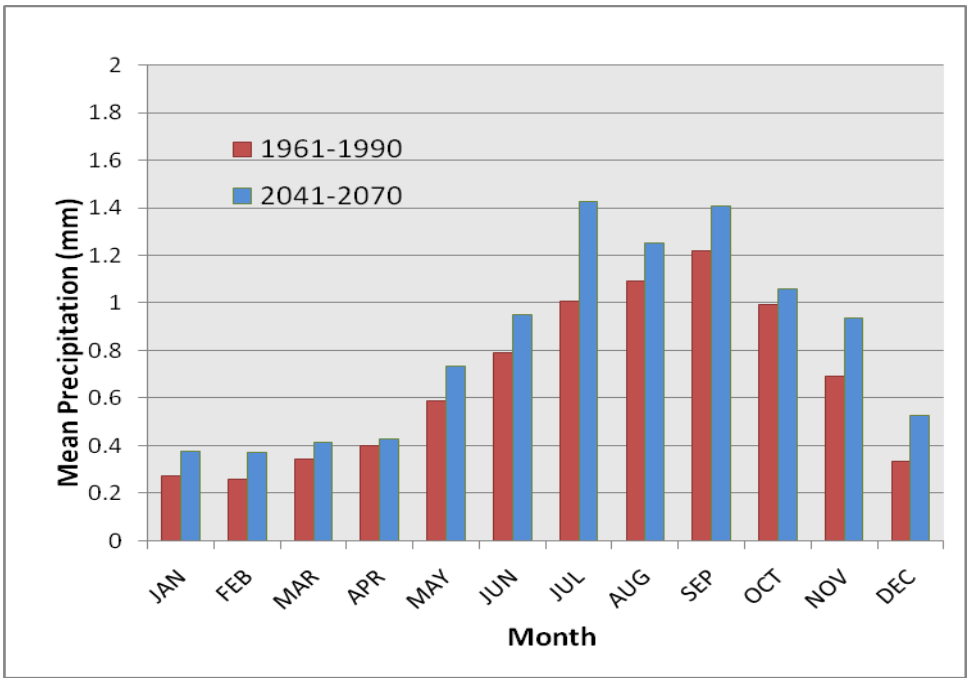

Figure 5.7: Mean daily precipitation for Cape Dorset (mm/day) by month over the 1961-1990 and 2041-2070 periods. Results were from the CRCM forced by CGCM over these two periods.

Figure 5.8 shows the daily precipitation events at Cape Dorset. Again, results similar to those at Iqaluit and Pangnirtung were detected with more 0-5 mm events detected in the hindcast simulation than the future projection scenario. The number of extreme events did decrease slightly with one 30-35 mm event detected in each of the simulations but more 15-20 and 20-25 mm events detected in the future projection. More intermediate events were detected in the future projection simulation as opposed to the larger events.

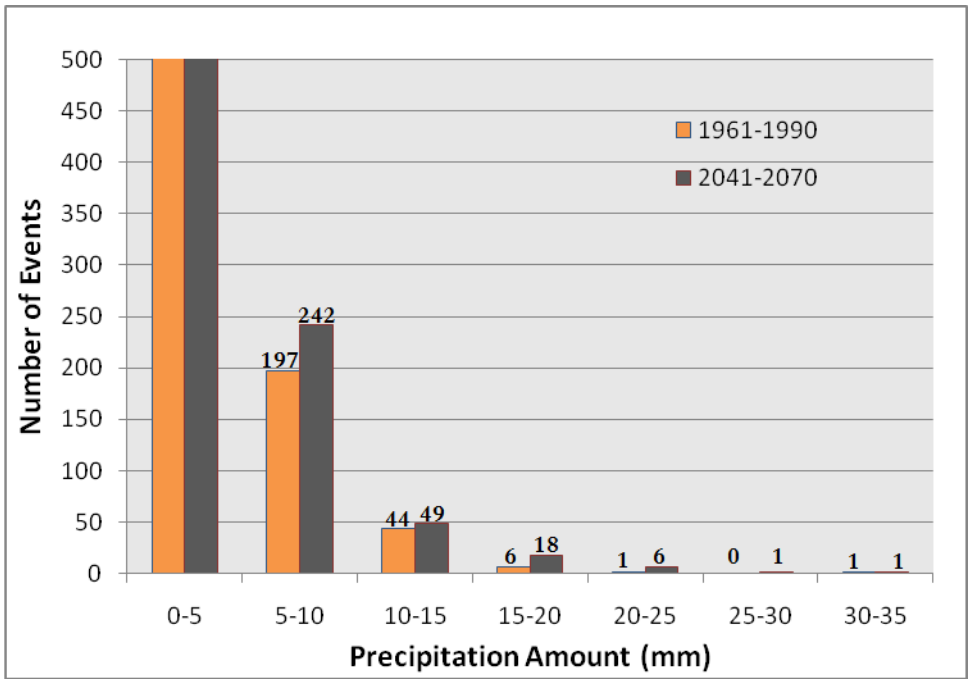

Figure 5.8: The number of events as a function of daily precipitation amount for Cape Dorset over the 1961-1990 and 2041-2070 periods. Results were from the CRCM forced by CGCM over these two periods. The vertical axis was scaled down to a maximum of 500 days so that the more extreme precipitation categories were visible and the number of events is shown at the top of each bar.

Figure 5.9 shows the maximum daily precipitation event in each month for Cape Dorset. Every month other than May and June showed slight or moderate increases in the maximum precipitation event. The most notable increases occurred in the winter and fall during the months of January, February, October and November. January showed an increase from 10 mm to 15 mm as a maximum daily precipitation value and February showed an increase from 7 mm to 14 mm, or doubling the hindcast maximum event for the month of February. During the fall months, the future projection showed an increase

from 15 mm to 22 mm in the month of October and an increase from 12 mm to 21 mm in the month of November.

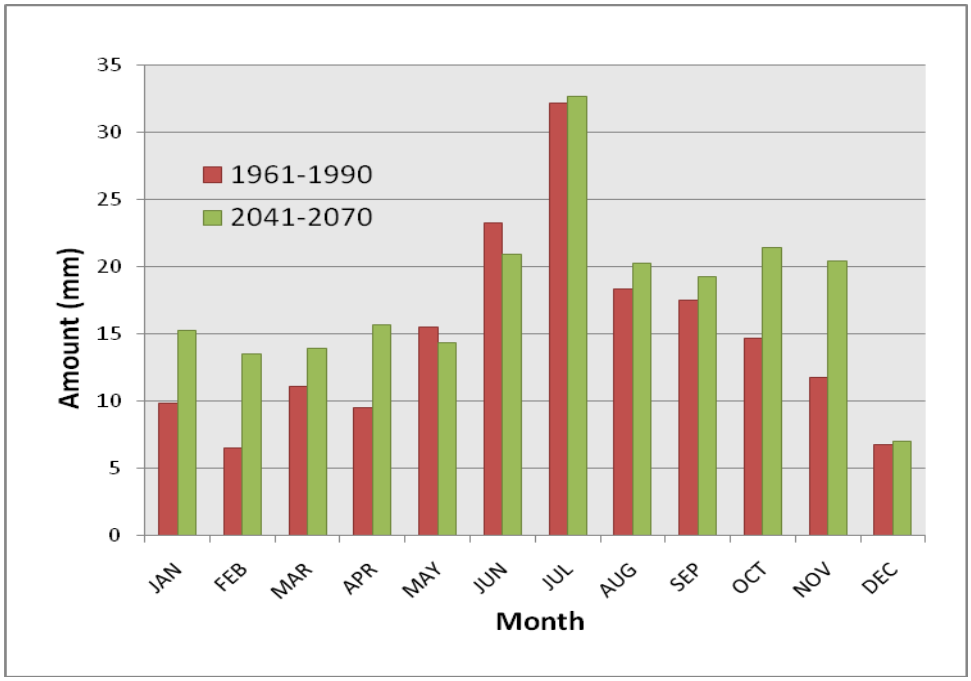

Figure 5.9: Maximum daily precipitation from events at Cape Dorset (mm) over the 1961-1990 and 2041-2070 periods. Results were from the CRCM forced by CGCM over these two periods.

5.2.4 Kimmirut precipitation assessment

Figure 5.10 shows the mean daily precipitation at Kimmirut. This graph shows that there is an increase in the mean daily precipitation for all 12 months from the hindcast data compared to the future projection data. The most notable increases in the mean daily precipitation are in the summer and fall months from July to November. Increases from 0.2 to 0.6 mm above the mean were observed during these months, with lesser amounts in the other months.

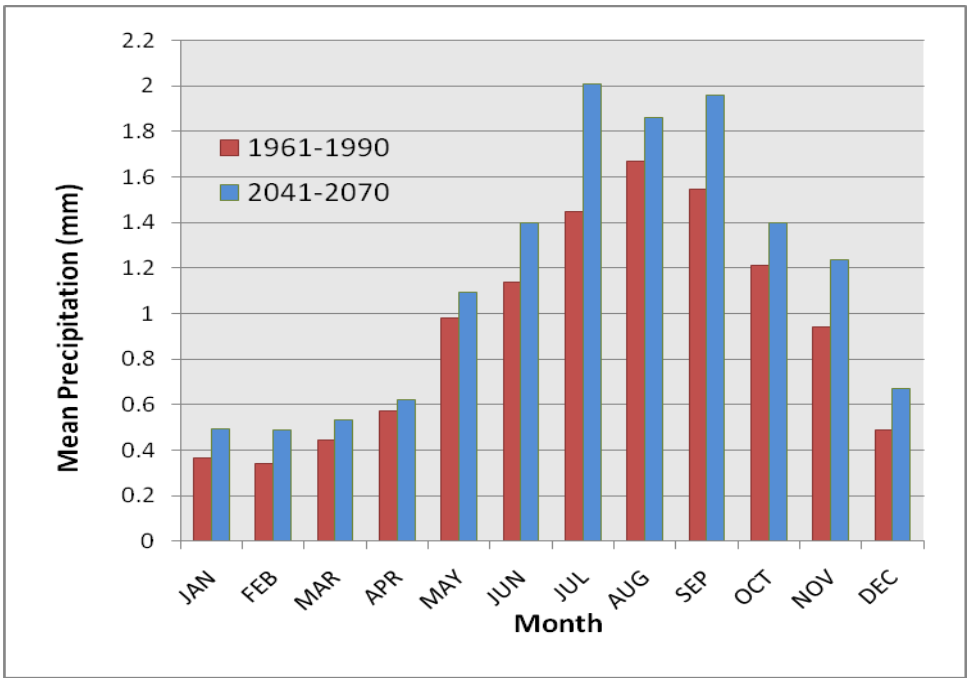

Figure 5.10: Mean daily precipitation for Kimmirut (mm/day) by month over the 1961-1990 and 2041-2070 periods. Results were from the CRCM forced by CGCM over these two periods.

Figure 5.11 shows the daily precipitation events at Kimmirut. The results were mixed; like all of the other communities more 0-5 mm events were detected in the hindcast simulation. The most extreme event was detected in the future projection with 1 event detected in the 50-55 mm category and none in the hindcast. However, there were no events detected in the 45-50 mm category for the future projection simulation and 1 event detected in the hindcast simulation in this category. Overall, there were more frequent large events in the future projection simulation but not in all categories.

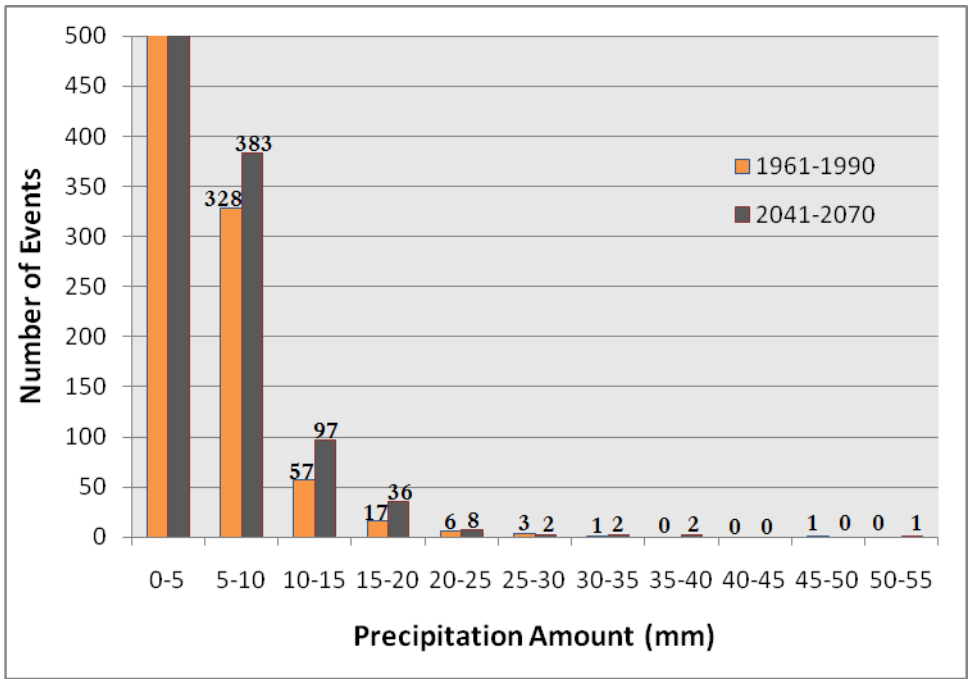

Figure 5.11: The number of events as a function of daily precipitation amount for Kimmirut over the 1961-1990 and 2041-2070 periods. Results were from the CRCM forced by CGCM over these two periods. The vertical axis was scaled down to a maximum of 500 days so that the more extreme precipitation categories were visible and the number of events is shown at the top of each bar.

Figure 5.12 shows the maximum precipitation event during the analysis periods for each month. Most months showed an increase in the maximum daily precipitation amount, other than February, August and December. The largest increase in precipitation events occurred in the fall, in October and November. In October, a maximum event of 20 mm increased to 32 mm in the future projection, and in November the maximum event increased from 17 mm to 39 mm in the future projection.

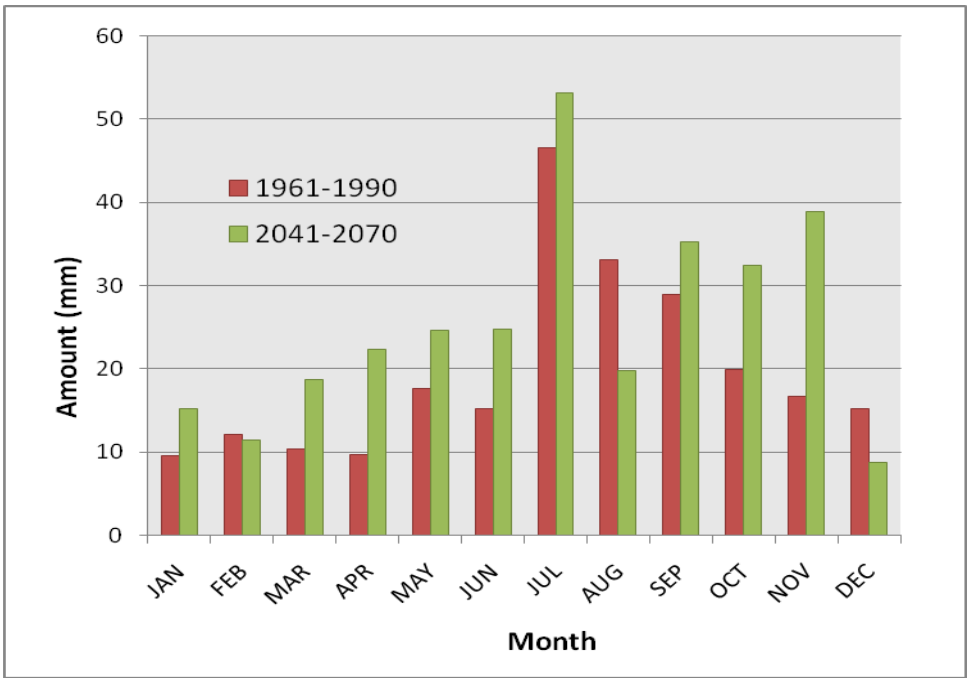

Figure 5.12: Maximum daily precipitation from events at Kimmirut (mm) over the 1961-1990 and 2041-2070 periods. Results were from the CRCM forced by CGCM over these two periods.

5.3 Wind Assessment

The following Sections describe the results obtained with the CRCM forced with CGCM hindcast and the CRCM forced with CGCM future projection.

5.3.1 Iqaluit wind assessment

An algorithm set up to detect sustained wind speeds of over 60 km/h was run for each of the CRCM datasets that were forced by the CGCM. Figure 5.13 shows the results at Iqaluit. In the 60-70 km/h category, Iqaluit showed an increase from 62 events in the hindcast dataset to 88 events in the future projection. In the 70-80 km/h category

there was a smaller increase, from 26 to 32 events and a decrease from 6 events to 5 events in the 80 km/h or greater category.

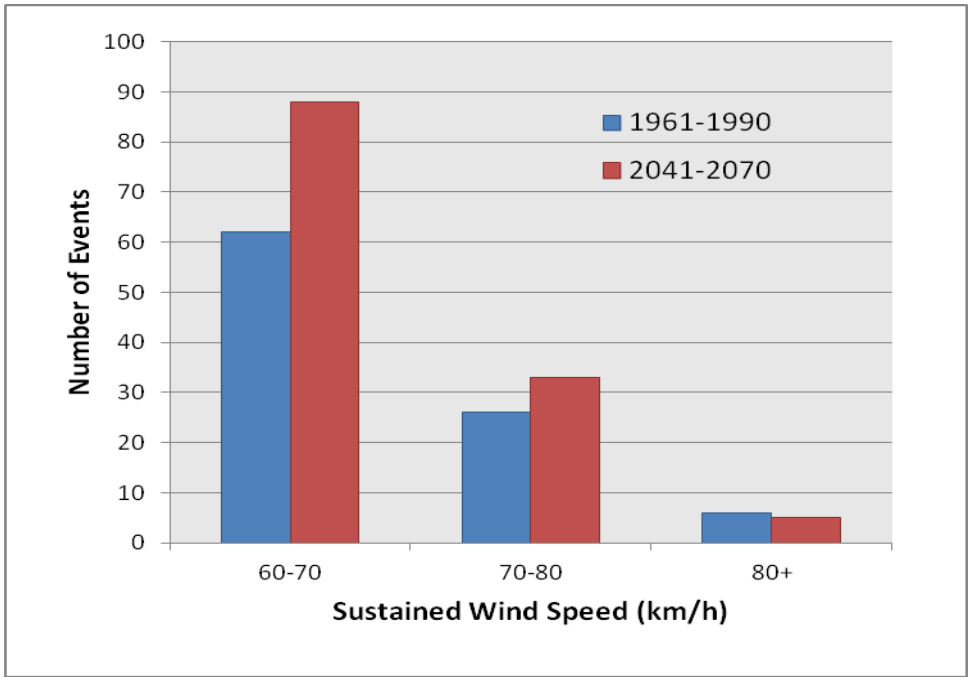

Figure 5.13: Number of extreme wind events at Iqaluit using CRCM forced with CGCM data.

5.3.2 Pangnirtung wind assessment

For Pangnirtung, the number of wind events decreased in each category from the hindcast to the future projection. The greatest decrease was observed in the 70-80 km/h wind category, with 32 events observed in the hindcast and only 15 events observed in the future projection (Figure 5.14).

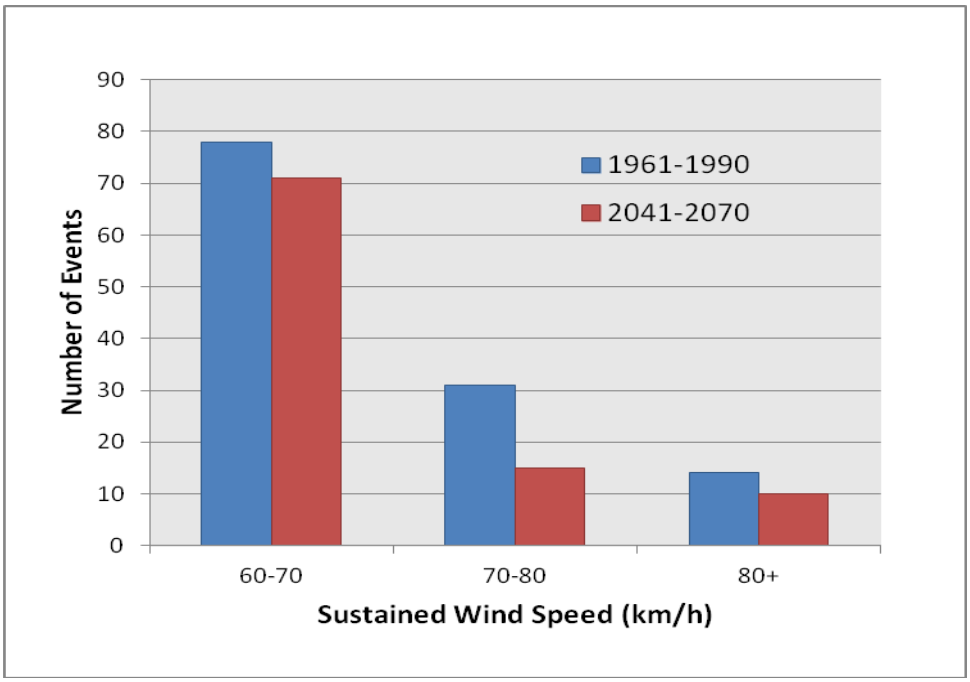

Figure 5.14: Number of extreme wind events at Pangnirtung using CRCM forced with CGCM data.

5.3.3 Cape Dorset wind assessment

Figure 5.15 shows the number of extreme wind events at Cape Dorset. In the 60-70 km/h category, there were over 3 times as many wind events in the future projection as there were in the hindcast scenario, an increase from 13 events to 41 events. In the 70-80 km/h category there was also an exponential increase in events in the future projection scenario with an increase from 2 events to 12 events. Neither of the models detected a wind event of 80 km/h or greater.

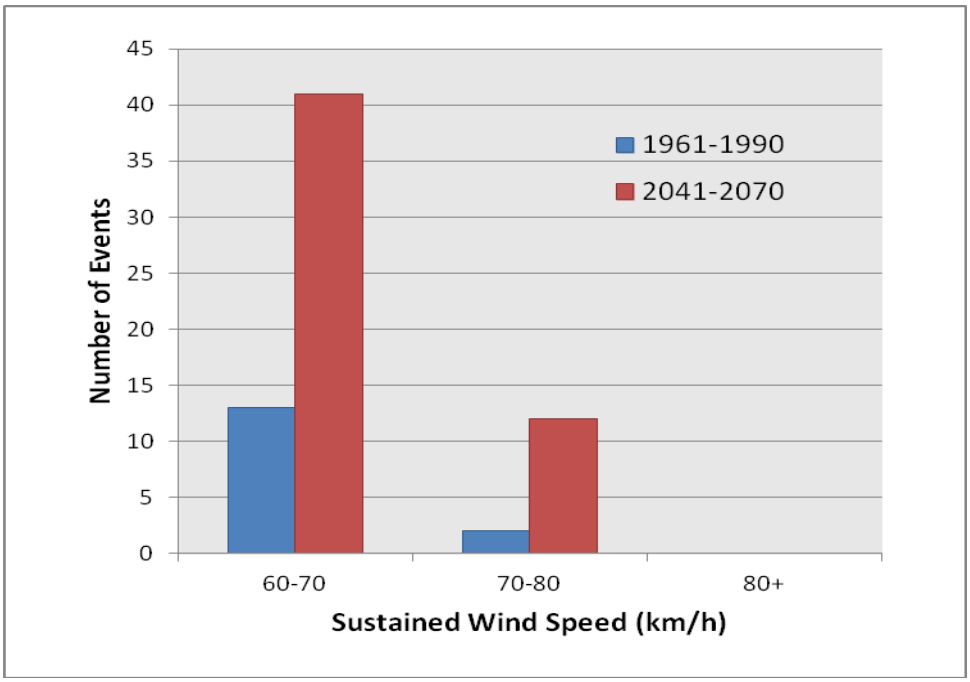

Figure 5.15: Number of extreme wind events at Cape Dorset using CRCM forced with CGCM data.

5.3.4 Kimmirut wind assessment

At the Kimmirut site there was an increase in all three of the wind event categories from the hindcast dataset to the future projections (Figure 5.16). In the 60-70 km/h event category, an increase from 70 events to 88 events was observed. In the 70-80 km/h category an increase from 13 events to 21 events was observed. In the 80 km/h or greater event category an increase of 5 events to 7 events was observed.

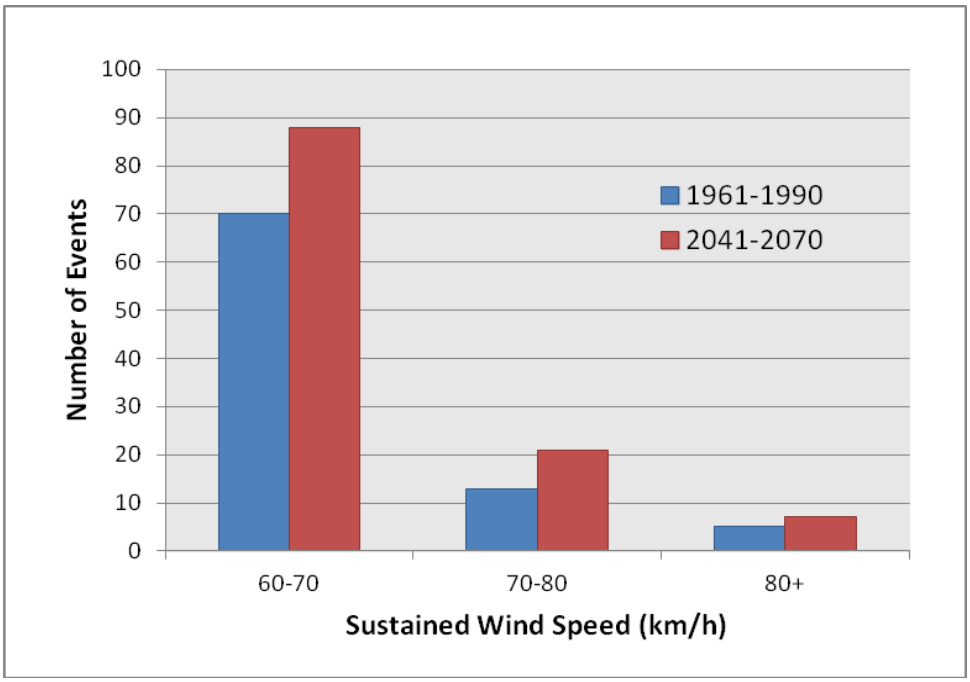

Figure 5.16: Number of extreme wind events at Kimmirut using CRCM forced with CGCM data.

5.4 Future scenario summary

In this Section, a summary of the frequency and intensity of extreme precipitation and wind events and how they have changed between the hindcast and future projection scenario are discussed.

Overall, Iqaluit, Kimmirut and Cape Dorset showed an increase in the mean daily precipitation amount as well as an increase in the intensity of the events (Figures 5.17 and 5.18). A trend towards more extreme events in the shoulder seasons, especially the fall was apparent at Iqaluit, Kimmirut and Cape Dorset. Pangnirtung showed an overall decrease in the mean daily precipitation amount and although the maximum precipitation

event didn't increase, the number of intermediately large precipitation events did (Figure 5.18).

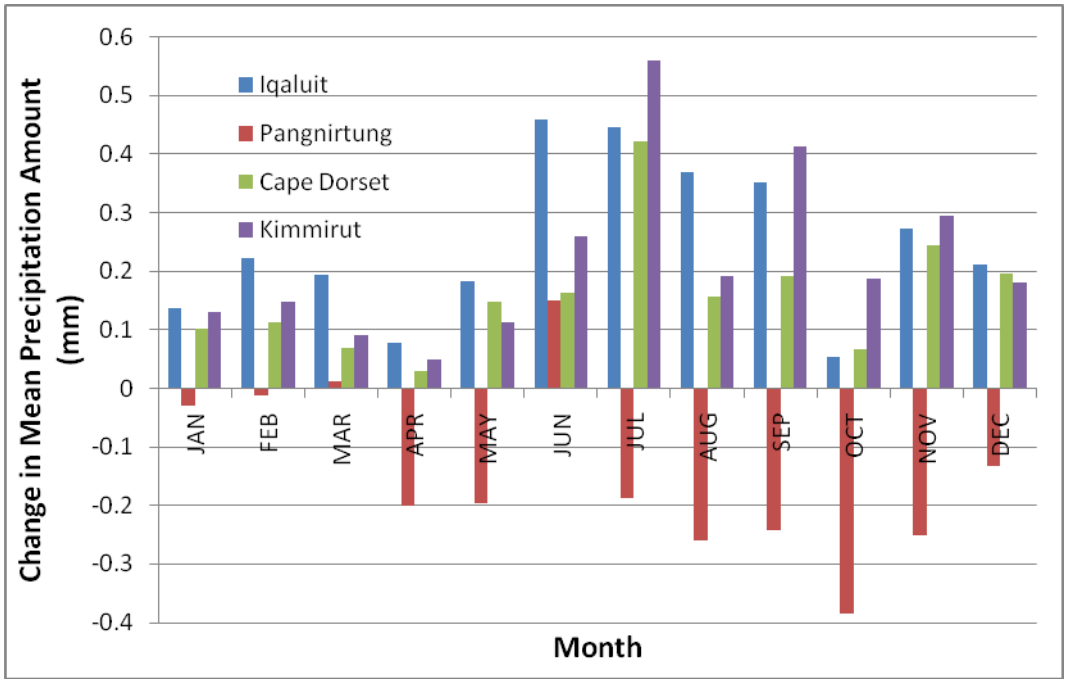

Figure 5.17: Change in mean monthly precipitation amount from the future projection (2041-2070) CRCM output to the CRCM hindcast (1961-1990).

The daily precipitation charts showed that for all four communities there was a decrease in the smallest precipitation events (0-5 mm) whereas there were more frequent large events in the future projection scenario. The future projection simulation showed more large events in all of the categories other than 0-5 mm for Iqaluit and Pangnirtung, whereas Kimmirut and Cape Dorset not only showed increases in the larger events, there was also an increase in the most extreme event (Figure 5.18).

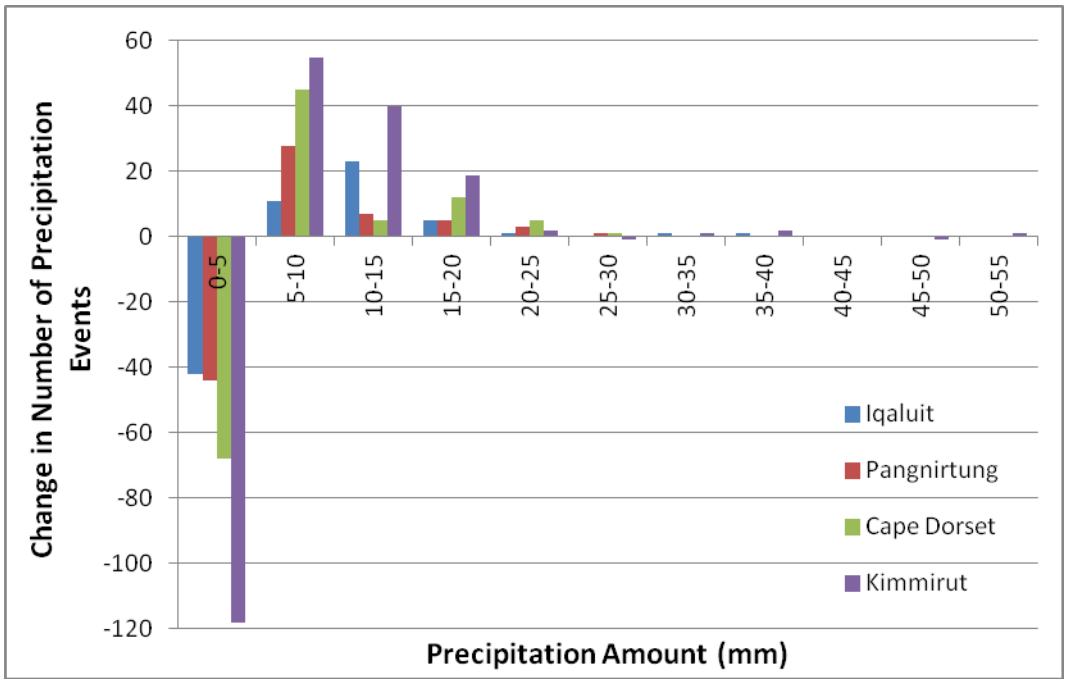

Figure 5.18: Change in number of precipitation events from the future projection (2041-2070) CRCM output to the CRCM hindcast (1961-1990).

For wind events, a similar trend was evident in which Iqaluit, Kimmirut and Cape Dorset showed an increase in extreme wind events whereas Pangnirtung showed a decrease (Figure 5.19). The largest increases were evident in the 60-70 km/h range. However smaller increases were also observed in the 70-80 km/h category for Iqaluit, Kimmirut and Cape dorset and in the 80 km/h or greater category for Kimmirut and Cape Dorset.

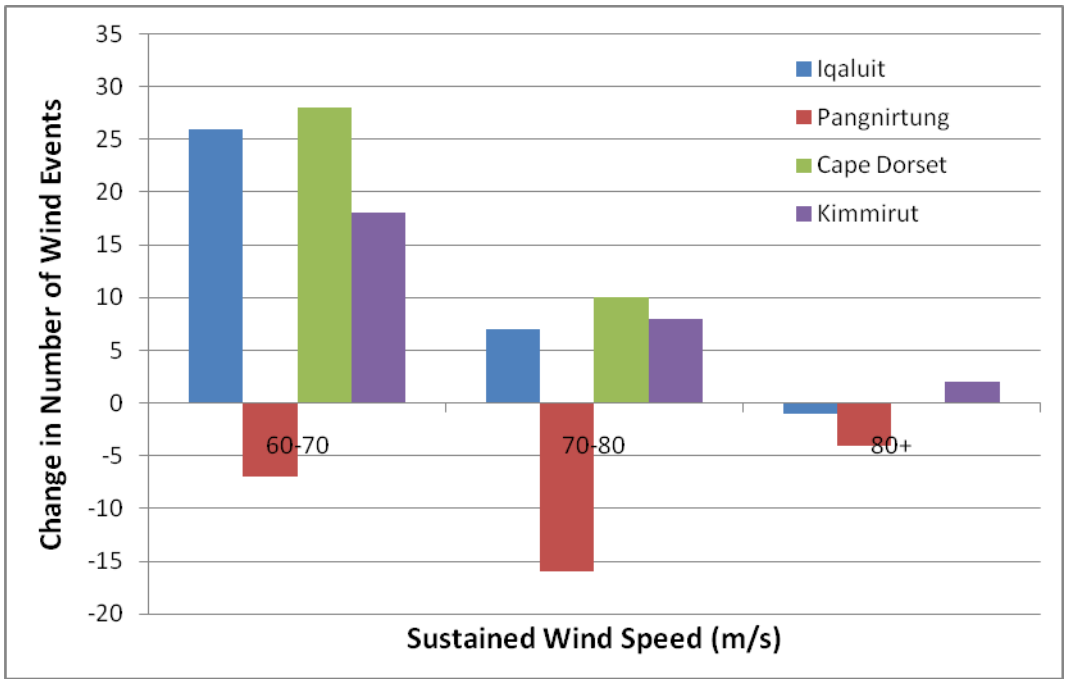

Figure 5.19: Change in number of extreme wind events from the future projection (2041-2070) output to the CRCM hindcast (1961-1990).

One potential reason for the increase in extreme weather events at Iqaluit, Cape Dorset and Kimmirut and the decrease in extreme weather events at Pangnirtung could be due to a shift in storm tracks. If, for example, more storms followed a south or west-originating storm track as described in by Gascon et al. (2010) and shown in Figure 2.1, then Iqaluit, Kimmirut and Cape Dorset would theoretically experience more frequent storms in the future. Another possible reason for heavier precipitation events at Kimmirut and Cape Dorset could be that with more open water, these sites may experience more convection off of open water hence more extreme events. Kimmirut may also be experiencing more of an upslope component to its precipitation events which could account for enhanced precipitation at the site. Although upslope precipitation

processes do occur at Pangnirtung as well, a change in storm tracking could potentially indicate a decrease in these events in the future with a change in storm tracks.

CHAPTER 6: FUTURE PROJECTION CASE STUDIES

6.1 Introduction

This Section analyzes case studies from the 2041-2070 CRCM dataset to identify projected atmospheric patterns that may produce extreme weather events.

The output from an algorithm that detected maximum precipitation events by month was used to select the case studies analyzed in this Chapter. This algorithm was discussed in Section 5.2. One of the top precipitation events at each community was chosen to analyze in depth. For Iqaluit, the top precipitation event was inferred on the same date as the 2nd highest precipitation event at Kimmirut (November 8, 2050).

An algorithm for calculating sustained wind speeds over southern Baffin Island was used to infer extreme wind events. This algorithm was discussed in Section 5.3. An extreme wind event at Iqaluit and Kimmirut was inferred on the same date as the most extreme precipitation event at Iqaluit (November 8, 2050). The other wind event analyzed affected both Kimmirut and Iqaluit and was inferred as one of the most extreme wind events by the future projection (September 24, 2054).

Table 6.1: Future projection case studies.

Event Date	Location	Type
November 8, 2050	Kimmirut and Iqaluit	Precipitation and Wind
September 24, 2054	Kimmirut and Iqaluit	Wind
August 27, 2068	Pangnirtung	Precipitation
July 31, 2070	Cape Dorset	Precipitation

6.2 November 8, 2050 at Iqaluit and Kimmirut

On November 8, 2050 the CRCM forced with CGCM future projection simulation inferred an extreme wind and precipitation event over Iqaluit and Kimmirut (Figure 6.1). According to the output, there was a large precipitation area that was inferred to affect almost all of southern Baffin Island. The model output inferred over 46 mm of precipitation over Kimmirut and over 38 mm of precipitation over Iqaluit that day (Figure 6.1 b). The output also inferred that these amounts were highly anomalous (Figure 6.1 d). The striking similarities between Figures 6.1 b, c and d indicate that this event had a large influence on the precipitation climatology for November 8 through the future projection study period.

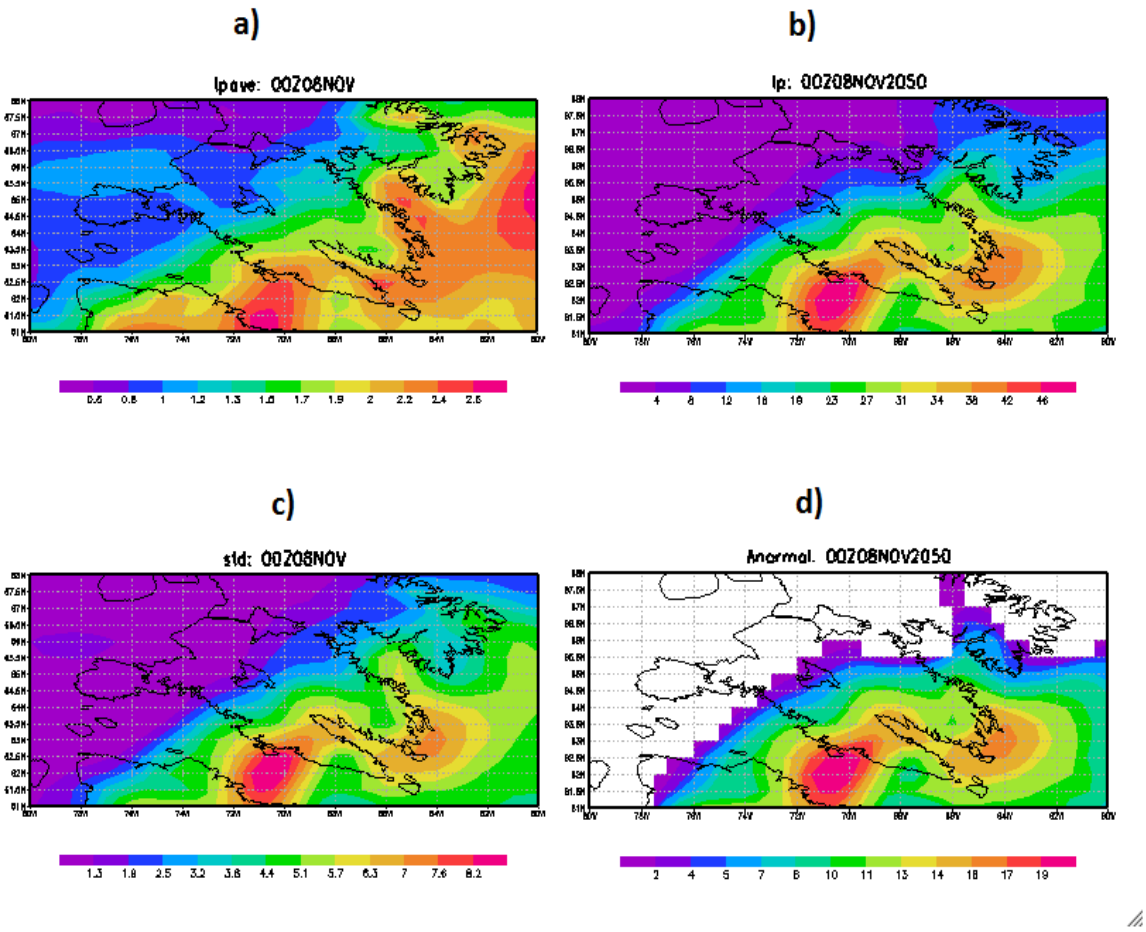

Figure 6.1: Daily values for CRCM precipitation (mm/day) data forced with CGCM data output. (a) shows the composite average daily precipitation amount from 00 UTC November 8 to 00 UTC November 9 for the 30-year period. (b) shows the precipitation amount from 00 UTC November 8, 2050 to 00 UTC November 9, 2050 specifically. (c) shows the standard deviation of the daily precipitation from 00 UTC November 8 to 00 UTC November 9 for the 30-year period. (d) shows precipitation amounts 3 standard deviations above (a) from 00 UTC November 8, 2050 to 00 UTC November 9, 2050 specifically.

At the surface, the future projection inferred a 960 mb low over eastern Hudson Strait just south of Kimmirut (Figure 6.2). The positioning of this low infers that Kimmirut and Iqaluit are on the 'back side' of the low, where precipitation often accumulates along a deformation zone once mature.

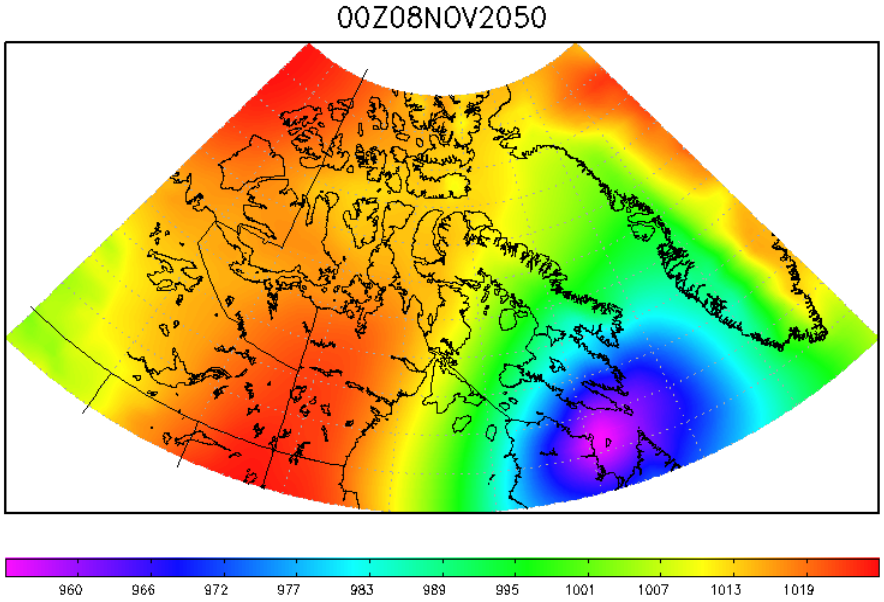

Figure 6.2: Composite mean sea level pressure (mb) from 00 UTC November 8, 2050 to 00 UTC November 9, 2050.

At 500 mb, the future projection inferred a 4760 m upper low over northern Quebec, with a weaker trough extending northward from the low into central Baffin Island (Figure 6.3). Conceptually, this makes sense with where the model inferred the high precipitation amounts over southern Baffin Island, as the affected area was downstream from the 500 mb low.

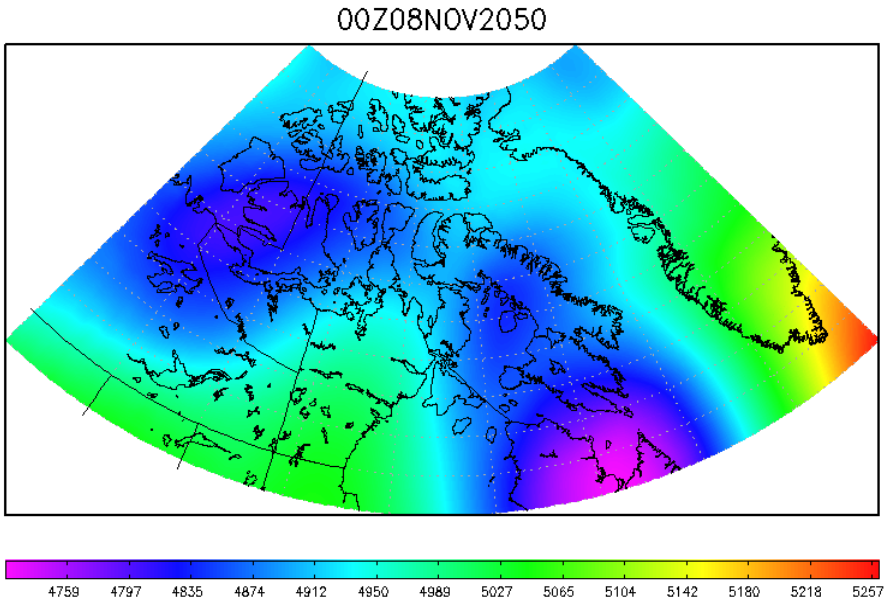

Figure 6.3: Composite mean 500 mb geopotential height (m) from 00 UTC November 8, 2050 to 00 UTC November 9, 2050.

The wind algorithm output showed a surface jet core just east of Iqaluit with sustained surface winds of approximately 26 m/s. Over Iqaluit, sustained surface wind speeds of approximately 23 m/s were inferred. Over Kimmirut, sustained wind speeds of approximately 22 m/s were inferred. Also apparent in the surface wind output is a secondary jet maximum over Pangnirtung with sustained wind speeds of approximately 23 m/s over the site (Figure 6.4).

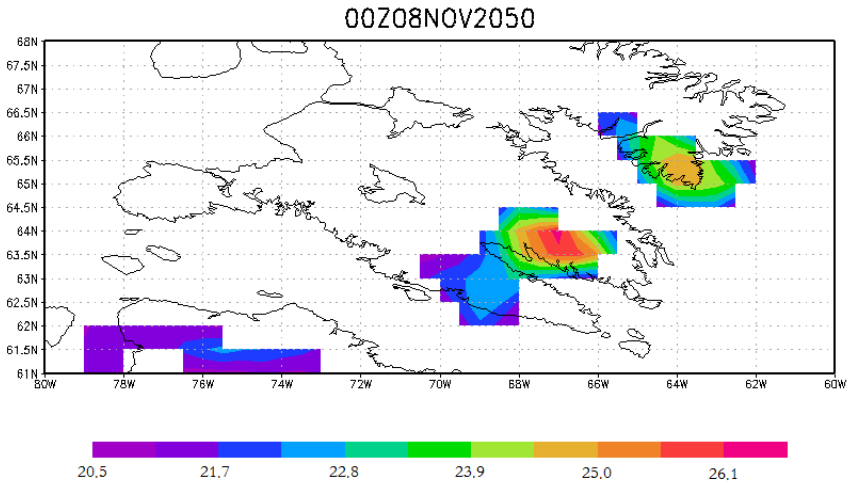

Figure 6.4: Composite average wind speed (m/s) from 00 UTC November 8, 2050 to 00 UTC November 9, 2050.

The 850 mb wind output inferred stronger northeasterly winds over Iqaluit at 22 m/s (Figure 6.5). The 850 wind chart also shows a strong cyclonic circulation in the Southern Baffin Island area with the main circulation just south of Kimmirut. The strongest winds were associated with the southwesterly flow with values of 30 m/s inferred over Ungava Bay.

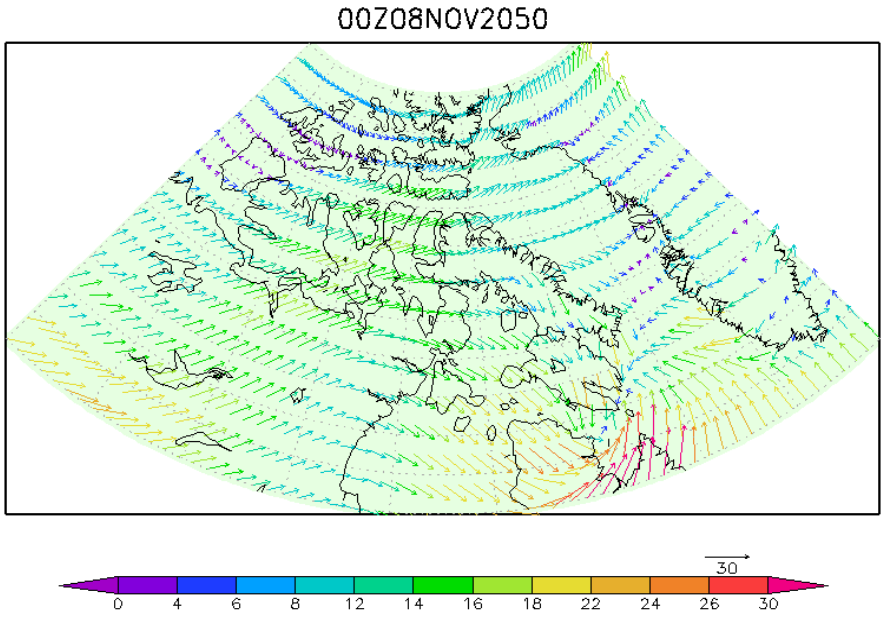

Figure 6.5: Composite mean 850 mb vector wind speed (m/s) from 00 UTC November 8, 2050 to 00 UTC November 9, 2050.

6.3 September 24, 2054 at Iqaluit and Kimmirut

On September 24, 2054 the CRCM future projection inferred an extreme wind event that impacted Kimmirut and Iqaluit.

Precipitation amounts inferred by the algorithm were approximately 20 mm over Iqaluit and Kimmirut (Figure 6.6b) with higher amounts inferred just southeast of these communities. The bulk of the precipitation was inferred in the extreme southeastern portions of Baffin Island with approximately 34 mm of rain inferred over Frobisher Bay. Slightly anomalous precipitation values of approximately 7 mm were inferred over Kimmirut but not over Iqaluit (Figure 6.6d).

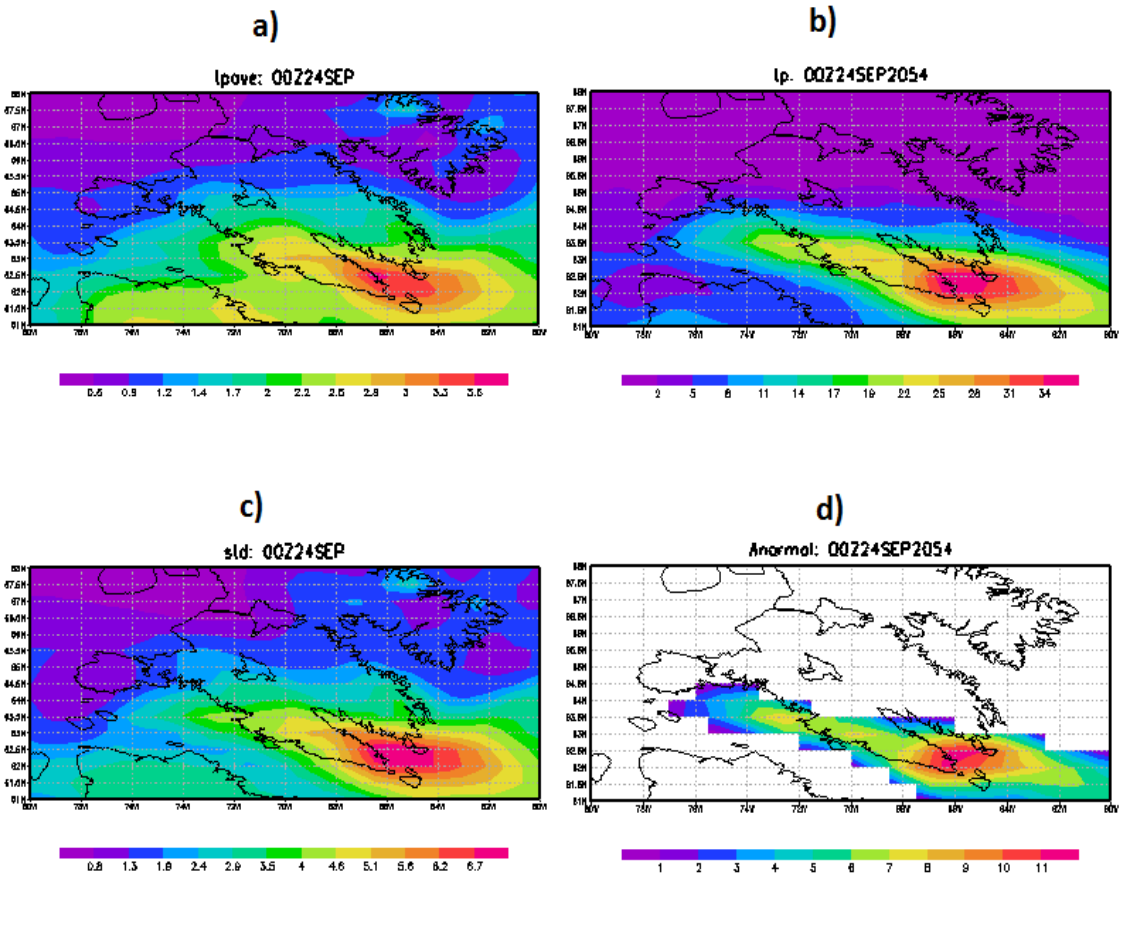

Figure 6.6: Daily values for CRCM precipitation (mm/day) data forced with CGCM data output. (a) shows the composite average daily precipitation amount from 00 UTC September 24 to 00 UTC September 25 for the 30-year period. (b) shows the accumulated precipitation amount from 00 UTC September 24, 2054 to 00 UTC September 25, 2054 specifically. (c) shows the standard deviation of the daily precipitation from 00 UTC September 24 to 00 UTC September 25 for the 30-year period. (d) shows precipitation amounts 3 standard deviations above (a) from 00 UTC September 24, 2054 to 00 UTC September 25, 2054 specifically.

The future projection inferred a 966 mb surface low pressure system over northwestern Quebec, over the northeastern portion of Hudson Bay (Figure 6.7). Conceptually, Kimmirut and Iqaluit would be experiencing south-southeasterly winds. The flow is inferred to be approximately parallel to Frobisher Bay, which would enhance the low level winds in the Iqaluit area.

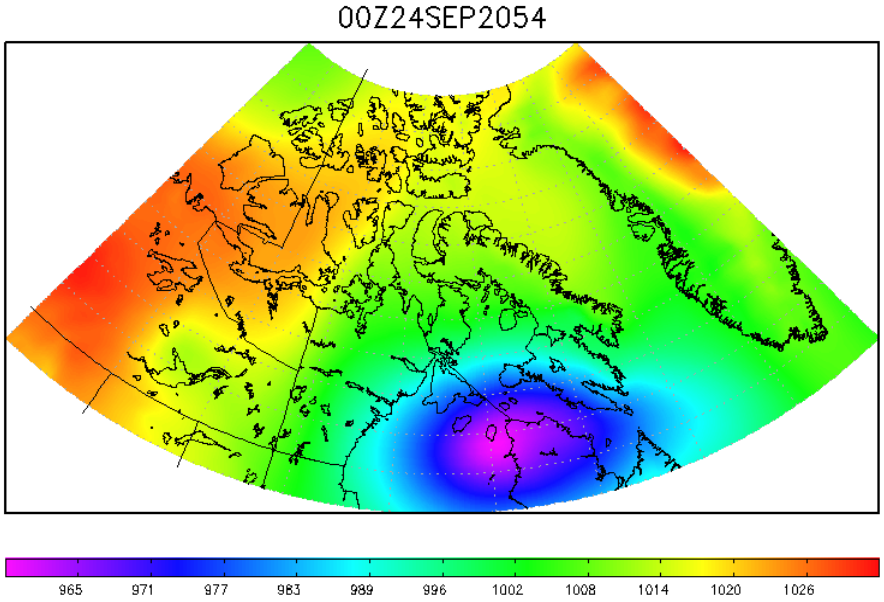

Figure 6.7: Composite mean sea level pressure (mb) from 00 UTC September 24, 2054 to 00 UTC September 25, 2054.

The 500 mb geopotential height chart for this event inferred a 4850 m low over northern Quebec (Figure 6.8). Kimmirut and Iqaluit are located downstream of this upper low and the flow aloft would conceptually be from the southeast.

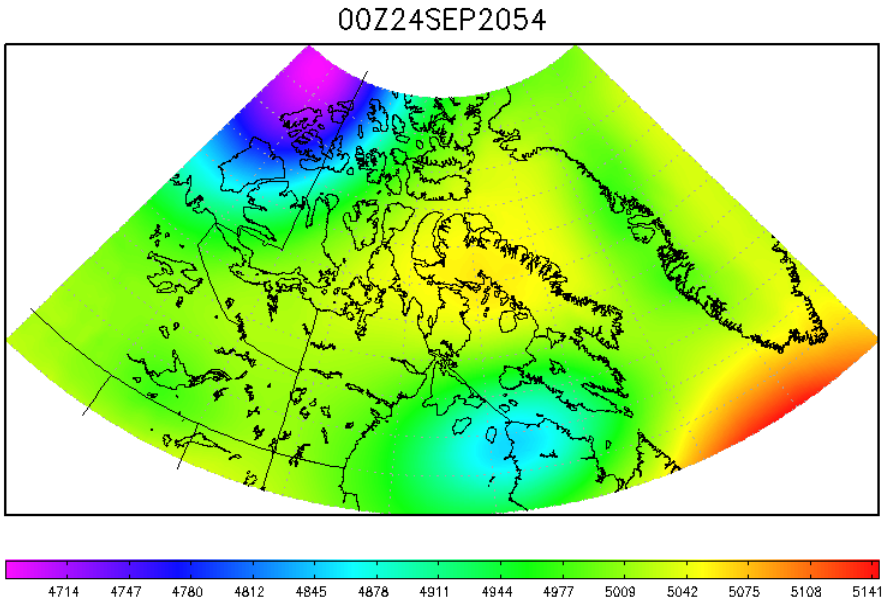

Figure 6.8: Composite mean 500 mb geopotential height (m) from 00 UTC September 24, 2054 to 00 UTC September 25, 2054.

The wind algorithm inferred a surface jet maximum over the Kimmirut and Iqaluit areas with sustained surface wind speeds of 23 m/s over the Iqaluit area and 22 m/s over Kimmirut (Figure 6.9). The highest sustained wind speeds were inferred just north west of Kimmirut at 24 m/s.

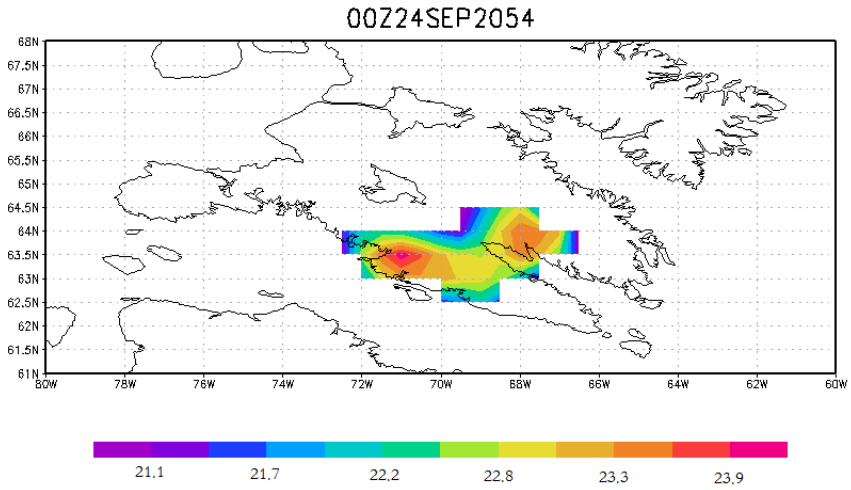

Figure 6.9: Composite average wind speed (m/s) from 00 UTC September 24, 2054 to 00 UTC September 25, 2054.

The 850 mb winds inferred a strong cyclonic rotation just south west of Baffin Island (Figure 6.10). A very strong 30 m/s southwesterly jet associated with this system was inferred just south of Kimmirut, with a slightly lighter northeasterly jet influencing Iqaluit. The flow over Iqaluit is perpendicular to the orientation of Frobisher Bay, which may indicate that this may have a downsloping and channeling event for Iqaluit. Most strong wind events at Iqaluit in the past have been events where the flow is parallel to Frobisher Bay allowing for the wind to be channeled through the bay, however as Deacu et al. (2010) noted, downsloping winds in combination with channeled winds may also enhance surface winds at Iqaluit.

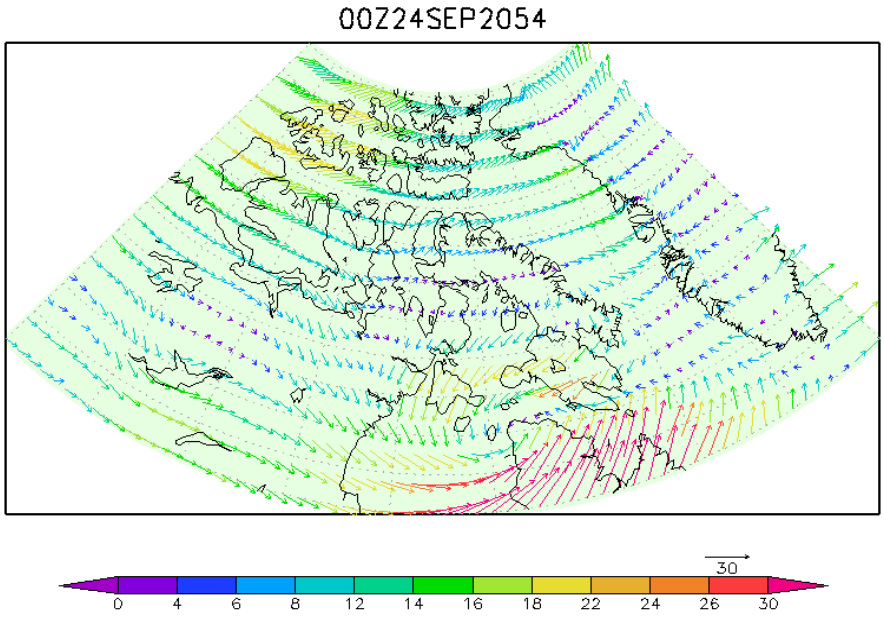

Figure 6.10: Composite mean 850 mb vector wind speed (m/s) from 00 UTC September 24, 2054 to 00 UTC September 25, 2054.

6.4 August 27, 2068 at Pangnirtung

The CRCM future projection analysis inferred an extreme precipitation event over Pangnirtung on August 27, 2068 (Figure 6.11). According to the model output, over 41 mm of rain was inferred at the Pangnirtung site (Figure 6.11b) with a large anomalous precipitation area that exceeded 3 standard deviations above the mean detected over northern Baffin Island (Figure 6.11d). The bulk of the precipitation would be occurring over the northern portion of Baffin Island.

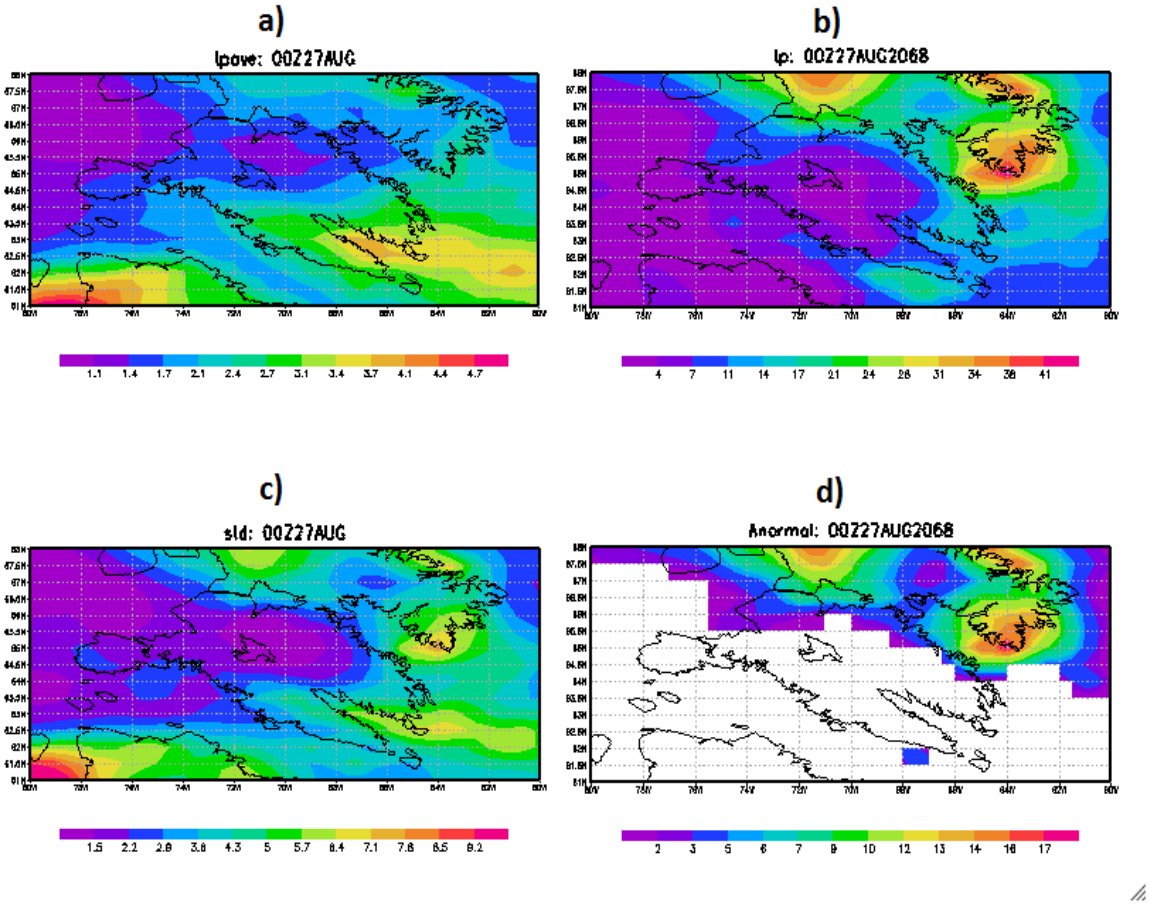

Figure 6.11: Daily values for CRCM precipitation (mm/day) data forced with CGCM data output. (a) shows the composite average daily precipitation amount from 00 UTC August 27 to 00 UTC August 28 for the 30-year period. (b) shows the precipitation amount from 00 UTC August 27, 2068 to 00 UTC August 28, 2068 specifically. (c) shows the standard deviation of the daily precipitation from 00 UTC August 27 to 00 UTC August 28 for the 30-year period. (d) shows precipitation amounts 3 standard deviations above (a) from 00 UTC August 27, 2068 to 00 UTC August 28, 2068 specifically.

The future projection inferred a 970 mb surface low over eastern Foxe Basin (Figure 6.12). Conceptually, the positioning of the low would infer that Pangnirtung would be under the influence of a southerly flow.

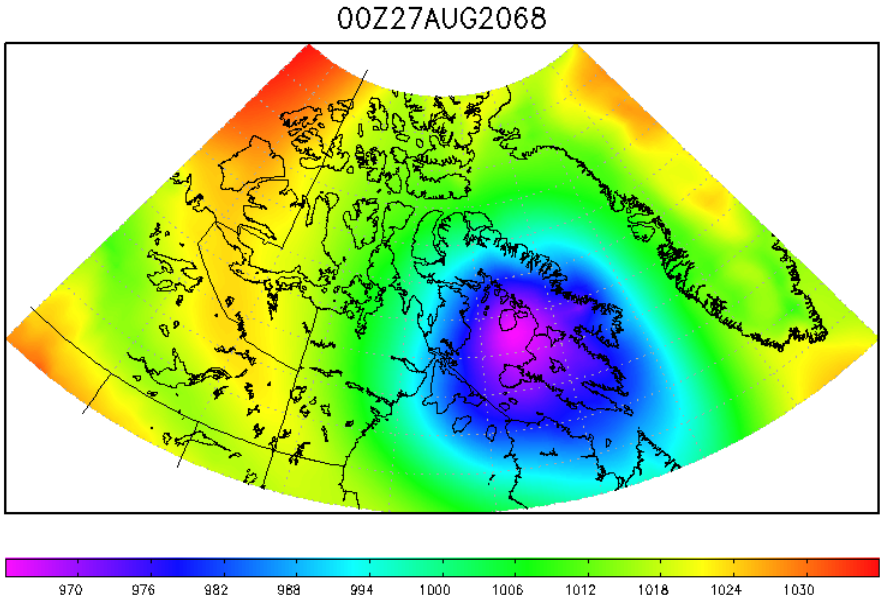

Figure 6.12: Composite mean sea level pressure (m) from 00 UTC August 27, 2068 to 00 UTC August 28, 2068.

The 500 mb chart inferred a 4770 m upper low over central Foxe Basin (Figure 6.13). This infers that all of southeastern Baffin Island would be in a prime area for upper level lift and support for a well developed storm system.

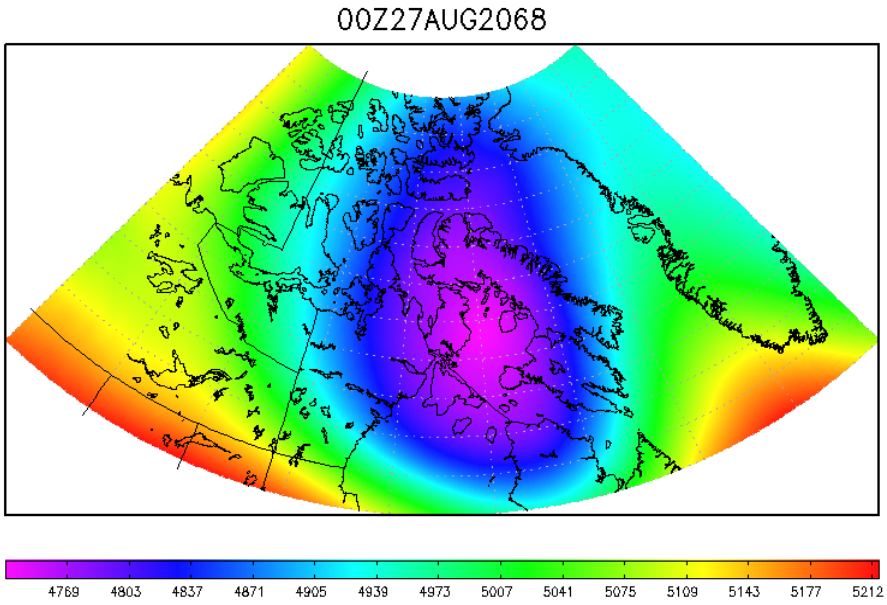

Figure 6.13: Composite mean 500 mb geopotential height (m) from 00 UTC August 27, 2068 to 00 UTC August 28, 2068.

The future projection did not infer any sustained winds over 60 km/h associated with this event therefore a surface wind chart was omitted from the analysis.

The 850 mb wind chart inferred very strong winds with this event, contrasting what the surface chart suggested (Figure 6.14). A 26 m/s southwesterly sustained wind was inferred over Pangnirtung with this event. This wind direction is an upslope wind for the Pangnirtung site, which could be one of the reasons that the future projection inferred enhanced precipitation over Pangnirtung on this particular day.

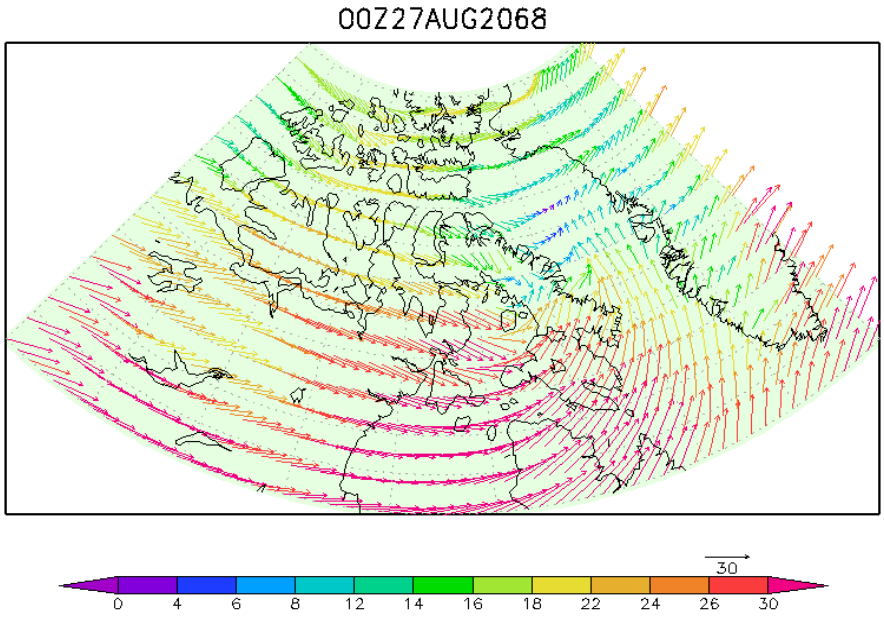

Figure 6.14: Composite mean 850 mb vector wind speed (m/s) from 00 UTC August 27, 2068 to 00 UTC August 28, 2068.

6.5 July 31, 2070 at Cape Dorset

On July 31, 2070 the CRCM forced with CGCM future projection inferred an extreme precipitation event over Cape Dorset (Figure 6.15). The model output inferred over 32 mm of rain that fell at the Cape Dorset site on this date (Figure 6.15b) with large anomalous values over the region (Figure 6.15d).

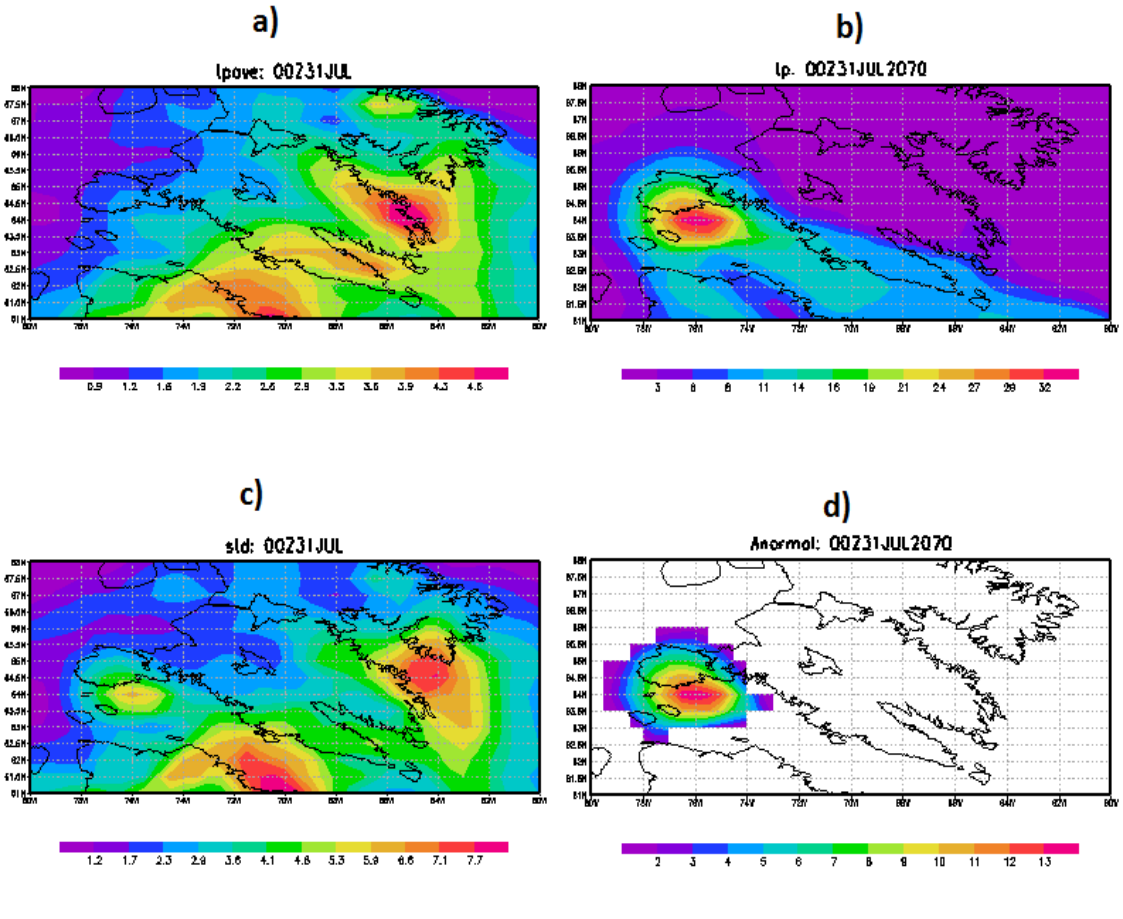

Figure 6.15: Daily values for CRCM precipitation (mm/day) data forced with CGCM data output. (a) shows the composite average daily precipitation amount from 00 UTC July 31 to 00 UTC August 1 for the 30-year period. (b) shows the precipitation amount from 00 UTC July 31, 2070 to 00 UTC August 1, 2070 specifically. (c) shows the standard deviation of the daily precipitation from 00 UTC July 31 to 00 UTC August 1 for the 30-year period. (d) shows precipitation amounts 3 standard deviations above (a) from 00 UTC July 31, 2070 to 00 UTC August 1, 2070 specifically.

The future projection inferred a 988 mb surface low over Hudson Strait, with Cape Dorset inferred to be on the northwest side of the low (Figure 6.16). Conceptually, Cape Dorset would be in a northerly flow and in this location would be in a prime area for heavy precipitation relative to the low.

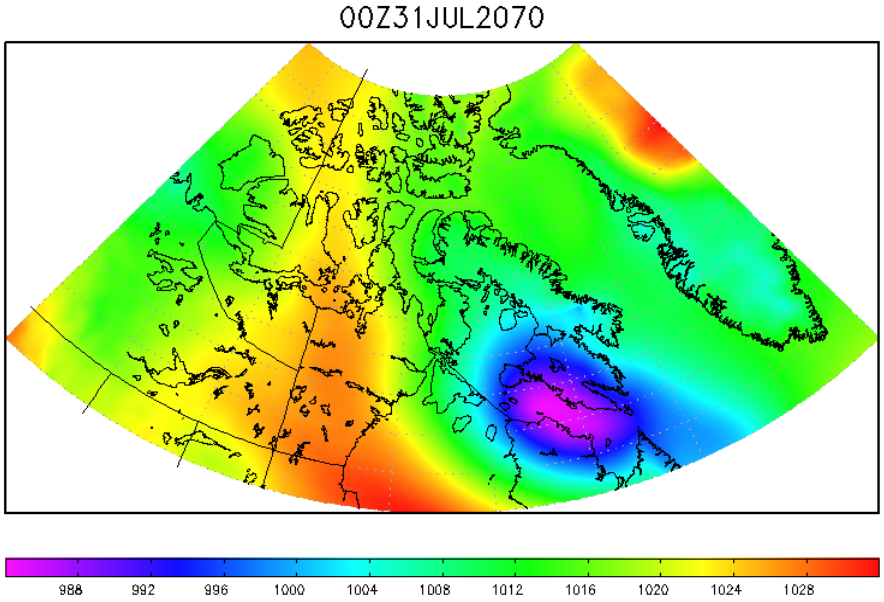

Figure 6.16: Composite mean sea level pressure (mb) from 00 UTC July 31, 2070 to 00 UTC August 1, 2070.

The 500 mb geopotential height chart inferred a 4850 m upper low over northern Quebec with a trough of low pressure extending northwestward from this low all the way up through to the high Arctic (Figure 6.17). The upper low was inferred to be southeast of Cape Dorset. However, relative to the upper trough Cape Dorset was upstream of the

flow and would have upper level support. Conceptually, the placement of the low would give Cape Dorset a southeasterly flow aloft.

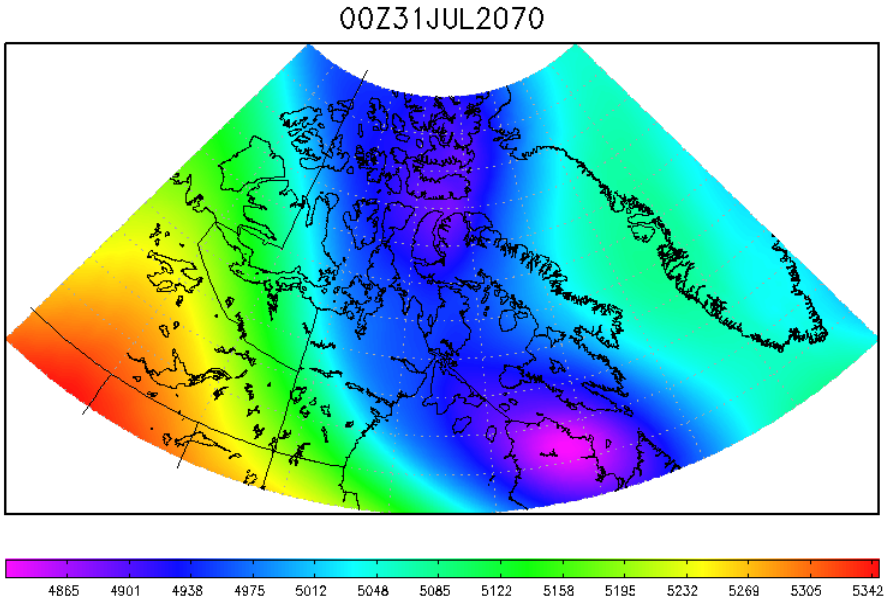

Figure 6.17: Composite mean 500 mb geopotential height (m) from 00 UTC July 31, 2070 to 00 UTC August 1, 2070.

The surface wind algorithm did not infer any sustained wind speeds above 60 km/h and was not included in the analysis.

The 850 mb wind chart inferred a strong westerly jet around Cape Dorset at the time of this event with an even stronger jet core just south of Pangnirtung (Figure 6.18). The 850 mb winds over Cape Dorset were inferred to be approximately 22 m/s and approximately 30 m/s in the jet core.

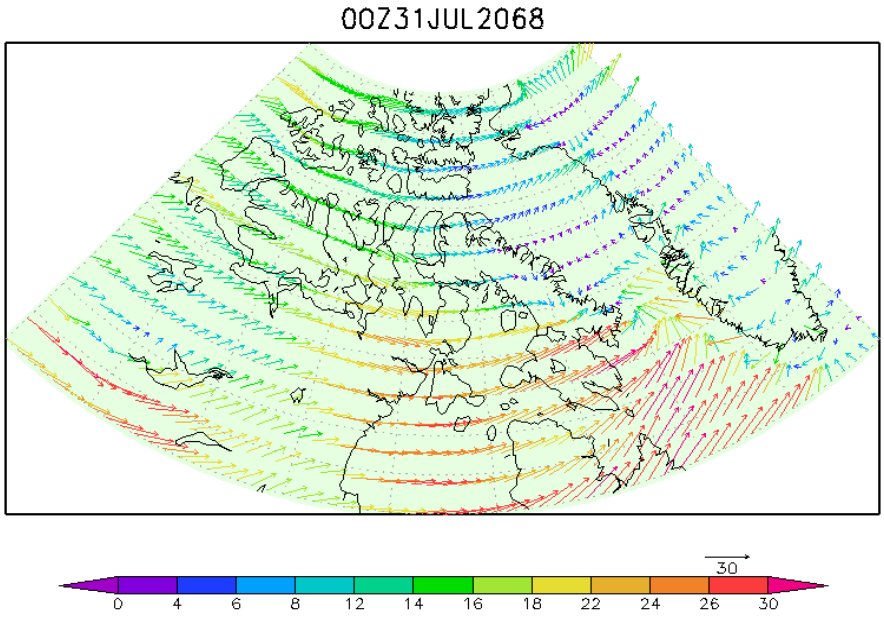

Figure 6.18: Composite mean 850 mb vector wind speed (m/s) from 00 UTC July 31, 2070 to 00 UTC August 1, 2070.

6.6 Summary of future projection case studies

The preceding four case studies provide a limited analysis of the future projection scenario and provide only a few scenarios of events that may occur in the future. These case studies were chosen to analyze in detail for their large scale and local features.

Some features were consistently found in the case studies. A strong surface low was inferred in all cases, and most were deeper than 970 mb in strength. The positioning of the lows made sense conceptually for each event. A strong 500 mb low or a strong 500 mb trough occurred in all cases and varied only slightly in strength (approximately 4750-4850 m between the events). In all of the wind events and most of the precipitation

events, a strong 850 mb jet was also inferred. Values of 20-30 m/s were consistently inferred for the wind events whereas these winds were more variable in strength for the precipitation events.

All of the wind events analyzed inferred sustained surface winds over 60 km/h. However, despite strong 850 mb wind values, the extreme precipitation events did not always exhibit strong surface winds. This may suggest that, as was seen in Chapter 4 with the analysis of the historical case studies, that 850 mb winds enhanced by local effects are not resolved well with such a coarse model resolution.

The magnitude of the precipitation events analyzed in this study was much greater than those of the historic case studies from Chapter 4. As an example, the future projection inferred a 46 mm event at Iqaluit on November 8, 2050 whereas the historic re-analysis detected a maximum precipitation event of only 28 mm at Iqaluit (see Figure 5.3).

CHAPTER 7: CONCLUDING REMARKS

With our warming climate and the Arctic being one of the most vulnerable regions on Earth, it is essential to understand how extreme weather events will change in this region in the future. Extreme precipitation and wind events have many impacts on northern communities, paralyzing transport and damaging structures.

This study addressed several aspects of this overall issue through an examination of historic and future extreme wind and precipitation events at four locations over Southern Baffin Island. This led to several key observations and conclusions.

Extreme precipitation and wind events have occurred over this region, some by themselves and some with both precipitation and wind events simultaneously. These events have occurred in different seasons.

For historic case studies, a strong low pressure system at 500 mb was a common element with the both extreme wind and extreme precipitation events, as well as an 850 mb jet, which was more consistent in the model output than the modeled surface winds when determining actual surface observations of historic extreme events. An absence of 850 mb winds over the Iqaluit site itself seen in historic case studies could be indicative that some of the meteorological features that cause extreme weather events are on a smaller scale than the NARR and the CRCM re-analyses could detect.

A comparison between actual observations and the CRCM forced with ERA-40 dataset showed that in general the CRCM model consistently under-predicted extreme precipitation events. Using this knowledge, we may also assume that the CRCM forced with CGCM runs may be under-predicting precipitation in their results as well. This

would mean that any increase in intensity of extreme precipitation events inferred by the future projection could also be under-predicted.

Comparisons of the two CRCM forced with CGCM datasets, one being a hindcast from 1961-1990 and the other being the future projection from 2041-2070, inferred an increase in frequency and intensity of extreme precipitation and wind events at three of the four communities over Southern Baffin Island. More frequent and more intense precipitation and wind events were inferred at Iqaluit, Kimmirut and Cape Dorset whereas Pangnirtung showed a decrease in frequency of both precipitation and wind events. However, Pangnirtung still showed a trend towards heavier precipitation events. This could be due to a shift in storm tracks, or more convection due to more open water in the Arctic. The maximum precipitation amount in events at Iqaluit and Kimmirut was inferred to increase by as much as 20 mm according to the future projection, as much as 10 mm at Cape Dorset. The maximum precipitation amount at Pangnirtung did not change.

Extreme wind events showed an overall increase at Iqaluit, Kimmirut and Cape Dorset by approximately 30 events in the 60-70 km/h category, 10 events in the 70-80 km/h category and 2 events in the 80 km/h or greater category whereas Pangnirtung showed a decrease in events for all categories. One reason for this may be that a change in storm tracks could have an impact on wind direction, which is important for Pangnirtung, where its climate is highly dependent on local effects.

For the future projection case studies, there were significant changes at surface and aloft. Surface low pressure systems were generally deeper than the historic case studies. A strong 850 mb jet was present in all wind events, whereas it varied for the

precipitation case studies. A 500 mb low pressure system was also a common element in both extreme precipitation and wind events.

Changes between the hindcast and future projection CRCM forced with CGCM runs showed the biggest increases in precipitation amounts and intensities in the shoulder season months. A shift in the heavy precipitation season could have a huge impact on precipitation typing. This could also mean that with more open water, the future projection may be hinting at more convection in the shoulder season months. A shift in storm tracks to more south and west originating storms as seen by Gascon et al. (2010) in the Arctic may be another reason why the future projection inferred an increase in extreme events to the Southern Baffin Island area.

It is recognized that this study has limitations. It would be desirable in future studies, for example, to examine an ensemble of future projections. Other limitations exist because of the lack of data points in the Arctic as well as data gaps within archived observations. The modeled data itself has a 45 km resolution, which is not sufficient, especially in the Arctic where many local effects have a large impact on the weather observed at the surface. Also, newer model runs may have different outcomes with different storm tracks. For example, a recent article on climate projections shows an equatorward shift of storm tracks relative to models with poor stratospheric resolution (Scaife et al. 2011). Another limitation of this study is the use of daily values instead of values in smaller blocks of time, such as 6 h time steps. By using daily values, the true depths of the low pressure systems were not captured and sustained wind values were less than the maxima experienced.

In summary, an analysis of the projected 2041-2070 extreme precipitation and wind events over southern Baffin Island shows that the area may receive more intense systems that produce stronger winds and more variable precipitation events. The peak precipitation season may also shift to the shoulder seasons, meaning the Arctic may see more convection in the ice-free months. Precipitation type forecasting may also become a bigger challenge as the bulk of the precipitation may fall during the transition months producing both rain and snow.

REFERENCES

ACIA Arctic climate impact assessment, 2005: scientific report. Cambridge University Press, Cambridge.

Bender, Frida A-M., V, Ramanathan and G. Tselioudis, 2011: Changes in extratropical storm track cloudiness 1983-2008: observational support for a poleward shift. *Climate Dynamics*, **DOI:** 10.1007/s00382-011-1065-6.

Bisson, M., 2008: Pangnirtung Flash Flood of June 8-9, 2008. PASPC Winnipeg weather report.

Chang, E. M. K. and Y. Fu, 2002: Interdecadal variations in northern hemisphere winter storm track intensity. *Journal of Climate*, **15**: 642-658.

DAI Catalogue, 2009: "Catalogue available datasets through DAI (Data Access and Integration)", version 1.0, April 2009, Montreal, QC, Canada, 24 pp.

DAI CGCM3 Predictors, 2008: "Sets of Predictor Variables Derived From CGCM3 T47 and NCEP/NCAR Reanalysis'', version 1.1, April 2008, Montreal, QC, Canada, 15 pp.

Data Access Integration (DAI) Portal, 2010: http://loki.qc.ec.gc.ca/DAI/login-e.php, page last modified May 3, 2010.

Deacu, D., A. Zadra and J. Hanesiak 2010: Simulating wind Channeling over Frobisher Bay and its Interaction with Downslope Winds during the 7-8 November 2006 Wind Event. *Atmosphere-Ocean*, **48** (2): 101-121.

Devine, K.A. and É. Mekis, 2008: Field accuracy of Canadian rain measurements. *Atmosphere-Ocean*, **46** (2): 213-227.

Environment Canada, 2011: http://www.climate.weatheroffice.gc.ca/Welcome_e.html, page last modified September 15, 2011.

Fedor, Mesinger et al, submitted to BAMS 2004: North American Regional Reanalysis: A long term, consistent, high-resolution climate dataset for the North American domain, as a major improvement upon the earlier global reanalysis datasets in both resolution and accuracy.

Gascon, G., R.E. Stewart and W. Henson, 2010: Major cold season precipitation events at Iqaluit, Nunavut. *Arctic*, **63**: 327-337.

Hanesiak, J., R. Stewart, P. Taylor, K. Moore, D. Barber, G. McBean, W. Strapp, M. Wolde, R. Goodson, E. Hudson, D. Hudak, J. Scott, G. Liu, J. Gilligan, S. Biswas, D. Desjardins, R. Dyck, S. Fargey, R. Field, G. Gascon, M. Gordon, H. Greene. C. Hay, W. Henson, K. Hochheim, A. Laplante, R. Martin, M.A. Melzer and S. Zhang, 2010: Storm Studies in the Arctic (STAR). *Bull. Am. Meteorol. Soc.* **91:** 47-68.

Henson, W., R. Stewart and D. Hudak 2010: Vertical reflectivity profiles of precipitation over Iqaluit, Nunavut during autumn 2007. *Atmospheric Research*, **99**: 217-229.

Hill, J. S., 2011: Catastrophic Arctic Storm Surge Linked to Global Warming. Reuters May 18, 2011.

Intihar, M. R., and R. E. Stewart, 2005: Extratropical cyclones and precipitation within the Canadian Archipelago during the cold season. *Arctic*, **58**: 162-174.

Jiao, Y., and D. Caya, 2006: An investigation of the summer precipitation simulated by the Canadian Regional Climate Model. *Mon. Wea. Rev.*, In Press.

Kalnay, E. and Coauthors, 1996: The NCEP/NCAR Re-analysis 40-year Project. Bull. Amer. Meteor. Soc., 77, 437-471.

Mekis, É. and R. Brown: Derivation of an adjustment factor map for the estimation of the water equivalent snowfall from ruler measurements in Canada. *Atmosphere-Ocean*, submitted.

Mekis, É. And W.D. Hogg, 1999: Rehabilitation and analysis of Canadian daily precipitation time series. *Atmosphere-Ocean* **37** (1): 53-85.

Mekis, É. And R. Hopkinson, 2004: Derivation of an improved snow water equivalent adjustment factor map for application on snowfall ruler measurements in Canada. Proc. 14th Conference on Applied Climatology. January 11-15 2004. 5 pp.

Mekis, É., 2005: J3.7 Adjustments for trace measurements in Canada. 15th Conference on Applied Climatology, Savannah, Georgia, USA, 20-24 June 2005.

Mesinger, F., G. DiMego, E. Kalnay, K. Mitchell, P.C. Shafran, W. Ebisuzaki, D. Jovic, J. Woollen, E. Rogers, E. H. Berbery, M.B. Ek, Y. Fan, R. Grumbine, W. Higgins, H. Li, Y. Lin, G. Manikin, D. Parrish, W. Shi, 2006: North American Regional Re-analysis. *Bull. Amer. Meteor. Soc.*, **87**: 343-360.

Nadeau, D., 2007: Impacts of synoptic atmospheric circulations and topographic conditions on sustained strong surface winds over southern Nunavut. Master's thesis, McGill University, Montreal, Quebec.

National Oceanic and Atmospheric Administration (NOAA): http://ww.esrl.noaa.gov/psd/data/narr, page last modified October 2011.

Nawri, N. and R. E. Stewart, 2006: Climatological features of orographic low-level jets within Frobisher Bay. *Atmosphere.-Ocean*, **44**: 397-413.

Nawri, N. and R. E. Stewart, 2008: Channeling of high-latitude boundary-layer flow. *Nonlinear Processes in Geophysics*, **15**: 33-52.

Nielsen, D., 2007: The City of Iqaluit's Climate Change Impacts, Infrastructure Risks & Adaptive Capacity Project. Nunavut Research Institute.

Pisaric, Michael F.J., J.R. Thienpont, S.V. Kokelj, H. Nesbitt, T.C. Lantz, S. Solomon and J.P. Smol 2011: Impacts of a recent storm surge on an Arctic delta ecosystem examined in the context of the last millennium. *Science*, **328**: 1517-1520.

Plummer, D.A., D. Caya, A. Frigon, H. Côté, M. Giguère, D. Paquin, S. Biner, R. Harvey, and R. de Elia, 2006: Climate and Climate Change over North America as Simulated by the Canadian CRCM. J. Clim., **19**: 3112-3132.

Raible, C. C., R. Blender, P. M. Della-Marta, C. Schwierz and H. Wernli, 2008: Northern Hemisphere Extratropical Cyclones: A comparison of detection and tracking methods and different reanalyses. *Monthly Weather Review* **136**: 880-897.

Riette, S. and D. Caya, 2002: Sensitivity of short simulations to the various parameters in the new RCM spectral nudging. Research activities in Atmospheric and Oceanic Modelling, edited by H. Ritchie, WMO/TD - No 1105, Report No. 32: 7.39-7.40.

Roberts, E., N. Nawri, and R. E. Stewart, 2008: On the storms passing over Southern Baffin Island during autumn 2005. *Arctic* **61**: 309-321.

Roberts, E. and R. E. Stewart, 2008: On the occurrence of freezing rain and ice pellets over the eastern Canadian Arctic. *Atmos. Research* **89**: 93-109.

Scaife, A. A., T. Spangehl, D.R. Fereday, U. Cubasch, U. Langematz, H. Akiyoshi, S. Bekki, P. Braesike, N. Butchart, M.P. Chipperfield, A. Gettelman, S.C. Hardiman,

M. Michou, E. Rozanov and T.G. Sheperd, 2011: Climate change projections and stratosphere-troposphere interaction. *Climate Dynamics*, doi: 10.1007/s00382-011-1080-7.

Stewart, R. E., D. Bachand, R. R. Dunkley, A. C. Giles, B. Lawson, L. Legal, S. T. Miller, B. P. Murphy, M. N. Parker, B. J. Paruk and M. K. Yau, 1995: Winter storms over Canada. *Atmos.-Ocean*, **33**: 223-248.

Vincent, L.A. and É. Mekis, 2009: Discontinuities due to joining precipitation station observations in Canada. *Journal of Applied Meteorology and Climatology*, Vol. **48** No. 1: 156-166.

Zhang, X. and J. E. Walsh, 2004: Climatology and interannual variability of Arctic cyclone activity: 1948-2002. *Journal of Climate* **17**: 2300-2317.